Data-Driven Optimization of Deep Brain Stimulation for Movement Disorders

Andrew J. Haddock

A dissertation
submitted in partial fulfillment of the
requirements for the degree of

Doctor of Philosophy

University of Washington

2017

Reading Committee:

Howard Jay Chizeck, Chair

Samuel A. Burden

Bingni M. Brunton

Andrew Ko

Katherine M. Steele, GSR

Program Authorized to Offer Degree:
Electrical Engineering

University of Washington

Abstract

Data-Driven Optimization
of Deep Brain Stimulation for Movement Disorders

Andrew J. Haddock

Chair of the Supervisory Committee:
Professor Howard Jay Chizeck
Electrical Engineering

Deep brain stimulation (DBS) is an effective therapy for ameliorating motor symptoms associated with Parkinson's disease (PD) and essential tremor (ET). DBS is a surgical procedure in which implanted electrodes are placed near brain structures believed to cause pathological motor disorder behaviors. Subcortical brain structures in thalamus and basal ganglia are typical DBS targets for PD and ET therapy, and modern DBS systems allow customization of therapeutic stimulation patterns through control of stimulation location, amplitude, pulsewidth, and frequency in order to optimize therapy on a patient-specific basis. Despite the technological capabilities of implanted DBS systems, current clinical implementation is limited by a scarcity of DBS specialty clinics and variable, subjective clinician performance in assessing patient symptoms and systematically selecting optimal DBS settings for therapy, a process known as programming. Compounding this problem is a dated and inefficient healthcare system that requires patients to travel to clinic to receive DBS programming updates, oftentimes at great expense both to patients and healthcare providers.

In this dissertation, we investigate and demonstrate experimental data-driven methodologies and algorithms aimed at improving DBS therapy for PD and ET patients. Particularly, we develop adaptive DBS systems by coupling low-cost commercial sensors with stimulation control and demonstrate the therapy potential through clinical experiments with human

subjects diagnosed with PD and ET. We make use of a commercially available wearable smartwatch and show that clinical ratings for tremor and bradykinesia can accurately be classified on the basis of inertial measurement unit (IMU) data. We embed this feature in a software algorithm for automated DBS programming that is demonstrated to perform at the level of expert clinicians in selecting optimal DBS settings for therapy in PD and ET patients. We further use this platform to investigate neural correlates and biomarkers of effective DBS in ET patients using recorded local field potentials (LFPs) from an electrocorticographic (ECoG) strip placed over motor cortex. Scalable methods and algorithms for automatically programming DBS when considering a large number of candidate DBS settings are also developed in detail. Finally, we address the problem of closed-loop DBS, in which stimulation is delivered in a responsive manner to patient symptoms, by formulating a model-based approach using system identification experiments, hybrid systems modeling, and predictive control.

The results presented in this dissertation may improve patient care, patient quality of life, and the cost-effectiveness of DBS therapy for PD and ET patients. Additionally, the novel results presented on neural stimulation optimization may be useful more broadly in the growing medical and research fields of neuromodulation and bioelectronic medicine. We conclude with a discussion concerning how to integrate this data-driven approach to DBS therapy in modern healthcare systems, and we discuss the relevance of these results in light of anticipated technological developments in DBS systems.

TABLE OF CONTENTS

ACKNOWLEDGMENTS

This thesis is the culmination of work conducted alongside, and with guidance from, many colleagues and friends. First, I would like to thank the members of my dissertation committee for their helpful comments and especially my advisor, Howard Chizeck, for his continual support.

Many fellow graduate students at UW deserve my sincerest thanks for their support, mentorship, and comraderie. Charlie Matlack and Tamara Bonaci were very helpful during my first few years as a graduate student. Many other members of the Biorobotics Lab, including Jeffrey Herron, Brady Houston, Margaret Thompson, Tim Brown, Katherine Pratt, Jack Lindsay, Andy Lewis, Vijeth Rai, Kevin Huang, and many others, greatly enriched my experience as a graduate student.

Collaborators from other institutions were essential to the results and research presented in this dissertation. Chapter 2 and Chapter 3 were products of collaborative work with the Center for Movement Disorders and Neuromodulation at the University of California, San Francisco (UCSF), and I especially thank Svjetlana Miocinovic, Kyle Mitchell, Andrew Miller, Jill Ostrem, Sarah Wang, and JC Morgenthaler. Chapter 5 was part of collaborative work carried out with Tom Foutz of Seattle Children's Hospital. Chapter 6 was a product of a collaboration with Helen Bronte-Stewart at Stanford University.

I also would like to graciously acknowledge support from the National Science Foundation Graduate Research Fellowship Program (NSF GRFP) during my first three years as a graduate student. The freedom and latitude to study as I wished as afforded by the NSF GRFP was invaluable to my growth as a graduate student and to the development of my research interests. Additionally, the NSF-funded Center for Sensorimotor Neural Engineer-

ing (CSNE) at the University of Washington provided support for my final two years as a graduate student and fostered a great environment for collaboration and discussion.

DEDICATION

To my family–
especially my parents,
Julie and Roger Haddock,
and my grandparents,
Beverly and Darwin Guinn.

Chapter 1
INTRODUCTION

1.1 Deep Brain Stimulation and Neuromodulation

1.1.1 Past, Present, and Future

Deep brain stimulation (DBS) is a type of neuromodulation therapy, a medical treatment paradigm in which targeted electrical stimulation is used to alter nerve activity and to elicit some type of therapeutic effect. Neuromodulation gradually emerged as a viable approach in medicine by the 1980s following centuries of scientific work elucidating the diverse functional interplay between the central nervous system (CNS), peripheral nervous system (PNS), and overt human behavior.

Neural tissue stimulation has long been used as a tool for functional mapping for the brain and as an intervention for pathological behaviors. Early studies in the 19th century showed that direct stimulation of motor cortex could evoke predictable movements in corresponding body parts [1], eventually resulting in a map of functional organization described by the cortical homunculus. In the mid-20th century, electroshock therapy was controversially used to deliver high currents to the skull, evoking a seizure in the patient that would serve to disrupt their psychotic or manic-depressive behaviors [2].

Spinal cord stimulation (SCS) has been used to treat intractable chronic pain following an initial clinical study showing its therapeutic promise in the late 1960s [3]. SCS was developed in response to a theorized mechanism of pain, called gate control theory, which posited that nociceptive (pain-inducing stimuli) signals and non-nociceptive (touch, vibration, or some other stimulus) signals, along with descending afferent signals from the brain, were summed in the dorsal horn of spinal cord [4]. According to gate control theory, if the combination of these signals exceeded some threshold, then a pain signal would be transmitted to sensory

cortex. SCS is currently used today to treat chronic pain, failed back surgery syndrome, and other types of intractable pain disorders.

DBS evolved from surgical procedures that were developed to address tremor in Parkinson's disease. Electrical stimulation of brain structures was originally performed during surgery to confirm the location of anatomical landmarks relative to targeted brain structures that were to be ablated via thalamotomy. When it was discovered that high frequency stimulation of the targeted areas in thalamus could also effectively treat tremor, DBS began to replace thalamotomy as a treatment for patients due to its reversibility and its flexibility in addressing other symptoms of Parkinson's disease. DBS therapy for Parkinson's disease began in the late 1980s before receiving official FDA approval alongside the indication for essential tremor in 1997. In 2003 dystonia was approved as an indication for DBS, and obsessive-compulsive disorder followed in 2009, both as humanitarian device exemptions (HDE) under the FDA. Currently, DBS is being investigated as a possible therapy for epilepsy, treatment-resistant depression, Tourette syndrome, post-traumatic stress disorder (PTSD) and schizophrenia.

Although most indications for neuromodulation have hitherto been neurological disorders, recent research revealing CNS involvement in inflammatory processes throughout the body has suggested its therapeutic value may extend much further [5]. Studies have shown that descending drive from the vagus nerve activates an inflammatory reflex in which efferent cholinergic neurons suppress cytokine production, generating an anti-inflammatory response to counter the immune system response to foreign pathogens. Furthermore, electrical stimulation of vagus nerve demonstrated potent inhibition of inflammation [6], suggesting that vagus nerve stimulation (VNS) may become a therapeutic approach for treating the myriad diseases characterized by excessive immune response. These diseases include many chronic, resource- and cost-intensive diseases such as diabetes, Alzheimers disease, rheumatoid arthritis, multiple sclerosis, congestive heart failure, and inflammatory bowel disease. Thus, VNS may significantly expand the diseases targeted by neuromodulation and has the potential to usher in a new era of bioelectronics medicine.

1.1.2 DBS Side Effects

DBS and neuromodulation potentially confer many advantages over conventional medical treatment with pharmaceuticals. While pharmaceuticals absorbed into the bloodstream typically act in a very diffuse manner with potential effects throughout the body, DBS relies on precise delivery of electrical stimulation to targeted neural tissue.

However, there are many side effects and potential risks associated with DBS. Initial implantation and battery replacement are both surgical procedures that carry the risk of infection, which has been estimated at 4.5% in one large series study [7]. Additionally, as the exact mechanism of action for DBS is not known, and neural stimulation produces a host of inhibitory and excitatory effects both localized and distributed throughout the larger brain network to which the targeted brain structure is connected, pinpointing the effects of chronic DBS is difficult and remain largely unknown.

DBS-induced side effects are a major consideration in the selection of electrical stimulation parameters for DBS therapy. Targeted brain structures for DBS therapy are close in proximity to several tracts and inadvertent, or in some cases unavoidable, stimulation of these tracts can produce a range of psychophysical effects. In PD patients, DBS of subthalamic nucleus (STN) commonly induces speech impairment, double vision, mood changes (depressive or anxious), dysphagia (swallowing difficulties), parasthesia (tingling sensation), and tonic muscle contractions due to proximity to medial STN, optic tract, oculomotor nerve, internal capsule, and lemniscal tract [8]. In ET patients, DBS of ventral intermediate nucleus of thalamus (VIM) commonly induces parasthesia (in up to 79% of patients) by stimulation spillover into the lemniscal tract [9]. Other side effects reported in ET patients during VIM DBS include pain, speech difficulties and gait deficits.

Most side effects attributed to DBS appear within seconds of turning DBS on and subside soon after the cessation of DBS. However, there are more elusive side effects caused by DBS, such as dyskinesia in PD patients, which is generally context-dependent, and changes in impulsivity [10], which may only be noted over time as patients uncharacteristically pursue

certain activities (such as sexual or gambling impulses).

1.1.3 DBS Systems

Presently, DBS systems are implanted in patients through an inpatient neurosurgical procedure and consist of several essential components: an implantable pulse generator (IPG) that is implanted in the upper chest area below the collar bone on the ipsilateral side of the brain to be targeted, a thin wire that is routed from the IPG up the neck and head to penetrate the skull, and an electrode lead that penetrates the brain and is located adjacent to the targeted brain structure after implantation. When required, patients may have separate DBS systems implanted on both sides, known as bilateral DBS, to control motor symptoms on both sides of their body.

Medtronic's current electrode lead design consists of four spatially separated electrode contacts that serve as the source of stimulation. Electrode contacts are circumferentially placed at the end of the lead and thus produce omnidirectional fields that extend radially outwards. Due to typical electrode placement, much of the omnidirectional electrical fields produced during DBS are non-essential towards therapy. Additionally, as omnidirectional electric fields only allow creation of relatively non-specific spatial stimulation of tissue, it can be challenging to find stimulation configurations that excite only targeted neural tissues while avoiding nearby tracts that can produce side effects. Therefore, next generation electrode lead design consists of segmented leads that allow for directional current steering [11], a prospect that suggests greater therapeutic potential but also a much greater number of possible stimulation configurations and parameters for consideration.

Implanted DBS systems are coupled with external systems to allow modification of electrical stimulation parameters to adjust and optimize therapy for patients. Medtronic's Nexus-D is an USB adapter for their Activa IPG series DBS systems that allows for software control over various stimulation parameters, albeit in a tightly controlled manner. This dissertation will make extensive use of Nexus-D and Activa IPG functionality to demonstrate real-time control of DBS parameters to automate the process of therapeutic stimulation parameter

selection.

An additional sensing component may be added to next generation DBS systems, and currently some patients enrolled in FDA-approved research studies have this extra component implanted. The Activa PC+S adds to the system an electrocorticography (ECoG) strip consisting of four independent channels. The cortical strip can sense local field potentials (LFPs) and either record data on-board a memory unit embedded in the IPG at a maximum sampling rate of 800 Hz, or stream data via Nexus-D at a maximum sampling rate of 422 Hz.

1.2 Movement Disorders

1.2.1 Parkinson's Disease

Parkinson's disease (PD) is a progressive neurodegenerative disorder that typically manifests as a host of motor impairments in afflicted patients that may also be accompanied by cognitive deficits and autonomic dysfunction, especially as the disease progresses. Development of PD has been attributed to both genetic and environmental factors, with head trauma and pesticide exposure increasing likelihood of the disease. PD is the second most common neurodegenerative disorder (after Alzheimer's disease) with an estimated 60,000 new cases in the U.S. per year [12].

The cause of PD is dopaminergic cell death in the substantia nigra pars compacta (SNpc), which leads to the decreased striatal inhibition to the cortico-basal-ganglia network that is hypothesized to cause the motor symptoms associated with PD [13]. As PD has no cure, all treatments currently available are palliative and serve merely to improve quality of life of the patients. Typically, PD patients are treated first with the pharmaceutical Levadopa, which effectively increases dopamine concentrations in the brain in order to offset the dopamine-deficient SNpc [14]. However, for many PD patients, treatment with Levadopa alone is often unable to manage the worsening symptoms, at which point neurosurgery for implantation of a DBS is recommended.

There are four cardinal motor symptoms associated with PD: tremor, rigidity, bradykinesia, and postural instability (or freezing of gait). Typically, Parkinsonian tremor is a type of rest tremor that occurs when the affected limb is at rest. PD patients may also exhibit postural tremor and kinetic tremor to varying degrees, the former arising when one is trying to maintain limb posture in a certain position, as when reaching out to shake someones hand, and the latter being present when performing a visually-guided movement such as eating or writing. Rigidity and bradykinesia describe slowness of movement and difficulty performing repetitive movements. Postural instability and freezing of gait is often more difficult to characterize as symptomatic episodes are generally more intermittent and context-dependent (walking indoors or outdoors). Neurologists assess PD symptom severity using the Unified Parkinson's Disease Rating Scale (UPDRS) [15].

There are several potential surgical targets for DBS intervention in PD patients [16]. A common target is the subthalamic nucleus (STN) as DBS at this site has been shown to treat the widest array of motor symptoms presented in PD, and, even if a patient exhibits only a subset of the previously described symptoms, they may present with others as the disease progresses. Another target for DBS is the ventral intermediate nucleus (VIM) of the thalamus, which has demonstrated especially effective tremor suppression across several diseases. Finally, the globus pallidus internus (GPi) is sometimes used as a DBS target when speech or cognitive symptoms are prominent [16].

1.2.2 Essential Tremor

The other major neurological disorder with tremor as a defining feature is known as essential tremor (ET). The most common movement disorder, ET affects more than 5 million Americans [17] and has an estimated incidence of 13% in those over 60 years of age [18]. Like PD, ET is thought to have both a genetic and environmental basis. ET was long thought to solely have a familial pattern of inheritance, though recent studies have suggested that consumption of alkaloids or lead may indeed be a risk factor for developing the disease [19].

In contrast to PD, wherein rest tremor, postural tremor, and kinetic tremor may all

be present and debilitating, ET is generally marked by postural and kinetic tremor. The neurophysiological mechanism of ET is thought to involve cerebellar degradation [19], which is perhaps not surprising given the results of well-known cerebellar lesioning studies and their visual similarity to kinetic tremor in which one has difficulty maintaining an endpoint during a visually-guided movement. Additionally, there is some evidence of cognitive decline in ET patients, possibly owing to its link to Lewy Body disease, which is also a feature of PD [19].

For many ET patients the symptoms of the disease are mild and they can proceed untreated without much impact on their daily life. For those whose symptoms cannot be ignored or managed due to severity, the first course of treatment is usually the drug propranolol [20]. While successful in the near term (two-thirds of patients have tremor reduced by 50%), treatment with propranolol is ineffective for 75% of patients after two years. Treatment with DBS is recommended for ET patients whose symptoms are severe and who have run their course of effectiveness with pharmaceuticals like propranolol. The target for DBS in ET patients is the VIM, and stimulation at this deep brain structure has shown to reduce tremor by 75-100% in between 70-90% of patients.

1.3 DBS Programming, Economics, and Optimization

Having introduced DBS and its use in treating symptoms of PD and ET, it is now prudent to motivate the contents of this dissertation via a foray into the economics of prolonged treatment and monitoring required for this dynamic, technologically advanced therapy. Surgical implantation is only the first step in achieving chronic DBS control of symptoms, as once the healing process from surgery is complete patients enter a phase of therapy in which the optimal electrical stimulation parameters are systematically selected, a process known as *programming*.

DBS programming is a highly patient-specific process and depends on a number of critical factors: the relative location of electrode leads to targeted deep brain structures, the relative location of electrode leads to tracts which may cause side effects, electrode impedance, targeted symptom(s), disease progression and neurodegeneration, and other factors. Presently,

DBS systems allow for considerable customization of stimulation parameters to target each patient's unique requirements for therapy. Medtronic's 3387/3389 electrode lead models consist of four independent stimulation contacts which can be activated in various configurations (monopolar, bipolar, double monopolar, double bipolar, etc.) to shape the electric field used to activate neural tissue. Together, the stimulation contact configuration, voltage amplitude, and pulsewidth determine the spatial extent of electrical stimulation, or the volume of tissue activated (VTA), during DBS. Clearly, the VTA that includes the targeted brain structure depends on the relative location of the electrode, which varies considerably between patients as surgical procedures are not exactly replicated nor are anatomical locations entirely uniform across patients. By contrast, stimulation frequency affects the temporal neuronal interactions in targeted deep brain structures that lead to aberrant, pathological behavior, such as tremor and bradykinesia. DBS programming thus requires the patient-specific selection of stimulation parameters from thousands of possible permutations.

Currently, successful DBS programming for PD and ET requires the services of expert clinicians who use standardized algorithms [21] to considerably reduce the number of parameters considered for therapy. Clinicians assess patient symptoms using standardized clinical rating scales and also use patient reports of side effects to adjust stimulation parameters to achieve optimal therapy. DBS programming is not an isolated event, however, and patients are generally required to return to clinic many times in order to achieve and maintain satisfactory therapy, especially in the first year after implantation as the neural tissue heals and adapts to electrode implantation. Disease progression and neurodegeneration may warrant further DBS programming updates over time.

The healthcare and societal costs of DBS for PD were examined in a study using claims data from the Department of Veterans Affairs (VA) and Medicare [22]. Patients averaged about 20 visits to the clinic per year, many of those due to programming requirements, and these visits accounted for roughly $130,000 (in 2010 US dollars) in direct healthcare provider costs over the three year post-operative period for each patient. In addition to billable insurance claims the cost of patient travel and time spent attending clinical visits for both

the patient and their caregiver(s) was estimated to be about $35,000, and this cost is borne by the patients themselves and is not typically reimbursable. This issue is compounded by the fact that most DBS clinics are located in large city centers and in large research-oriented university clinics, far removed from the rural areas in which many patients reside.

A growing patient population, increased adoption of DBS as a mainline therapy for PD and ET, and independent increases in the cost of healthcare delivery suggests these expenditures for DBS management could rise considerably over time if methodology is unchanged. As of 2009 there were approximately 5,000 yearly surgical procedures in North America for PD alone [23], and, when coupled with the cost figures presented above, DBS expenditures for PD care could exceed $200 million per year without even factoring in the cost of the device and surgical procedure. This figure could be higher if present day number of implants and cost of therapy data were available.

The preceding anaylses suggest that DBS care for PD and ET could be delivered much more efficiently to improve both patient quality of life and use of healthcare resources. Deficits in DBS programming outcomes are particularly costly and may be attributed to several factors. First, DBS clinicians may be improperly trained or inadequately equipped to contend with selecting an optimal DBS setting for therapy given the multitude of candidate settings. DBS programming has been acknowledged as a particularly difficult task for clinicians, and training in electrophysiological principles may be lacking in typical medical education programs [24]. Therefore one cause of inadequate DBS programming may be a lack of sufficient skill and training. Second, as previously mentioned, patient neurophysiology adapts to the electrode following implantation, causing fluctuations in impedance that affect how DBS parameters excite targeted neural tissue. Additionally, the progressive, degenerative nature of PD and ET suggest that more intense stimulation may be required to achieve satisfactory therapy as disease progresses. Therefore, the dynamic response of neural tissue to DBS implantation and disease progression may require regular DBS parameter updates to maintain acceptable therapy.

These issues illustrate a gulf between the technological capabilities of DBS systems and

their present clinical deployment. Clearly, DBS therapy requires a level of patient symptom monitoring, treatment refinement and adjustment, and large-scale information integration that is beyond the reach of modern healthcare provision. Indeed, the rise of neuromodulation, DBS, and other neurotechnologies may spur a revolution in how healthcare is delivered.

In this dissertation, we propose that DBS treatment and distribution of resources can be optimized through automation of DBS programming and stimulation control. Particularly, we submit a collection of methodologies, algorithms, and experimental results that support a data-driven approach to optimizing the selection of DBS parameters for therapy of symptoms related to PD and ET. The primary hypothesis of this dissertation is that an automated software system can program DBS for PD and ET patients as effectively as expert clinicians.

This data-driven approach to DBS therapy consists of two fundamental components of treatment: *perception* and *decision-making*. Perception is required for assessment of disease state and severity, and this information is primarily derived from wearable and neural sensor data trained against standardized clinical assessments of symptoms provided by movement disorder neurologists. Decision-making, in this context, is a mapping from perception of symptom severity to choices about what DBS setting to select for therapy, how to search for similar DBS settings that may be therapeutically valuable, or how to optimize DBS in real-time in closed-loop DBS applications.

1.4 Dissertation Outline

The contents of this dissertation focus primarily on supporting automated DBS programming and stimulation control technology development for the treatment of PD and ET symptoms. In Chapter 2, we pursue classification of clinical ratings of tremor and bradykinesia using smartwatch data. In Chapter 3, we develop an automated DBS programming software platform and conduct a clinical study comparing its efficacy in selecting optimal DBS settings to that of expert clinicians. In Chapter 4, perception and analysis of symptom severity is extended to investigate neural correlates of effective DBS in essential tremor patients. Chapter 5 expands the decision-making capacity of automated DBS programming software

by developing a "search engine" for stimulation parameters based on electric field models of neural tissue activation. Chapter 6 motivates an approach to model-based closed-loop control of DBS for Parkinsonian tremor through system identification experiments, hybrid systems modeling, and simulation of model predictive control. In Chapter 7 we conclude the dissertation with a discussion on future applications of data-driven DBS optimization, and we discuss some avenues for future research including telemedicine and the future of healthcare delivery in the age of neuromodulation.

Chapter 2

SMARTWATCH CLASSIFICATION OF TREMOR AND BRADYKINESIA CLINICAL RATINGS

This chapter serves as the foundation for the rest of the dissertation. We examine some clinical tests for symptom assessment in Parkinson's disease and essential tremor, particularly for different types of tremor and bradykinesia, and we investigate data-driven methods for quantification and classification of clinical ratings for these tests based on inertial measurement unit data obtained from a smartwatch. The classification of tremor and bradykinesia clinical ratings on a smartwatch platform enables the automated deep brain stimulation programming explored in subsequent chapters, and may also enable future remote monitoring applications in Parkinson's disease and essential tremor patients.

2.1 Background

2.1.1 Clinical Ratings of Tremor and Bradykinesia

Movement disorders are treated and assessed clinically by neurologists who receive extensive and specialized training in order to capably discern the subtleties of abnormal movement features and prescribe personalized treatment regimens. Neurologists make assessments of movement disorder severity through the use of widely used clinical scales, which provide standardized metrics to enable comparison of treatment efficacy and disease progression. In this thesis, we will concentrate on two rating systems developed for Parkinson's disease and essential tremor: the Unified Parkinson's Disease Rating Scale (UPDRS) [15] and The Essential Tremor Rating Assessment Scale (TETRAS) [25]. These rating scales have seen widespread adoption through the international neurological community and were developed through input from a large cohort of movement disorders specialists and thorough clinical

observation.

Both the UPDRS and TETRAS assess various aspects of movement disorder severity through a neurologist's visual observation or patient questionnaire. Some components of movement disorder severity can be observed continuously or on-demand by subjecting a patient to various tests which may provoke symptoms. In PD patients the cardinal symptoms of tremor, bradykinesia, rigidity, and postural instability all have direct UPDRS components which are routinely assessed in clinic by neurologists. Likewise, the various types of tremor experienced by ET patients, including tremor of the hands, head, and legs, can be examined and rated according to various components of the TETRAS test. However, other movement disorder symptoms require query of patients to understand the level of impairment throughout a typical day, such as dyskinesia, which is characterized by abnormal, uncontrollable muscle contractions and may only be present in patients under intermittent or context-dependent conditions. Additional aspects of movement disorder evaluation require a patient to judge its impact on daily living, including interruptions to sleep and bodily functions, and changes in mood, cognition, and perception.

In this chapter, we will examine an experimental platform and methods for classification and quantification of clinical UPRDS/TETRAS ratings for movement disorder severity for the following battery of tests: rest tremor, postural tremor, kinetic tremor, and pronation-supination of the hands, which is referred to subsequently as wrist turning. The first three are standard types of tremor that may affect PD and ET patients; typically PD patients exhibit rest tremor or postural tremor, while ET patients exhibit postural tremor or kinetic tremor. Wrist turning is used to assess bradykinesia severity, as patients with bradykinesia will have a difficult time performing the rapid, repetitive movement. All of these tests and associated symptoms can be observed continuously in PD and ET patients, and in this chapter we aim to quantify and classify their clinical severity using a smartwatch equipped with inertial measurement unit (IMU) on the affected hand(s). Although tremor can affect additional parts of the body, hand tremor is generally the most important to treat as it can interrupt any number of activities of daily living, including eating, writing, typing, using a

smartphone, and more.

Table 2.1: UPDRS for Rest, Postural, Kinetic Tremor

Rating	Tremor Amplitude
0	No tremor
1	Less than 1 cm (slight)
2	Between 1 cm and 3 cm (mild)
3	Between 3 cm and 10 cm (moderate)
4	Greater than 10 cm (severe)

Table 2.2: UPDRS for Pronation-Supination (Wrist Turning)

Rating	Rhythm (Interruptions)	Speed	Amplitude (Decrement)
0	No interruptions	Normal speed	No decrement
1	1-2	Slight slowing	Near end of sequence
2	3-5	Mild slowing	Midway in sequence
3	5+	Moderate slowing	After first sequence
4	Cannot or can only barely perform task		

Each UPDRS/TETRAS test of interest has specialized instructions for patient evaluation: *rest tremor*, or parkinsonian tremor, is performed with the patient seated comfortably and their tested hand/arm supported against gravity on an armrest; *postural tremor* is performed by having the patient extend their arm directly in front of their chest; *kinetic tremor*, or action tremor, is performed by having the patient perform a visually-guided movement in which they alternately touch their tested hand's forefinger to their own nose and then to a clinician's forefinger which is approximately an arm's length away; and *wrist turning* is performed by having the patient hold their arm in front of their chest and then alternately orienting their palm face-up and face-down as quickly as possible. Table 3.2.4 lists the possible UPDRS ratings for each tremor test, indicating that these tests are rated based on visual assessment of tremor amplitude by neurologists, and Table 2.2 lists the different UPDRS ratings and

associated components for wrist turning assessment, showing that neurologists must rate this test based on different factors. With multiple components in the evaluation of wrist turning, neurologists assign the rating based on the most severe component observed, e.g. if a patient has normal speed ("0") and no decrement in amplitude ("0"), but has 3-5 interruptions ("2"), then they will assign a "2" rating.

2.1.2 Data-Driven Ratings for Tremor and Bradykinesia

The most notable limitation of UPDRS/TETRAS-based assessments of movement disorder severity in PD and ET patients is the requirement of a neurologist's time and presence for evaluation. Neurologists, like all physicians, have limited time to devote to any one patient for evaluation, and they also necessarily remain in the clinic, removed from most of a patient's life and removed from the daily fluctuations in their impairment. Despite this, movement disorder symptoms and their severity in PD and ET may change over time, both due to these diseases being progressive neurodegenerative disorders and due to the dynamic nature of different types of tremor. And, as we will explore in subsequent chapters, DBS is a dynamic medical technology, the parameters of which can potentially be adapted as patient symptoms change in severity to maintain a consistent, optimized level of therapy. Another limitation of the clinical UPDRS/TETRAS assessments of movement disorder severity is the relatively coarse, integer-based scale used to distinguish different levels of severity and the subjective nature of having individual neurologists rate severity based on visual observation. These factors necessitate a more continuous and precise method for assessment of movement disorder severity.

Several data-driven approaches for quantifying various aspects of PD and ET symptoms have been studied and pursued in the literature. Early approaches to quantifying tremor included the use of laser systems [26], which can provide very precise measurements of displacement amplitude and thus tremor severity (see Table 1). However, the last decade has seen the rise of Internet of Things (IoT) and associated ubiquitous and wearable computing technology, which is more appropriate for ambulatory monitoring than laser or video sys-

tems. The most popular approaches have been based on the use of miniaturized, wearable sensors called inertial measurement units (IMUs). Although IMUs cannot provide reliable estimates of displacement amplitude due to drift errors in the accelerometer and gyroscopic sensors, several relevant time-domain and frequency-domain features have been correlated with UPDRS/TETRAS assessments of severity.

One early study in wearable inertial sensing attempted to identify symptoms of tremor and bradykinesia from data in a non-controlled setting where patients are simply performing daily activities with a video recording used to provide UPDRS ratings of symptoms [27]. While this study produced some valuable data features that have been subsequently validated in other studies, the problem of quantifying movement disorder symptoms from IMU data alone without context can limit its actual application. Particularly with bradykinesia, severe symptoms can be indistinguishable from a lack of movement such as when a patient is resting or sleeping, so it is important to provide the proper context by having patients explicitly perform testing items from the UPDRS or TETRAS. Thus, the remainder of the studies addressed will be focused on simultaneous IMU data recording and UPDRS/TETRAS item testing, as opposed to "free-monitoring" approaches as in [27].

One of the well-known platforms for clinical tremor severity quantification is the Kinesia system, which features a wrist-worn and finger-worn IMU [28]. In a study with PD patients they found that the natural logarithm of the peak power in the 3 to 7 Hz range (tremor band) correlated highly with UPDRS scores for rest tremor and postural tremor. For kinetic tremor they found that the root mean square (RMS) value across all gyroscope and accelerometer channels achieved a moderate correlation with UPDRS scores. However, this study was limited by low sample size, especially for kinetic tremor, and, although these metrics may correlate highly with UPDRS scores, this type of analysis says little about how accurately such empirical models can actually predict UPDRS scores from raw IMU data. Additionally, although patients tested indicated they would find the device useful for testing at home (94% positive of patients polled), substantially fewer felt they would be comfortable wearing the device in public (55% positive of patients polled), indicating that perhaps the device was

too burdensome or noticeable for continuous monitoring outside the clinic. This limitation indicates the importance of developing monitoring solutions for patients that will be widely accepted.

Bradykinesia has been more difficult to quantify than tremor as the corresponding UPDRS tests (finger tapping, wrist turning, hand movements) require complex, repeated movements that do not evoke quite the same gross movement features as tremor. Many studies have sought to quantify wrist turning and finger tapping, with some opting for a simplified approach using RMS across the appropriate gyroscope channel (i.e. along the axis of movement) to quantify severity and predict UPDRS ratings [29][30]. Although this single-metric approach may work well to describe selective patient variation in bradykinesia ratings, it is not adequate for capturing the multi-faceted evaluation performed by UPDRS raters, which from Table 1 takes movement rhythm, speed, and amplitude into account. In order to predict UPDRS ratings based on these multiple components, more comprehensive studies have taken the approach of deriving several features from IMU data in order to classify and predict different bradykinesia ratings [31][32][33]. These studies appear to be more robust for detecting the spectrum of bradykinesia features that are manifested into performance of motor tasks across a wide swath of PD patients.

2.1.3 Mobile, Smartphone, and Smartwatch Platforms for Remote Monitoring

While the IoT revolution spurred the approach of using IMU sensing platforms for quantification and prediction of movement disorder severity, the next step in this evolution is to make use of widely available, ubiquitous computing capabilities present in mobile, smartphone, and smartwatch technology. These devices have high quality IMUs embedded in their hardware almost without exception, and the prospect of performing remote monitoring of movement disorder symptoms using devices that are already owned, or very likely to be accepted, by patients is attractive. Particularly with regards to the lack of complete acceptance of custom IMU platforms for every day use in monitoring [28], the use of smartphones and smartwatches to monitor symptoms should see greater acceptance owing to their established

status among the general population. And the ability to develop custom applications that can be widely disseminated and downloaded through app stores by patients adds further heft to the advantages of using mobile smartphone and smartwatch technology for monitoring.

There have been many studies investigating the capabilities of smartphone and smartwatch platforms and their ability to collect and analyze data relevant to UPDRS items. One notable feature of smartphones and smartwatches is the embedded microphone for recording audio, which can potentially provide speech-related assessments, an important aspect of UPDRS evaluation and understanding PD severity [34][35]. Other studies have focused on capture and analysis of IMU signals related to tremor [36], although apparently not with respect to UPDRS/TETRAS clinical scales. Although large-scale and popular applications have yet to be developed for monitoring PD and ET symptoms, these early studies show the promise of an integrated platform that can go beyond the capture and analysis of motion data and scrutinize other aspects of disease, such as speech and sleep.

2.2 Methods

2.2.1 Experiment Description

This experiment was performed at the University of California, San Francisco with approval from the Institutional Review Board (IRB). We recruited 10 patients (6 with PD, 4 with ET) with age 66.2 $\pm$ 8.2 years who had implanted DBS and were at least 6 months post-implantation. These patients were enrolled in the automated DBS programming study that is described in greater detail in Chapter 3. For each patient we tested several DBS settings (typically 15-30), both effective and ineffective for therapy, which allowed us to observe a range of symptom severity and corresponding UPDRS/TETRAS scores. For each DBS setting we tested a subset of tremor and bradykinesia tests, depending on the patient's exhibited symptoms; typically for PD patients we tested rest tremor, postural tremor, and wrist turning, while for ET patients we tested postural tremor and kinetic tremor. Patients were prompted to perform each test for 10 seconds, while an attending movement disorders

neurologist, who was blinded to the DBS setting being tested, observed the test and provided an appropriate UPDRS or TETRAS score.

2.2.2 Data Recording

While each test was being performed, IMU data from an LG G Smartwatch was streamed over Bluetooth at 100 Hz to a custom Windows application running on a PC laptop. Accelerometer and gyroscope data was collected and logged across all three channels (x, y, z) for each test. Table 2.2.2 shows the number of tests that were recorded at each MDS-UPDRS rating for the 10 patients who participated in the experiment.

Table 2.3: Number of Tremor and Bradykinesia Tests

MDS-UPDRS Test	**Number of Tests**					
	0	**1**	**2**	**3**	**4**	**Total**
Rest Tremor	127	53	40	17	0	237
Postural Tremor	98	123	20	12	43	296
Kinetic Tremor	33	21	43	3	34	134
Wrist Turning	15	45	43	14	15	132

It is instructive to look at the raw IMU data for these various tests and ratings to understand, qualitatively, how difficult it may be to distinguish between different levels of neurologist-assessed severity. Here, we will just present gyroscope data for tests of interest; accelerometer data, while useful for classification, is largely complementary to information present in gyroscope data with the additional effect of gravity impacting the linear acceleration recordings.

Figure 2.1 shows representative gyroscope plots from two rest tremor trials of differing severity. The top plot shows a rest tremor trial with UPDRS = 0, indicating no tremor, and the plots showing very low amplitude rotational velocities confirm the lack of movement. On the contrary, the bottom plot shows a rest tremor trial with UPDRS = 3, indicating "moderate tremor", and the plots show oscillatory angular velocity traces with amplitude

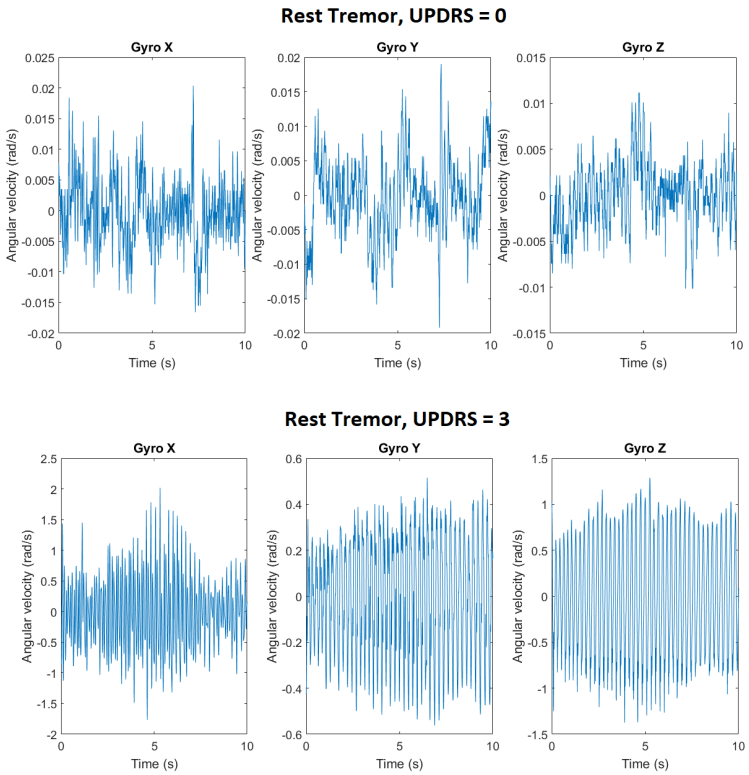

Figure 2.1: Top: gyroscope plots for a rest tremor test a neurologist rated "0". Bottom: gyroscope plots for a rest tremor test a neurologist rated "3"

approximately one hundred times greater than that of the top plot. Postural tremor plots appear quite similar to rest tremor plots, owing to the fact that in each patients are trying to maintain a stationary pose, so example plots for these tests will be omitted.

Figure 2.2 shows three different kinetic tremor tests of increasing severity as rated by the TETRAS scale. The top plot shows a trial rated "0" and clearly shows the oscillatory, low-frequency motion of the visually-guided movement performed for kinetic tremor testing. The middle plot contains the same basic structure but shows, most clearly on the "Gyro X" plot, that there is some oscillatory tremor, which typically occurs as the movement reaches an endpoint (either the clinician's finger or the patient's own nose), resulting in a rating of "2",. In the bottom plot the movement is almost entirely obscured by a strong tremor signal,

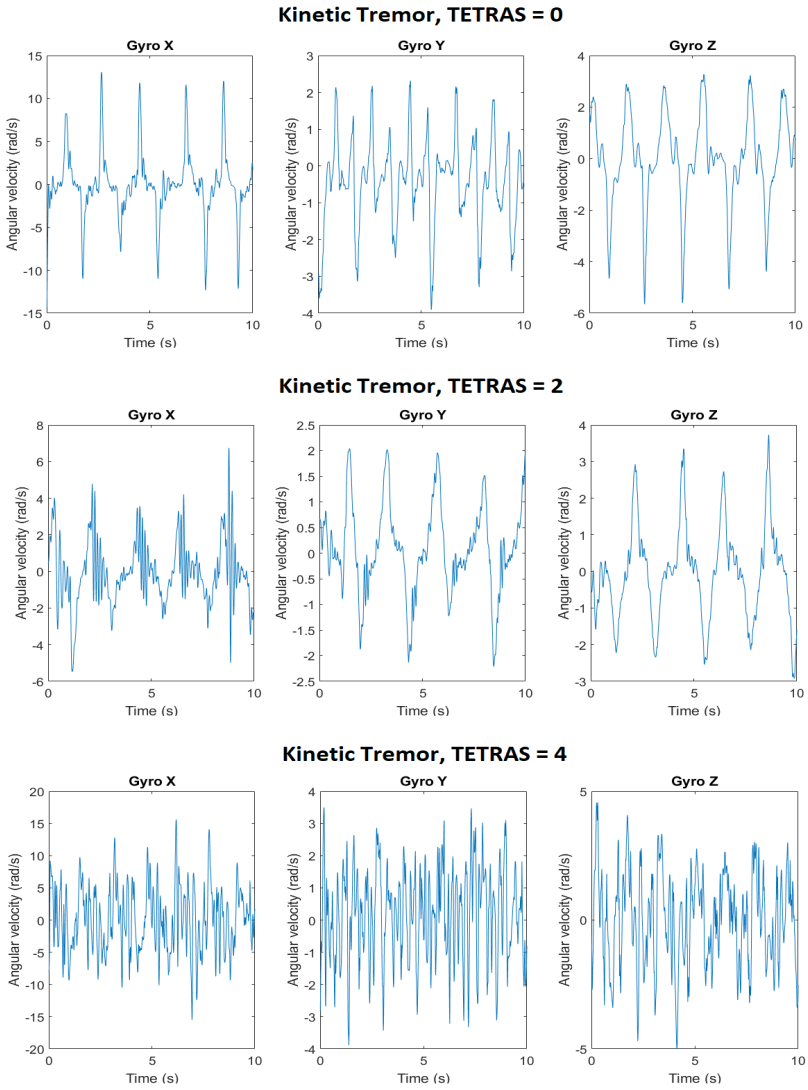

Figure 2.2: A collection of kinetic tremor tests with different TETRAS ratings (see text for details).

which resulted in a rating of "4" indicating severe tremor.

Figure 2.3 shows a sample of wrist turning tests and illustrates the challenge in classifying these signals to their corresponding UPDRS-assessed severity. Each test is plotted only in terms of the gyroscope's x-channel, as this is the axis along which the arm and hand rotate

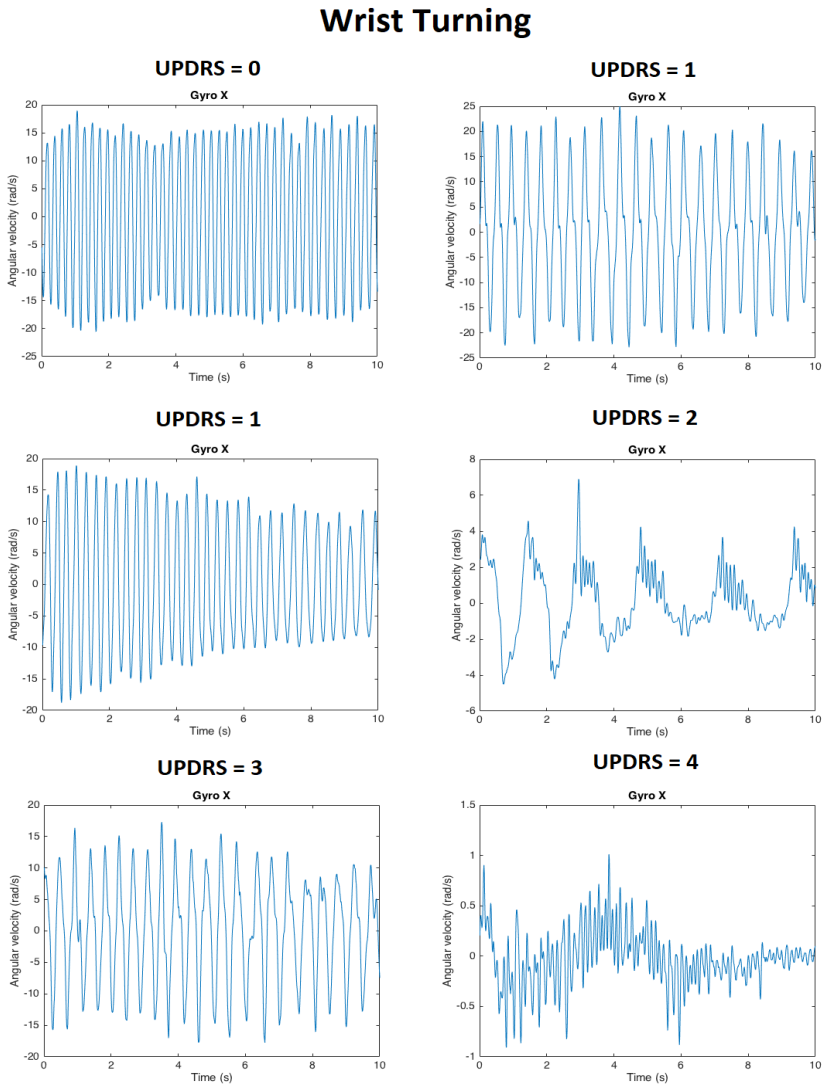

Figure 2.3: A collection of wrist turning tests with different UPDRS ratings (see text for details).

during the wrist turning test. The top left plot shows a trial rated "0", showing regular, repetitive oscillatory motion. The top right plot shows a trial rated "1"; the magnitude of wrist turning speed was not significantly different from the trial rated "0", however between 8 and 10 seconds there appears to be some irregularity - perhaps a few interruptions - in the

movement. The middle left plot shows another trial rated "1", and this data shows a marked decrement in movement amplitude as the trial progresses. The middle right plot shows a trial rated "2", which may have been due to a reduction in amplitude halfway through the trial. Note also that this trial featured much lower amplitude movements than trials rated "0", "1", or even "3"; this is due to the specific patient's overall slowness of movement, and illustrates the hazard of trying to use a single feature, such as RMS, to classify ratings. The bottom left plot shows a trial rated "3", which is possibly due to several irregularities (i.e. interruptions) in the data. And finally the bottom right plot shows a trial rated "4", and this data clearly shows an almost complete lack of movement as the patient was unable to perform the test due to severe bradykinesia.

2.2.3 Signal Processing & Classification

Signal Processing

Tremor test data was first filtered to remove any low amplitude movement artifacts using a type II Chebyshev band pass filter (2-12 Hz). Signal power in the tremor band (4-12 Hz) was estimated by computing a short-time fourier transform with a 1 second Hanning window in 200 ms intervals for each 10 second trial. A tremor band power magnitude estimate for each sensor (accelerometer, gyroscope) was computed as the 2-norm across every channel (x, y, z). Wrist turning test data was not filtered, as the movement could occur at different frequencies and was mostly analyzed using time domain features from raw data on the x-channel of the gyroscope.

Classification Features

Several classification algorithms studied in this chapter require data features as input to fit a model for classification. Features are typically derived from data based on intuition of what quantitative properties may be used to distinguish different classifications. For tremor tests selection of features is fairly straightforward and has been studied in the past: various

statistics of tremor band power from the accelerometers and gyroscopes are used, as are measures of RMS signal level after filtering out voluntary movement artifacts. Table 2.4 lists the features used for classification of UPDRS/TETRAS ratings for rest, postural, and kinetic tremor tests.

Table 2.4: Features for Rest, Postural, Kinetic Tremor Classification

Data Feature	**Description**
$gyro\_med\_tremorBP$	Median tremor band power magnitude (4-12 Hz) of gyroscope channels
$gyro\_avg\_tremorBP$	Average tremor band power magnitude (4-12 Hz) of gyroscope channels
$acc\_med\_tremorBP$	Median tremor band power magnitude (4-12 Hz) of accelerometer channels
$acc\_avg\_tremorBP$	Average tremor band power magnitude (4-12 Hz) of accelerometer channels
$gyro\_RMS$	RMS of gyroscope channels
$gyro\_dRMS$	RMS of "rate of change" of gyroscope channels
acc_RMS	RMS of accelerometer channels
acc_dRMS	RMS of "rate of change" of accelerometer channels

Representative wrist turning features are more elusive to obtain, as there are a range of behaviors that could lead to various ratings of severity, which Figure 2.3 illustrates. Table 2.2, offering the basis of wrist turning ratings, can aid in the pursuit of data features that capture the variation between severity ratings. Speed and amplitude decrement can be estimated using RMS measures, specifically ones that window data at various points in the test to detect a decline in amplitude. Rhythm, or interruptions, is more difficult to assess; the ideal wrist turning test is performed at a single, consistent frequency and amplitude, thus approximating a sinusoidal trace. Therefore, some features for gauging wrist turning rhythm include the autocorrelation function, which can be used to assess the periodicity of a signal, and measure of interpeak distance and deviation of the gyrosocope data, which can be used to measure the uniformity of repetition for the test. The candidate data features for

the wrist turning test are listed in Table 2.5.

Table 2.5: Features for Wrist Turning

Data Feature	**Description**	**UPDRS Feature**
Gx_RMS	RMS of gyroscope x-channel	Speed/Amplitude
min_Gx_RMS	Minimum RMS of gyroscope x-channel detected using sliding 1 s window	Speed/Amplitude
auto_Gx	Maximum value of autocorrelation function detected after 10 shifts	Rhythm
peak_interval_dev	Standard deviation of time between successive peaks for gyroscope x-channel	Rhythm

Standard Classification Algorithms

We first consider three standard classifiers for the UPDRS/TETRAS tests: linear discriminant analysis (LDA), multinomial logistic regression (MLR), and the support vector machine (SVM). These algorithms have been widely used in machine learning and statistics applications, and here we explore their distinct advantages in accurately predicting UPDRS/TETRAS ratings from IMU data.

LDA assumes gaussian distributions for the features and that the covariance of features for each class is the same. However, both these assumptions may be challenged when attempting to fit an LDA model for UPDRS/TETRAS ratings of tremor and bradykinesia. For instance, given the different tremor amplitude observations corresponding to severity ratings in Table 3.2.4, the covariance of tremor band power and other features for a "2" (tremor amplitude between 1 and 3 cm) and a "3" (tremor amplitude between 3 and 10 cm) may not be equivalent. Furthermore, the assumption of Gaussianity for each class and feature may fail, especially with the wrist turning test. Table 2.2 and Figure 2.3 show that wrist turning depends on several features from the data, and that the expectation of unimodal distributions for each feature and class may be unacceptable.

MLR departs from the LDA algorithm in several notable aspects. First, LDA makes use of marginal probability density information while MLR does not. This, in principle, can boost LDA performance in describing available data, however, as a result, MLR performance may be more robust for accurately describing new data. MLR also makes use of conditional probability density functions for prediction, and has more flexibility beyond just representing data generated by Gaussian processes, extending probabilistic representations for classification to the entirety of the exponential family, which includes Bernoulli, Poisson, and many others. MLR models may be harder to train because they require iterative optimization procedures, however online implementations of MLR and LDA do not vary much in complexity.

Another advantage of MLR models is their ability to capture *ordinal*, or ordered, classifications of data. In the case of the UPDRS/TETRAS tests, there is a natural ordering of ratings, with "0" indicating no symptoms and each subsequent higher rating indicating increasing severity. An ordinal MLR model uses a proportional log odds model to yield the odds that a set of data features belongs a rating that is at most some nominal value. For instance, a proportional log odds model will compute, for each set of data features, the log odds that the set is classified as a "0", a "0" or "1", a "0" "1" or "2", a "0" "1" "2" or "3", and a "0" "1" "2" "3" or "4". The proportional log odds model can be rearranged such that model supplies the probability of data feature membership to each rating class.

SVM is a method for classification which optimally fits a hyperplane in n-dimensional feature space to maximally separate the training data. SVM is attractive due to the underlying theory and considerable performance analysis devoted to its use; it may also provide models achieving comparable performance with fewer required parameters for prediction. However, some analyses have concluded that the SVM may have reduced classification performance for non-Gaussian distributions compared with MLR models [37].

These classifiers (LDA, MLR, and SVM) will be applied to the tremor and bradykinesia data to assess their ability to accurately predict clinical ratings of severity for PD and ET patients.

Convolutional Neural Networks

A more recent approach to classification problems has been the use of convolutional neural networks (CNNs). While "conventional" neural networks have been used for classification and other problems in artificial intelligence for several decades, recent studies in image processing have demonstrated that neural networks built on cascaded layers of processing units, or *deep* neural networks, can achieve high classification performance on a number of benchmark problems and datasets [38]. Though originally applied to image processing problems, CNNs have been shown to achieve superior classification performance in applications such as human activity recognition (HAR) where the objective is to automatically infer a person's activity (e.g. walking, sitting, standing, running, walking down stairs, etc.) from body-worn IMUs [39]. These studies suggest that movement disorder feature analysis and classification may also benefit from the use of CNNs.

CNNs differ from typical classification approaches in that feature extraction is automated and performed in sequence with model fitting for prediction. Unlike the "standard classification algorithms", CNNs do not require specification and computation of features, such as tremor band power or RMS levels. Rather, raw time series data is input to the CNN and the computing power of cascaded processing layers and large numbers of processing units is leveraged to extract salient features from the data. In this sense, CNNs allow classification to be potentially performed without requiring domain-specific knowledge of how the data was created and collected. However, the potential power of this approach requires in-depth knowledge about how the CNN architecture is connected and how to set relevant hyperparameters in order to achieve the best results.

CNNs have a modular architecture that is composed of several fundamental units, the arrangement and sequencing of which can be customized for the problem at hand. Figure 2.4 shows the architecture employed for classification of rest tremor, postural tremor, kinetic tremor, and wrist turning. The *input layer* (INPUT) consists of the six channels of raw IMU data (three channels each of accelerometer and gyroscope), each of which contain 1000 data

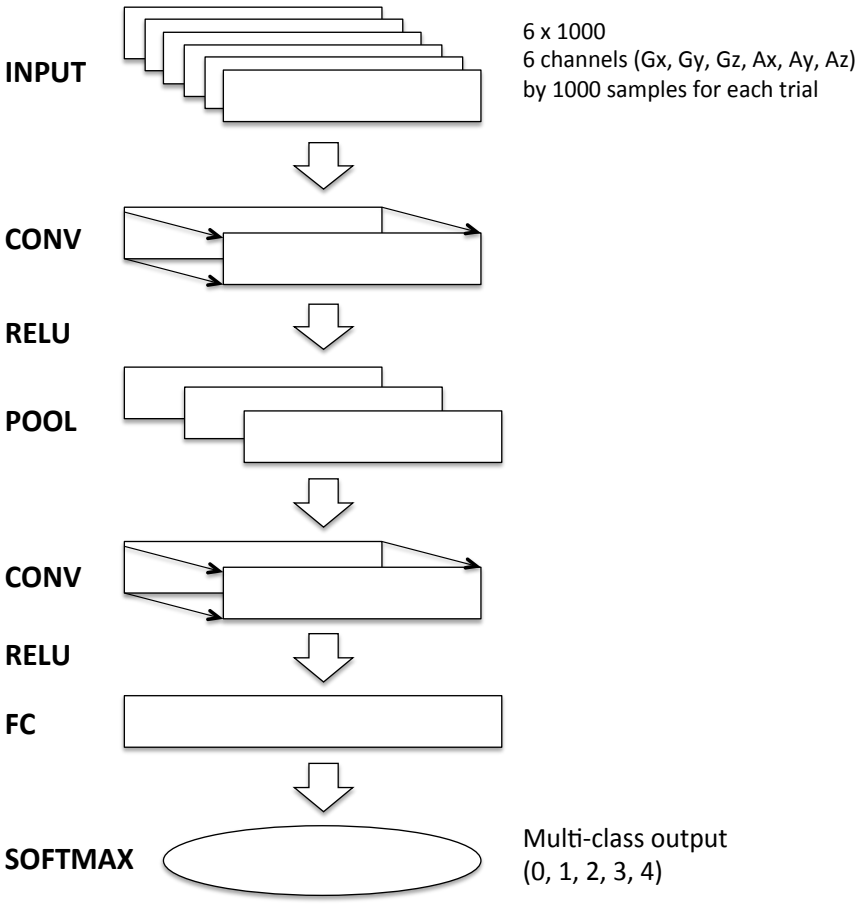

Figure 2.4: Convolutional neural network model for classifying clinical ratings of tremor and bradykinesia based on raw IMU input.

points for the ten seconds of 100 Hz sampled data recorded for each trial.

The next layer is a *convolutional layer* (CONV) in which one-dimensional convolution is applied to each input channel. The convolutional layer is defined by three hyperparameters: width, stride and depth. Width determines the size of the convolutional filter and consequently how many consecutive input samples are analyzed at once. Stride determines the amount of time samples by which the convolutional filter shifts to produce each output element of the convolutional layer, and consequently, the size of the output layer. Depth

determines the number of stacked convolutional filters in the layer, each of which may learn different parameters to detect different features from the input data.

Following the CONV layer is a *rectified linear unit layer* (RELU) that applies a nonlinear activation function to each output of the CONV layer. In this application a positive thresholding function is used for the RELU layer, outputting the element if it is positive and 0 if it is not. After the RELU layer there is a *max-pooling layer* (POOL) which performs a downsampling operation by taking the maximum element within a specified window. Next, another CONV layer is applied with smaller width and depth to account for the smaller input shape following the POOL layer.

The two seperate CONV layers allow the CNN to collate and assess potentially salient data features at different scales. The first CONV layer operates on raw data samples and thus detects features such as local oscillations. The second CONV layer operates on groupings of data, which may pertain to successions or inconsistencies of tremor oscillations or wrist turns. It is this ability to automatically perform data analysis at different time scales that can result in high CNN classification performance.

The last two layers in the CNN are the *fully-connected layer* (FC) and the *softmax layer* (SOFT). The FC layer is a typical neural network layer where neuron weights are learned and mapped onto the space of categorical variables. In this layer all channels, which have been until now processed in parallel, are mapped to provide a probability of membership to any of the provided classifications. Finally, the SOFT layer takes the maximum probability of this layer and assigns the predicted classification for the input sequence.

2.3 Results

The classification performance for each of the classifiers (LDA, MLR, SVM, and CNN) is listed in Table 2.3. Performance for each classifier is assessed by its *Accuracy* (percentage of classifications correctly predicted out of total) and *F-Score* which is a measure of precision and recall. The results in Table 2.3 indicates that the CNN models outperformed the LDA, MLR, and SVM models for each test. The classification results for LDA, MLR, and SVM

models were mostly interchangeable, and no significant differences can be reported between them.

Table 2.6: Tremor and Bradykinesia Classification Performance

Classifier	**Rest Tremor**		**Postural Tremor**		**Kinetic Tremor**		**Wrist Turning**	
	Accuracy	F-Score	Accuracy	F-Score	Accuracy	F-Score	Accuracy	F-Score
LDA	75.0%	75.0%	77.2%	77.0%	75.6%	74.9%	57.5%	56.4%
MLR	77.3%	77.2%	76.8%	76.4%	76.2%	74.7%	60.1%	57.1%
SVM	78.1%	78.2%	79.1%	78.9%	76.4%	73.0%	59.3%	56.5%
CNN	**79.1%**	**77.8%**	**80.5%**	**80.1%**	**87.5%**	**88.3%**	**86.5%**	**85.6%**

In order to obtain a higher resolution rating for each test, we summed over the mixed probability that each test belonged to each rating classification to obtain a continuous rating on the interval 0 to 4 rather than the coarse, integer-based MDS-UPDRS. Such a rating may provide a more accurate discrimination of tremor and bradykinesia tests while also remaining interpretable to clinicians. Additionally, mixed probabilities embed a measure of classification uncertainty into the ratings, whereas softmax operations can remove some of the information regarding uncertainty of rating and prediction.

The IMU-predicted ratings for MLR and CNN models of rest tremor are shown in Figure 2.5. For each collection of MDS-UPDRS ratings provided by a movement disorders neurologist, the distribution of IMU-predicted ratings based on MLR and CNN models is plotted. Wilcoxon rank-sum tests were used to identify significant differences between successive MDS-UPDRS distributions, and the level of significance is indicated by stars on the plots ($* = p < 0.05, ** = p < 0.01, *** = p < 0.001$). Figure 2.5 shows significant differences (p < 0.001) between each successive distribution, and also shows that the CNN IMU-predicted ratings generally have less variation than the MLR IMU-predicted ratings.

The IMU-predicted ratings for MLR and CNN models of postural tremor are shown in Figure 2.6. Each successive MDS-UPDRS rating distribution shows significant differences (p < 0.001), and again the CNN IMU-predicted ratings have less variation than the MLR

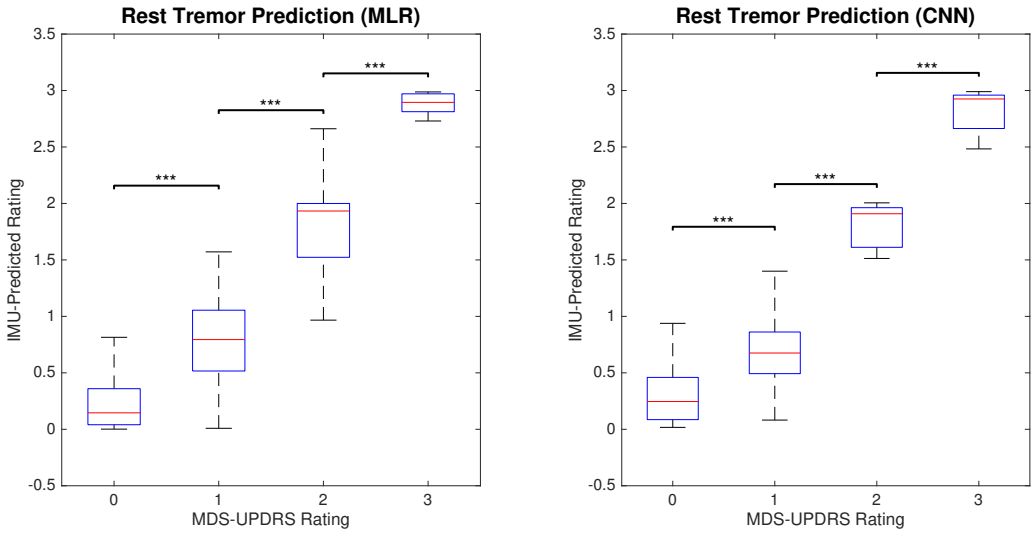

Figure 2.5: IMU-predicted ratings for MLR and CNN models of rest tremor.

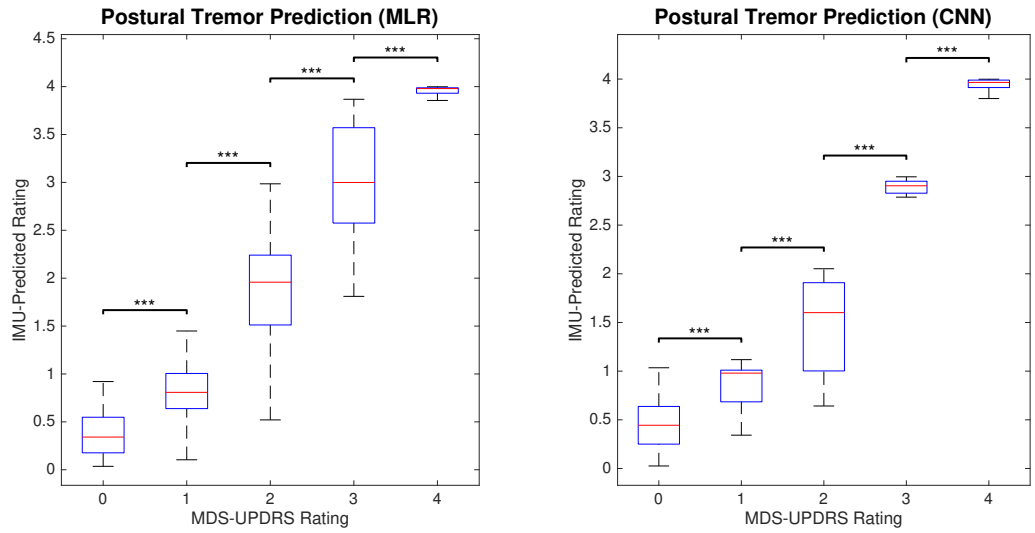

Figure 2.6: IMU-predicted ratings for MLR and CNN models of postural tremor.

IMU-predicted ratings.

The IMU-predicted ratings for MLR and CNN models of kinetic tremor are shown in Figure 2.7. Each plot shows highly significant differences between ”0” and ”1” and ”1” and

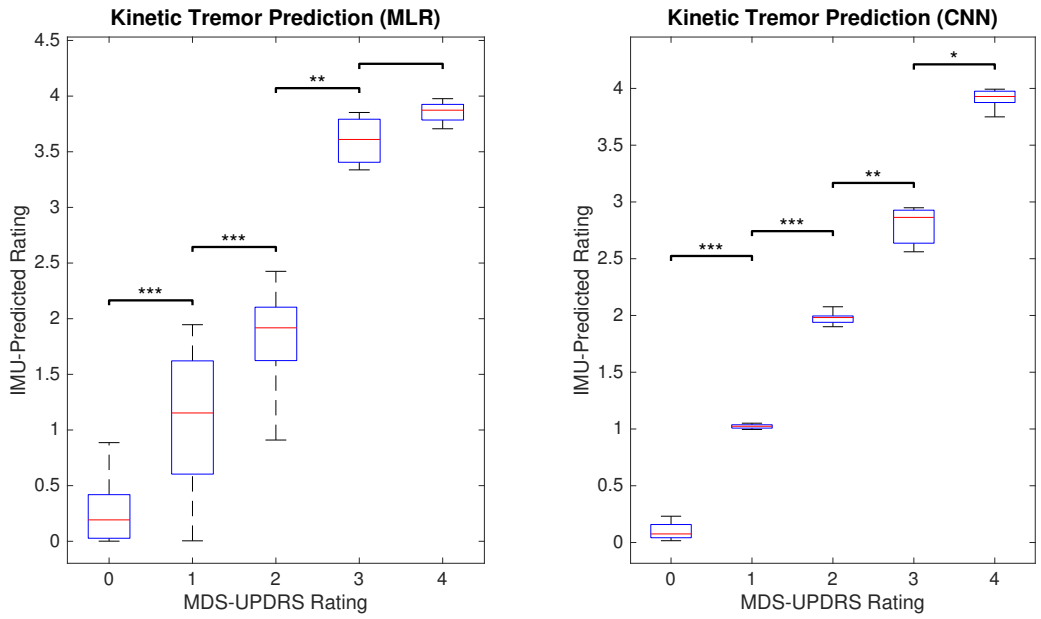

Figure 2.7: IMU-predicted ratings for MLR and CNN models of kinetic tremor.

"2" MDS-UPDRS distributions ($p < 0.001$), and a less significant difference between "2" and "3" MDS-UPDRS distributions ($p < 0.01$), likely due to a small sample size for "3" ratings. Additionally, there is no significant difference between "3" and "4" ratings for MLR model, while there is a significant difference for the ratings in the CNN model ($p < 0.01$). The CNN model distributions generally have less variation than the MLR ratings, aside from the "1" MDS-UPDRS rating.

The IMU-predicted ratings for MLR and CNN models of wrist turning are shown in Figure 2.8. Each plot shows highly significant differences between "1" and "2" and "3" and "4" MDS-UPDRS ratings ($p < 0.001$). The CNN model shows a less significant difference ($p < 0.01$) between "0" and "1" than the MLR model ($p < 0.001$), and the MLR model shows a less significant difference ($p < 0.01$) between "2" and "3" than the CNN model ($p < 0.001$). The CNN model distributions generally have less variation than the MLR ratings for wrist turning, aside from the "0" MDS-UPDRS rating.

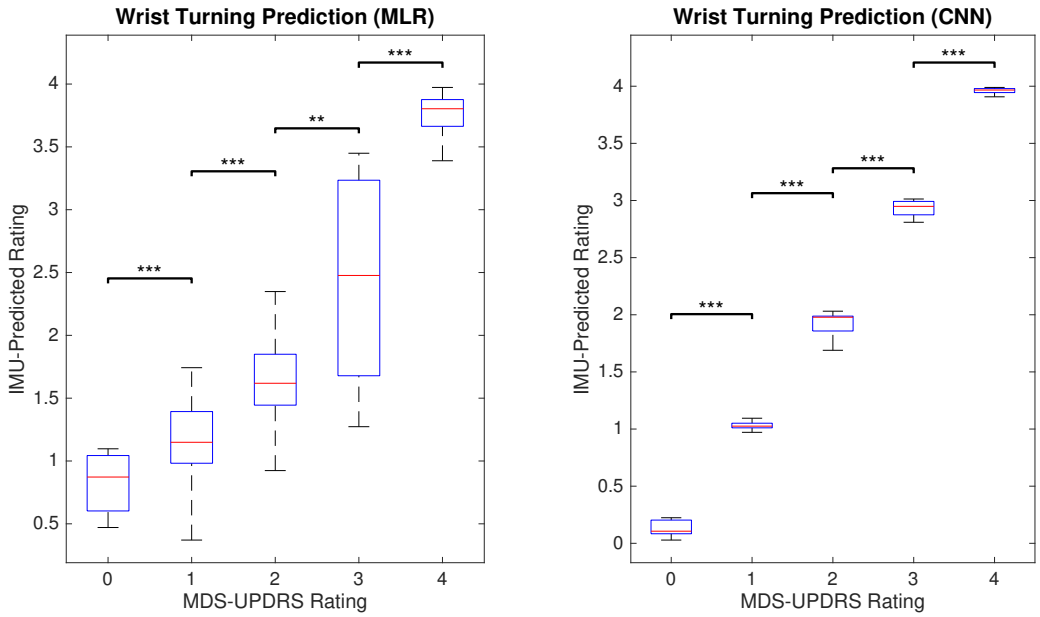

Figure 2.8: IMU-predicted ratings for MLR and CNN models of wrist turning.

Next, we analyzed the IMU-predictions for MLR and CNN models for each test to determine if either provided a significant advantage in predictive ability. In order to make comparisons between the models, we computed the mean absolute error (MAE) between the IMU-predictions and the MDS-UPDRS neurologist-provided ratings (Table 2.3). This analysis indicates that CNN models for kinetic tremor and wrist turning performed significantly better than MLR counterparts ($p < 0.001$), while there was no significant difference in performance for CNN and MLR models for rest tremor and postural tremor tests. These results support the classification performance analysis presented in Table 2.3, which show that CNN models for rest tremor and postural tremor provide a slight performance improvement over standard classification algorithms and that CNN models for kinetic tremor and postural tremor provide a much greater performance improvement.

Table 2.7: MLR and CNN Prediction Performance

MDS-UPDRS Test	MLR MAE	CNN MAE	p-value	Significance?
Rest Tremor	0.29	0.34	0.09	No
Postural Tremor	0.29	0.28	0.16	No
Kinetic Tremor	0.32	0.23	2×10^{-5}	Yes
Wrist Turning	0.48	0.11	3×10^{-9}	Yes

2.4 Discussion

The analysis showed that CNN models could provide significant advantages in classification performance and accuracy compared with standard classification algorithms, among them LDA, MLR, and SVM. Particularly, CNN models performed slightly better than standard classification algorithms for characterizing rest tremor and postural tremor clinical ratings, and CNN models performed significantly better than standard classification algorithms for characterization of kinetic tremor and wrist turning. In view of CNNs as a method for automated feature extraction and data fitting, these results suggest that the selected features for rest tremor and postural tremor (Table 2.4) are nearly optimal, while the selected features for kinetic tremor (Table 2.4) and wrist turning (Table 2.5) are incomplete.

However, in selecting classification algorithms for use in applications such as automated DBS programming or remote monitoring of symptoms, one should consider the limitations of algorithms as much, if not more, as apparent advantages. Despite their apparent advantage in classification, there may be some pitfalls in CNN use for classification in online applications. CNNs are trained by extracting features present in the data, while standard classification algorithms (LDA, MLR, SVM) require feature selection by the user, and thus require some level of domain knowledge for the specified problem. This difference in model construction means that CNN models will rely on data that is sufficiently representative of expected variation in the untested collection of data to be used in application, while standard classification algorithms make use of generalized features.

To understand the importance of this difference for CNN versus standard classification algorithms, consider the classification of pathological tremor, which is generally an oscillation of the hand occurring between 4 and 12 Hz. Consider a population of patients with tremor between 4 and 6 Hz and whose tremor data is fit to both a CNN and MLR (using the features in Table 2.4) model relating IMU data to clinical ratings of tremor. Now consider the application of these models (CNN and MLR) to predict clinical ratings of a selected group of patients whose tremor varies between 6 and 10 Hz. Because the CNN model was trained only on 4-6 Hz tremor data, it may not generalize well to recognize the 6-10 Hz tremor patients as having clinically-relevant tremor, while the MLR model may perform better in this aspect as the features used for model-fitting span the range of expected clinically-relevant tremors.

One notable observation about classification performance for CNN models vs. MLR models is that the CNN models for tests with a movement component, namely the kinetic tremor and wrist turning tests, had significant improvements compared with the MLR models whereas the static tests, namely rest tremor and postural tremor, did not confer such an advantage. While the CNN models and extracted features are difficult to interpret, it can be speculated that perhaps this advantage was due to coupling between different IMU channels during movement tasks that is unlikely to be as significant during less complex motions, and that CNN feature extraction is more adept at discovering these obscure components to movement tests.

The results presented in this chapter demonstrate that a smartwatch can effectively discriminate between clinical ratings of tremor and bradykinesia using standard classification algorithms, including LDA, MLR, and SVM, and that further performance gains may be achieved using CNN models. In subsequent chapters of this dissertation we will leverage this platform for a number of automated DBS programming applictions to discriminate between DBS settings and select optimal DBS settings for patient therapy, which are quantified in terms of tremor assessment and side effects reports.

Chapter 3

AUTOMATED DEEP BRAIN STIMULATION PROGRAMMING FOR TREMOR

Deep brain stimulation (DBS) programming is the systematic selection of electrical stimulation parameters that deliver maximal therapeutic benefit while limiting side effects, and this process poses several challenges in the treatment of movement disorders. DBS programming requires expertise of trained neurologists or nurses who assess patient symptoms according to standardized clinical rating scales and use patient reports of DBS-related side effects to adjust stimulation parameters and optimize therapy. In this chapter, we motivate and describe an automated software platform for deep brain stimulation programming for tremor in Parkinson's disease (PD) and essential tremor (ET) patients. Each tested DBS setting is ranked according to its effect on patient tremor, which is assessed using classification of smartwatch inertial measurement unit data (from Chapter 2), and patient side effects, which patients report through a user interface. We use blinded neurologist assessments to show that the automated programming method performs at least as well as clinical standards in PD and ET patients for selection of therapeutic DBS settings, and we demonstrate a method for optimization in which a patient-specific model of DBS response is used to guide selection of new parameters for testing. The results of this chapter may improve DBS programming procedures and enable DBS programming, troubleshooting and adaptation outside of specialty clinics.

3.1 Background

Deep brain stimulation (DBS) is an effective therapy for ameliorating tremor in patients with Parkinson's disease (PD) and essential tremor (ET) when maximal medical management

fails. While DBS can significantly improve patient motor symptoms and quality of life, there are many challenges to its successful clinical implementation. Programming DBS for therapy has been acknowledged as an especially difficult task for clinicians [24], and many reports of patient dissatisfaction with DBS therapy rank suboptimal stimulation parameters as the primary concern [40][41]. Additionally, DBS programming is a costly and time-consuming procedure, especially in the 3 to 6 month post-operative period when patient visits to clinic are frequent to optimally manage DBS settings and medication dosage [42]. DBS management incurs expenses both to healthcare providers and patients [22], who are subject to high travel costs as DBS clinics are typically isolated in large city centers and far removed from rural areas. These studies suggest that an improvement in DBS programming methodology could lead to greater patient satisfaction and cost-effectiveness of therapy.

Current DBS systems allow considerable customization of stimulation parameters to optimize therapy for patients. Medtronic's Activa PC implanted pulse generator (IPG) allows for control over stimulation via contact configuration, intensity (through voltage-controlled or current-controlled modes of operation), frequency, and pulsewidth, resulting in thousands of potential stimulation permutations. Accordingly, clinicians have developed standard approaches for greatly reducing the number of parameters in consideration for therapy [21]. However, as next generation DBS systems are poised to enable greater specificity of the electric fields generated for therapy via directional current steering with segmented leads [11], clinicians will be faced with a more difficult task in arriving at optimal DBS configurations for patients. Therefore, automated and objective DBS programming approaches are necessary to ensure that clinical therapy keeps pace with advancements in electrode technologies.

Prior works have investigated various methods for automated or computer-guided selection of DBS parameters for patient therapy. Some studies have employed biophysical models of the pathological cortico-basal-ganglia circuit in PD to determine optimal parameters for conventional stimulation [43] and novel waveforms [44]. However, it is unclear how these methods may address interpatient variability in both electrode location and response to DBS, and, in the case of the latter study, novel stimulation waveforms were shown to

be about half as effective for suppressing tremor as standard clinical stimulation, indicating that approaches to automatically selecting DBS parameters solely based on biophysical models may be insufficient for clinical use. Another approach has proposed combining DBS-generated electric field estimates with patient imaging and brain atlas data to predict stimulation parameters for therapy, which has been demonstrated to be as effective as clinical DBS stimulation at treating symptoms and more effective for avoiding cognitive impairment side effects [45].

Other recent studies have capitalized on the increasing prevalence of sensors and their ability to give feedback about patient symptoms in order to select DBS parameters, and these approaches may be useful alone or in complement to aforementioned modeling and imaging strategies. A study in PD patients implanted with Medtronic Activa PC+S, which enables sensing of local field potentials (LFPs) from the implanted electrode, showed that spectral estimates of LFPs in subthalamic nucleus (STN), including the beta band frequency range (13-30Hz), could be used to predict the clinically used stimulation contacts to a high degree of accuracy [46]. Another approach has been to make use of wearable sensing devices such as the Kinesia system [28] to give feedback on various movement disorder features in order to assist clinicians in selecting DBS settings [47][48]. These studies demonstrate the utility in using empirical measurements and models of patient-specific DBS response to successfully program patients for DBS therapy. This approach may confer several advantages over modeling- and imaging-based approaches to programming, including utilizing fewer assumptions about patient response to DBS and requiring less computational and medical imaging resources.

In this chapter we describe the development and testing of a fully automated software platform for programming deep brain stimulation for tremor in PD and ET patients. We use inertial measurement unit (IMU) data from a commercially available smartwatch to classify and predict clinical ratings of different types of tremor, and we use patient reports of DBS-related side effects to quantify and rank each DBS setting tested according to its therapeutic value. We embed these features into an integrated software platform that sends stimulation

commands directly to the Activa system, removing clinicians from the loop of device control and decision making in DBS programming. We show that this system can identify DBS settings that reduce tremor at least as well as standard clinical, human-mediated programming according to blinded movement disorder neurologist and IMU-predicted tremor ratings.

3.2 Methods

3.2.1 Patient Selection

Patients were recruited from the UCSF Movement Disorders and Neuromodulation Center. We recruited patients with ET or tremor-dominant PD who were implanted with Medtronic Activa PC series IPG systems for at least 6 months and had completed clinical programming optimization. Patients were asked to hold their tremor or PD medications for at least 12 hours prior to testing. The Institutional Review Board (IRB) at UCSF approved this study, and all patients signed written informed consent.

3.2.2 System Description

We performed the automated DBS programming experiment using a custom software application developed for a Windows PC laptop, a block diagram for which is shown in Fig 3.1. The application was built in C# with embedded C++ modules for asynchronously receiving smartwatch IMU data over Bluetooth using the Android Wear platform, and communicating with the Nexus-D, a Medtronic adapter that allows software commands to update IPG stimulation parameters within safety limits defined by a clinician. The laptop receives 6-axis IMU data from an LG G Smartwatch at 100 Hz over Bluetooth and side effect reports from patients entered through a user interface, and sends stimulation commands over USB to the Nexus-D, which communicates with a patient's Activa IPG. Raw IMU data is both logged and used online for tremor severity assessment, and this data is used along with side effect reports to assess the therapeutic value of DBS settings. Stimulation commands are sent from the laptop to the Nexus-D and logged every 200 ms.

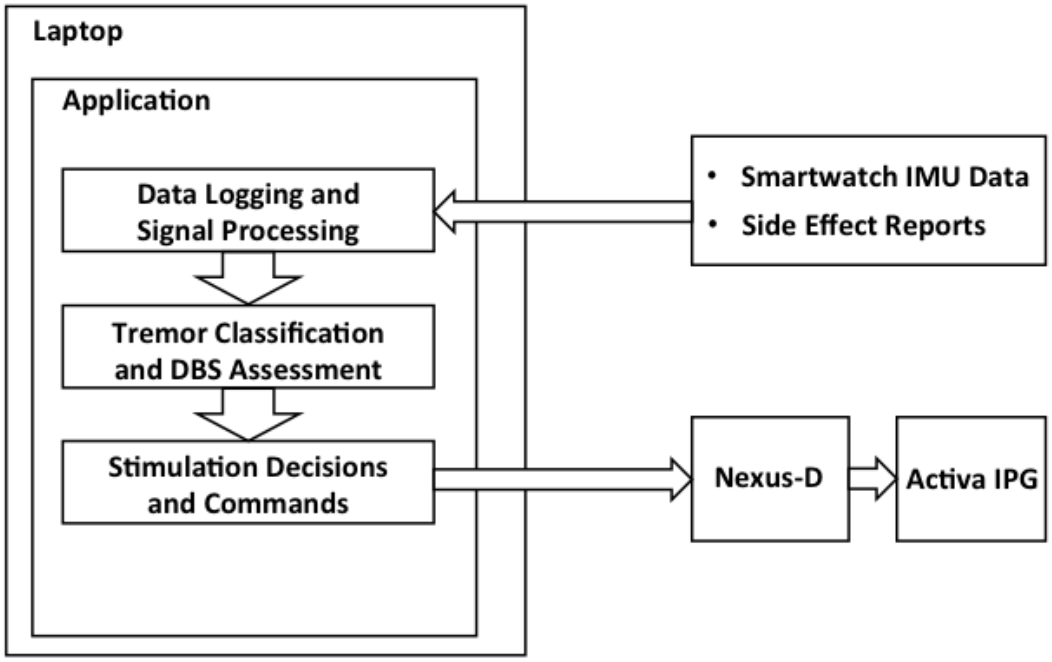

Figure 3.1: A conceptual block diagram of the automated programming system. The software application receives IMU data over a Bluetooth connection from a smartwatch worn by patients, and also receives side effects reports from patients submitted through a user interface. The application performs IMU signal processing and evaluates side effects reports to assess DBS settings. The software application sends stimulation commands to the Nexus-D which communicates with patients' implanted Activa IPG.

3.2.3 Experiment Description

We developed the platform for automated DBS programming of tremor using a standard clinical decision algorithm for DBS programming [21]. In typical clinical DBS programming sessions, the monopolar screen is used first to determine the therapeutic response to DBS by separately testing each of the four electrode contacts as the cathode and using the IPG case as the anode. DBS frequency is often set to 130 Hz and DBS pulsewidth is set to 60 μs. Each monopolar contact is separately tested by incrementally increasing DBS amplitude while assessing patient tremor and noting any side effects experienced. If a DBS setting is found that provides satisfactory suppression of tremor without side effects, then that monopolar

setting is used for therapy. However, if the DBS settings found to provide satisfactory suppression of tremor also cause side effects, then it is suggested that bipolar configurations are tested, which narrow the electrical field to lower side effect thresholds. If the DBS settings found in a monopolar screen do not provide satisfactory suppression of tremor nor induce side effects, then it is suggested that double monopolar configurations or increased frequency and/or pulsewidth be tested, which can expand the electric field created by DBS and potentially provide greater levels of therapy.

At the beginning of each experimental session, we evaluated a patient's tremor in their clinical DBS settings to later serve as a comparison to the optimal DBS setting determined by the automated programming method. This was done using both smartwatch IMU data and clinical rating scales (neurologist was not blinded for this assessment). For patients with bilateral DBS implants, we tested the hand with more severe tremor. After the initial tremor assessment, the patients IPG was shut off for 30 minutes to washout the effects of chronic stimulation.

We then performed a pseudorandom monopolar screen for which the evaluation of tremor and side effects and command over DBS parameters was under automated control by the computer program. Prior to starting the automated procedure, a movement disorders neurologist configured a patient's IPG to enable this screen and determined maximum tolerable stimulation amplitude for each contact (i.e. the safety limit). These limits for each stimulation contact were used to parameterize the monopolar screen in 1 V increments, and the stimulation contacts and amplitudes were tested in a random order. A baseline condition in which the stimulator was "off" (0 V) was tested for each contact at evenly spaced intervals to assess baseline tremor levels throughout the monopolar screen. Each experiment was tailored to clinical tremor experienced by the patient, using a subset of rest tremor, postural tremor, and kinetic tremor for evaluation (described below).

During the monopolar screen, the software tested each parameterized DBS setting and evaluated its effect on patient tremor and side effects. The automated programming state transition sequence is shown in Figure 3.2 to illustrate how each DBS setting was evaluated.

To begin each DBS setting evaluation, the IPG was automatically set to the desired stimulating contact and amplitude was gradually ramped up over several seconds, after which followed a "settling" phase typically lasting 15 seconds, allowing the transient effects of stimulation changes on patient tremor and side effects to resolve. Next, the patient was prompted to perform their subset of tremor tests sequentially and also asked about side effects experienced. Side effects reports were submitted to the software through a user interface, and included reports of magnitude ("none", "mild", "moderate", "severe"), type (sensory, motor, speech, vision, mood, autonomic, dyskinesia) and body location ("face", "arm", "leg", "trunk"). After the tremor testing was completed for each DBS setting, the IPG was turned "off" (0 V) for a "washout" period lasting 30 seconds so that the therapeutic effects of that DBS setting would not interfere with evaluation of subsequent DBS settings. This process of DBS setting evaluation was continued for all settings parameterized by the monopolar screen (typically 24 settings tested from 0-5 V unless maximum tolerable threshold was lower for any given contact).

3.2.4 DBS Setting Assessment and Quantification

The foundation for an automated DBS programming system is a method for quantification of DBS setting value and the ability to rank and select the optimal DBS setting amongst the many tested. DBS value should incorporate both clinical benefit for mitigating tremor as well as negative aspects of therapy such as the side effects induced by stimulation. In this study we use a simple method for quantification of DBS setting value J_{DBS^i} based on the results of tests performed while the patient's IPG was active in a particular DBS setting DBS^i:

$$J_{DBS^i} = J_{tremor^i} + J_{SE^i} \tag{3.1}$$

Each tested DBS setting DBSi is evaluated in terms of a tremor rating J_{tremor^i} and a side effects rating J_{SE^i}. The tested DBS setting DBS^{i*} with maximum $J_{DBS^{i*}}$ is chosen as the

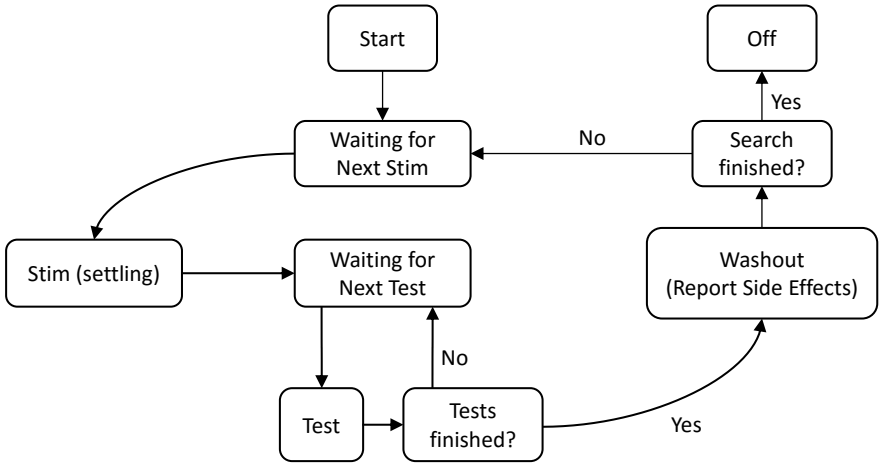

Figure 3.2: A sequence of automated programming states during an experiment.

optimal DBS setting for therapy at the end of the experiment.

Tremor Assessment and Quantification

Tremor severity was assessed in each tested DBS setting by performing a subset of rest tremor, postural tremor, and kinetic tremor tests, which were chosen on a patient-specific basis. Typically PD patients performed rest tremor and postural tremor tests, while ET patients performed postural tremor and kinetic tremor tests. Patients were seated comfortably with each test lasting 10 seconds for evaluation of different types of pathological tremor: *rest tremor* testing was performed with the patients affected hand supported against gravity on a chair's armrest; *postural tremor* testing was performed with the patients arm outstretched directly in front of their chest; and *kinetic tremor*, or action tremor, testing was performed with the patient performing a visually-guided movement which required they alternately touch

their affected hand's forefinger to their nose and then to an examiner's forefinger which was approximately an arm's length away.

After each tremor test was performed a movement disorders neurologist, blinded to the DBS setting currently being tested, provided a clinical rating according to the Movement Disorder Society update to the Unified Parkinsons Disease Rating Scale (UPDRS) [15]. Although there are rating scales developed for ET specifically [25], we used only the UPDRS to assess tremor in PD and ET patients to provide consistent and comparable clinical assessments of tremor across all patients. The UPDRS provides the following numerical ratings based on visual assessment: 0 for no tremor; 1 for slight tremor with amplitude less than 1 cm; 2 for mild tremor with amplitude between 1 cm and 3 cm; 3 for moderate tremor with amplitude between 3 cm and 10 cm; and 4 for severe tremor with amplitude greater than 10 cm.

Various features from IMU accelerometer (linear acceleration) and gyroscope (angular velocity) were used to quantify and predict the magnitude of clinical tremor ratings. Raw gyroscope and accelerometer data was first processed with a Type II Chebyshev band pass filter (2-12Hz) to remove low amplitude voluntary movement artifacts. Tremor band power (4-12Hz) for gyroscope and accelerometer channels was then estimated using a short time Fourier transform with a 1 second Hanning window computed in 200 ms intervals over the course of a tremor test, and then a magnitude estimate was computed across each sensor over the 3-channels (x, y, z). We used the natural logarithm of estimated tremor band power of both accelerometer and gyroscope channels, which has been shown previously to be linearly correlated to clinical tremor ratings [28], and we used average and median statistics from each tremor test to reduce the influence of noise from movement artifacts during testing. We also computed the root-mean-square (RMS) level of signal across both accelerometer and gyroscope channels.

These features from gyroscope and accelerometer data during the tremor test were used to fit an ordinal multinomial logistic regression (MLR) model based on the neurologist's provided tremor ratings. We assessed models for each tremor test by dividing data into

training (70%) and testing (30%) sets randomly and performing classification analysis. Table I shows the average classification performance for each MLR tremor model (over 1000 random initializations of training and testing data), with the predicted rating for each test being the one computed with highest probability. In order to reflect uncertainty of tremor rating classification and to obtain a higher resolution tremor rating, we summed over the mixed probability of tremor classification for each test and obtained a rating on a continuous scale from 0 to 4.

Table 3.1: Tremor Classification Performance

Test	**Accuracy**	**F-Score**
Rest Tremor	78.3%	77.0%
Postural Tremor	79.7%	79.4%
Kinetic Tremor	76.2%	75.3%

Thus, after each tremor test the predicted clinical rating was computed and recorded for the current DBS setting. A composite average tremor rating, J_{tremor^i}, was used to assess the total therapeutic value of a DBS setting across all types of tremor tests, compared to the baseline predicted tremor rating, $tremor_0$, when DBS was off (0V):

$$J_{tremor^i} = tremor_0 - tremor_{DBS^i} \tag{3.2}$$

As therapeutic DBS is expected to mitigate tremor severity, it is expected that $tremor_0$ has higher predicted tremor ratings than $tremor_{DBS^i}$, and that more effective DBS settings for tremor would have higher J_{tremor^i} ratings.

It should be noted that the tremor models were developed over the course of the experiments with the 10 patients; the first 5 patients had tremor quantified using only the natural logarithm of tremor band power estimate. However, the computation of J_{tremor^i} was consistent across all experiments, and tremor models from the first 5 patients were used to develop predictive MLR clinical rating models that were iteratively updated after each of

the next 5 patients were tested.

Side Effect Assessment and Quantification

Side effect reports from patients were obtained for each tested DBS setting, and these were used to quantify the side effect magnitude of each DBS setting for use with algorithmic decision-making. Side effect magnitude was submitted to the program through a user interface, and a side effects penalty J_{SE^i} was computed and scaled by the factor α according to the severity ($\alpha = 0$ for "no side effects", $\alpha =$ for "mild", $\alpha = 1$ for "moderate", $\alpha = 2$ for "severe"). The side effects penalty was computed as

$$J_{SE^i} = \alpha(tremor_{DBS^i} - tremor_0) \tag{3.3}$$

The side effect penalty was thus used to offset the benefit to tremor for assessment of DBS setting value J_{DBS^i} for selection of optimal DBS settings and advanced programming decision making. For example, a DBS setting that induced moderate side effects ($\alpha = 1$) would have a computed DBS value $J_{DBS^i} = 0$, suggesting that such a DBS setting was no better for therapy than a DBS setting that did not reduce tremor at all.

3.2.5 Advanced DBS Programming

At the end of the monopolar screen, the software displayed recommendations for advanced programming based on the tremor and side effects results of every DBS setting tested. The decision space for advanced programming recommendations is shown in Fig. 3.3. If the monopolar screen resulted in at least one DBS setting that yielded predicted tremor ratings below 1 and no side effects, then monopolar optimization was suggested to narrow in on the optimal DBS setting. If the monopolar screen resulted in DBS settings with predicted tremor ratings below 1 but these settings also induced side effects, then bipolar settings were suggested based on the most effective contact(s) for therapy. If the monopolar screen resulted in no DBS settings with predicted tremor ratings below 1, and also no settings that

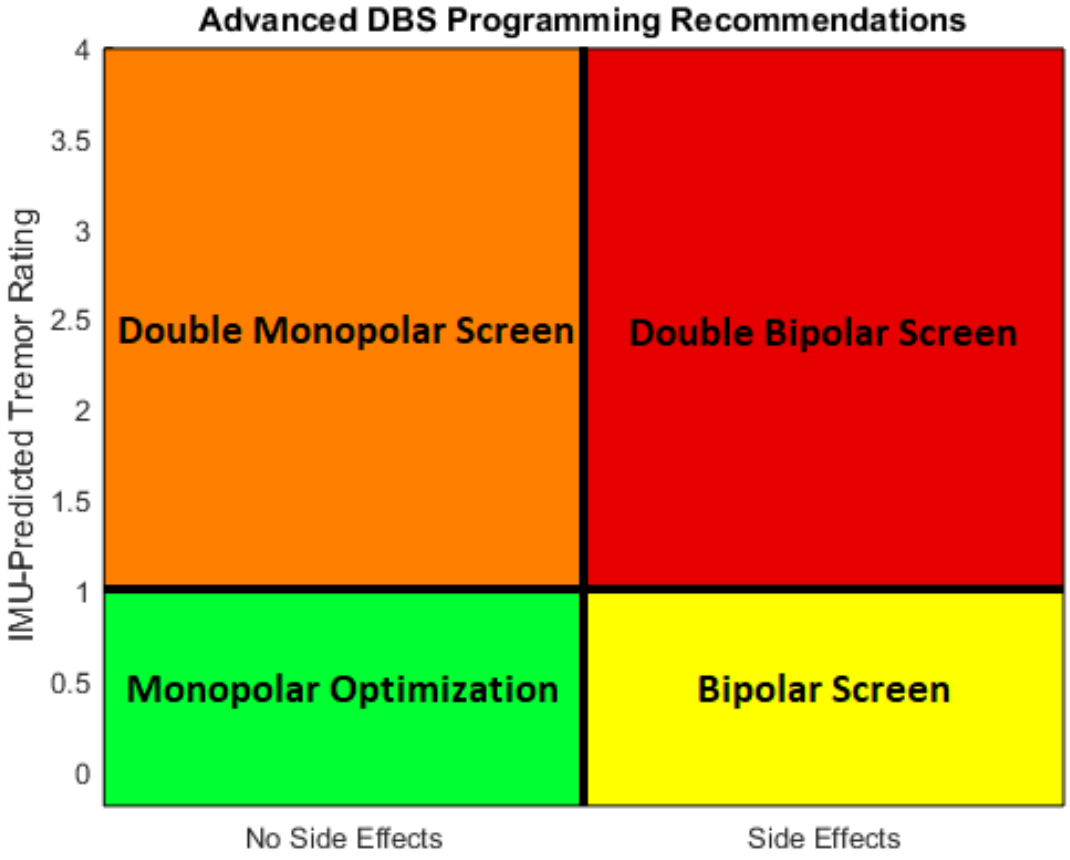

Figure 3.3: Advanced programming recommendations for DBS based on the results of the automated monopolar screen. The software displays various recommendations, shown in each region, to the user based on the results of the monopolar screen. Stimulation contacts for each advanced programming decision are recommended based on their effectiveness during the monopolar screen.

induced side effects, then double monopolar settings, in which two stimulation leads with the best tremor control were used as cathodes, and settings with increased frequency and pulse width were suggested. Finally, if the monopolar screen resulted in no DBS settings with predicted tremor ratings below 1 and the most effective settings induced side effects, then double bipolar configurations were recommended, with 2 leads set as cathodes and one lead set as anode based on the most effective contacts for therapy. Due to limitations of

Medtronics Activa IPG series, stimulation contact settings could not be changed directly by the software system; instead, reconfiguring the IPG for bipolar, double monopolar, double bipolar, and increased frequency and pulse width DBS settings had to be performed manually by a clinician before the advanced programming screen was performed.

3.2.6 DBS Setting Optimization

A procedure for optimization was used to narrow in on the best DBS setting for patient therapy. The results from the monopolar screen or advanced programming screens were used to formulate a predictive model of untested DBS settings. We estimated J_{DBS} at intermediate amplitude levels in 0.1 V increments by interpolating the J_{DBS^i} results available in 1V increments from the previously completed monopolar or advanced programming screens. We then iteratively selected the DBS setting with the maximum predicted value and evaluated it for therapy using the same procedure previously outlined for assessing DBS settings during the monopolar screen. Each optimization session tested 6 previously untested DBS settings in addition to the prior DBS settings tested during the monopolar or advanced programming screens. The optimization procedure was used to evaluate the predictive capabilities of a patient-derived model of DBS response from the monopolar screen, and it was also useful for clarifying the thresholds and tradeoff between DBS settings that were beneficial for tremor reduction and DBS settings that induced side effects, which are both associated with higher amplitude settings.

3.3 Results

We recruited 10 patients (4 ET, 6 PD) to undergo automated DBS programming using the custom software system. All ET patients had leads implanted in ventral intermediate nucleus of thalamus (VIM), and all PD patients had leads implanted in subthalamic nucleus (STN). Patients had been implanted with Medtronic Activa PC, RC, or SC IPGs at least 6 months prior to their enrollment in the study. Table II shows a summary of each patients characteristics including age, diagnosis, clinical DBS settings and tremor ratings, automated

Table 3.2: Automated Programming Experiment Summary

ID No.	**Age, Sex**	**Dx**	**DBS Target(s)**	**Clinical DBS Setting**	**Clinical DBS Tremor Ratings**	**Automated DBS Setting**	**Automated DBS Tremor Ratings**	**Patient Preference**
1	69, M	ET	**L**/R VIM	2+1-, 3.1 V, 90 μs, 130 Hz	Rest: 1, Postural: 1, Kinetic: 1	0-1+, 1.8 V, 60 μs, 130 Hz	Rest: 0, Postural: 0, Kinetic: 0	Automated
2	57, M	ET	L/**R** VIM	C+8-, 4.1 V, 60 μs, 180 Hz	Rest: 0, Postural: 4, Kinetic: 3	C+8-, 2.7 V, 60 μs, 180 Hz	Rest: 0, Postural: 4, Kinetic: 4	Neither
3	66, M	PD	**L** STN	1-2+3-, 3.7V, 60 μs, 130 Hz	Rest: 0, Postural: 0	1+2-, 4.0 V, 60 μs, 130 Hz	Rest: 1, Postural: 0	Automated
4	68, M	PD	**L**/R STN	1-2+, 5.9 V, 60 μs, 120 Hz	Rest: 0, Postural: 2	C+0-, 2.7 V, 60μs, 120 Hz	Rest: 0, Postural: 1	Automated
5	66, M	PD	**L**/R STN	C+0-, 4.1 V, 60 μs, 60 Hz	Rest: 0, Postural: 1, Kinetic: 1	C+0-, 4.0 V, 60 μs, 60 Hz	Rest: 0, Postural: 0, Kinetic: 0	Same
6	66, M	ET	L/**R** VIM	10-11+, 4.0 V, 60 μs, 170 Hz	Postural: 1, Kinetic: 0	C+10-, 1.6 V, 60 μs, 170 Hz	Postural: 1, Kinetic: 1	Automated
7	81, F	ET	L/**R** VIM	8-9+, 2.2 V, 60 μs, 130 Hz	Postural: 0, Kinetic: 1	8-9+, 2.7 V, 60 μs, 130 Hz	Postural: 0, Kinetic: 1	Clinical
8	47, M	PD	**L**/R STN	C+1-, 5.6 V, 60 μs, 140 Hz	Rest: 0, Postural: 0	C+1-, 4.5 V, 60 μs, 140 Hz	Rest: 0, Postural: 0	Same
9	59, M	PD	**L** STN	C+1-, 3.5 V, 60 μs, 130 Hz	Rest: 0, Postural: 0	C+0-, 3.7 V, 60 μs, 130 Hz	Rest: 0, Postural: 0	Clinical
10	52, M	PD	**L**/R STN	C+1-, 3.3 V, 60 μs, 160 Hz	Rest: 2, Postural: 1	C+1-, 2.0 V, 60 μs, 160 Hz	Rest: 1, Postural: 1	Clinical

DBS settings and tremor ratings, and the preferred DBS setting at the conclusion of the experiment. Of the 10 patients who enrolled, 4 preferred the automated DBS settings, 3 preferred their clinical DBS settings, 2 had no preference, and 1 did not like either setting.

All patients underwent the automated monopolar screen, and 3 patients additionally

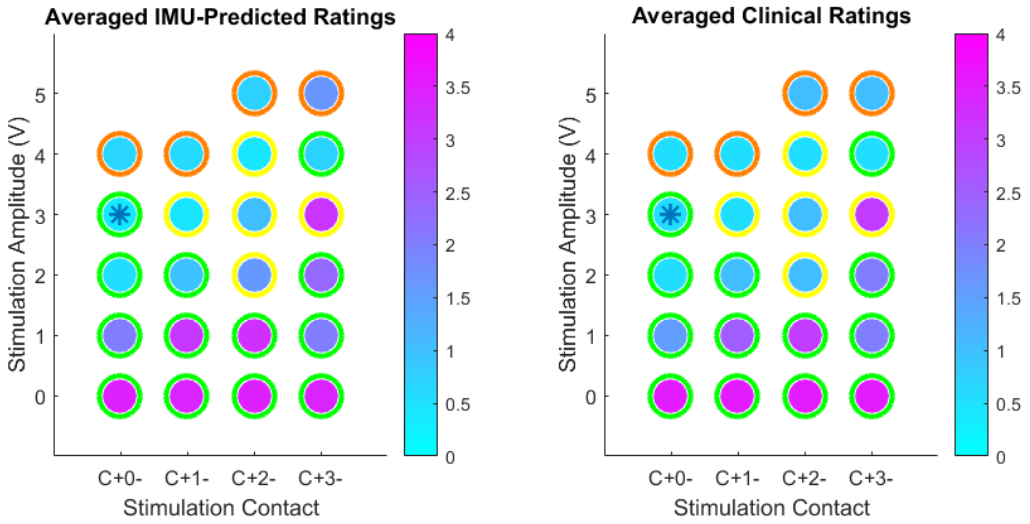

Figure 3.4: IMU-predicted tremor ratings vs. blinded neurologist tremor ratings for a representative monopolar screen. Inner circle shading represents average tremor ratings for each DBS setting on a 0 to 4 scale, and outer circle color represents the reported side effects from the patient (green = no side effects, yellow = mild, orange = moderate, red = severe). The IMU-predicted results and blinded neurologist results show general agreement in the monopolar screen assessment, including identifying the same optimal DBS setting for therapy.

underwent a bipolar screen per the advanced programming recommendations, with an optimization session following each. An average of 28.8 ± 6.6 DBS settings were tested for each patient. Fig. 3.4 shows a representative plot of monopolar screen results for patient number 4 with IMU-predicted tremor ratings on the left and blinded neurologist UPDRS tremor ratings on the right. For each unique stimulation contact (x-axis) and stimulation amplitude (y-axis) pair, the average tremor ratings and side effects are plotted; the inner circle coloring represents the tremor rating on the UPDRS scale, and the outer ring coloring denotes the reported side effect severity (green = no side effects, yellow = mild, orange = moderate, red = severe). On each plot an asterisk denotes the optimal DBS setting.

The optimization procedure followed the monopolar or advanced programming screens, and examples of this procedure for patient numbers 4 and 8 are shown in Fig. 3.5. The plot at

left shows the J_{DBS} values for the most effective stimulation contact of the monopolar screen (C+0- in the left plot of Fig. 3.4) plotted as solid circles using (1) to reference tremor scores and side effect ratings against baseline tremor scores. The interpolated lines connecting the solid circles denotes the predicted J_{DBS} values at these intermediate stimulation amplitude settings, and the hollow circles are the results of testing 6 previously untested DBS settings during the optimization procedure. The results indicate that 2.7 V has optimal DBS value, and this setting was chosen for automated DBS settings results for patient 4 (see Table II). The plot at right shows optimization results after a bipolar screen for patient 8, and this plot reveals how the optimization procedure could identify DBS settings that provided greater reduction of tremor without inducing side effects than DBS settings tested during the monopolar or advanced programming screens. At 2 V the J_{DBS} value was about 2, indicating that the tremor rating was predicted to be about 2 points lower than at baseline (0 V). However, at 3 V and 4 V, the patient reported speech-related side effects of "mild" and "moderate" severity respectively, so the J_{DBS} value for these settings was penalized accordingly. During optimization, intermediate settings between 2 V and 3 V were tested, and among these 2.7 V provided optimal tremor benefit while not inducing any patient-reported side effects.

We next analyzed the results from optimization sessions performed after monopolar screens and advanced programming screens to determine whether the optimization procedure was able to effectively search for and test new DBS settings that would provide acceptable levels of therapy. To accomplish this, we compared the tremor ratings of DBS settings tested during optimization with tremor ratings of randomly selected DBS settings during the monopolar or advanced programming screens. Since the amount of tremor improvement due to DBS varied across patients, we made the comparison using percentage of total tremor rating improvement seen across all DBS settings for each patient, rather than simply using the tremor rating. We compared the differences between optimized DBS settings and randomized DBS settings for both IMU-predicted tremor ratings and blinded clinician tremor ratings using the Wilcoxon signed-rank test to establish significance. Figure 3.6 shows the

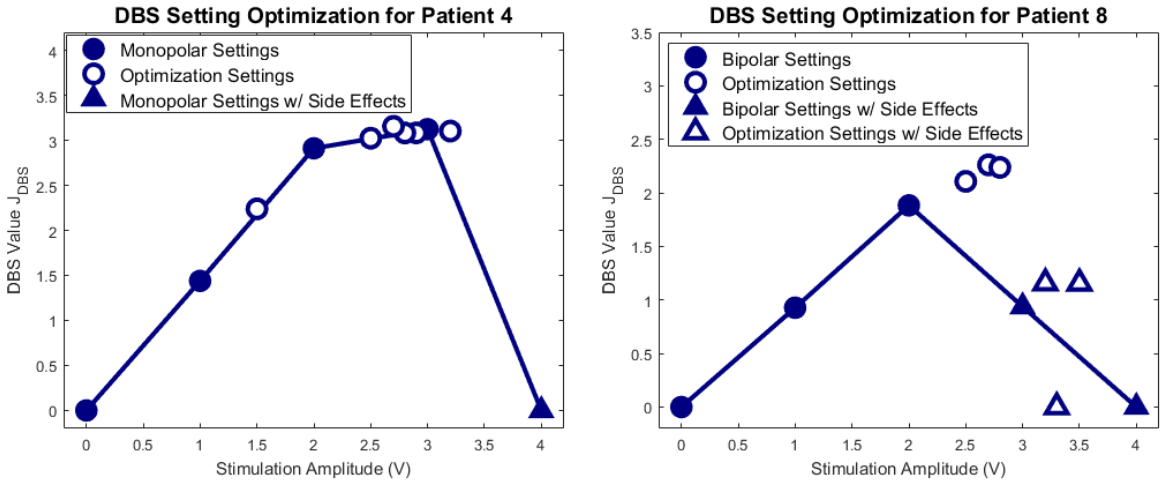

Figure 3.5: Results of the optimization procedure following a monopolar screen for patient 4 (left) and following a bipolar screen for patient 8 (right). The DBS value (J_{DBS}) for each monopolar/bipolar setting is plotted as solid circles, with triangles denoting DBS settings that induced side effects (as reported by the patient). Hollow circles represent the DBS value of DBS settings tested during optimization, with hollow triangles representing DBS settings that induced side effects. After each optimization procedure, the DBS setting with maximum value was selected for therapy by the automated programming algorithm, and 2.7 V was selected for both patient 4 and 8 (see Table 2).

distribution of tremor improvement for optimized DBS settings and randomized DBS settings for both IMU-predicted tremor ratings and blinded clinician tremor ratings. Wilcoxon signed-rank tests allow us to reject the null hypothesis that these results belong to the same distribution for both the IMU-predicted tremor ratings ($p < 0.001$) and the blinded clinician tremor ratings ($p < 0.001$). As expected, the distribution of improvement in tremor ratings for randomized DBS settings spanned the entire range, whereas the distribution of improvement in tremor ratings for optimized DBS settings was mostly concentrated in the top quartile. These results validate the hypothesis that a patient-specific model can be used to predict DBS settings that are effective for tremor therapy.

In order to assess the algorithm's performance in automatically selecting optimal DBS settings, we compared tremor ratings for automated DBS settings with tremor ratings for

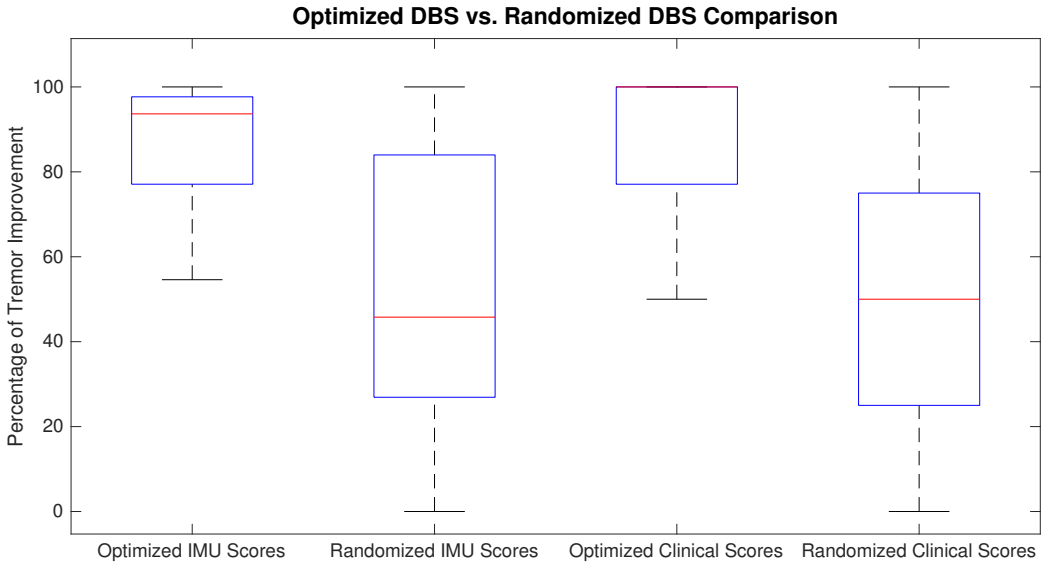

Figure 3.6: A comparison between optimized DBS settings and randomized DBS settings for IMU-predicted and blinded neurologist in terms of percentage of tremor improvement. In both cases, optimized DBS settings provide significantly more improvement in tremor ratings (p ¡ 0.001) than randomly selected DBS settings from the monopolar screen, which validates the patient-specific model generated by the monopolar screen.

clinical DBS settings (i.e. chronic DBS settings in which patients were evaluated at the beginning of experiment before washout). Fig. 3.7 shows the distribution of differences between both IMU-predicted tremor ratings and blinded clinical tremor ratings for the automated DBS settings and clinical DBS settings. Negative values for the difference between automated DBS tremor ratings and clinical DBS tremor ratings indicate that tremor ratings were lower in the automated DBS settings than clinical DBS settings. Wilcoxon signed-rank test results indicate that comparisons between the automated DBS settings and clinical DBS settings for both IMU-predicted tremor ratings and blinded UPDRS ratings resulted in no significant differences between the distributions. Furthermore, we assessed whether this distribution was significantly greater than zero (i.e. clinical DBS resulted in significantly lower tremor scores than automated DBS) or significantly less than zero (i.e. automated

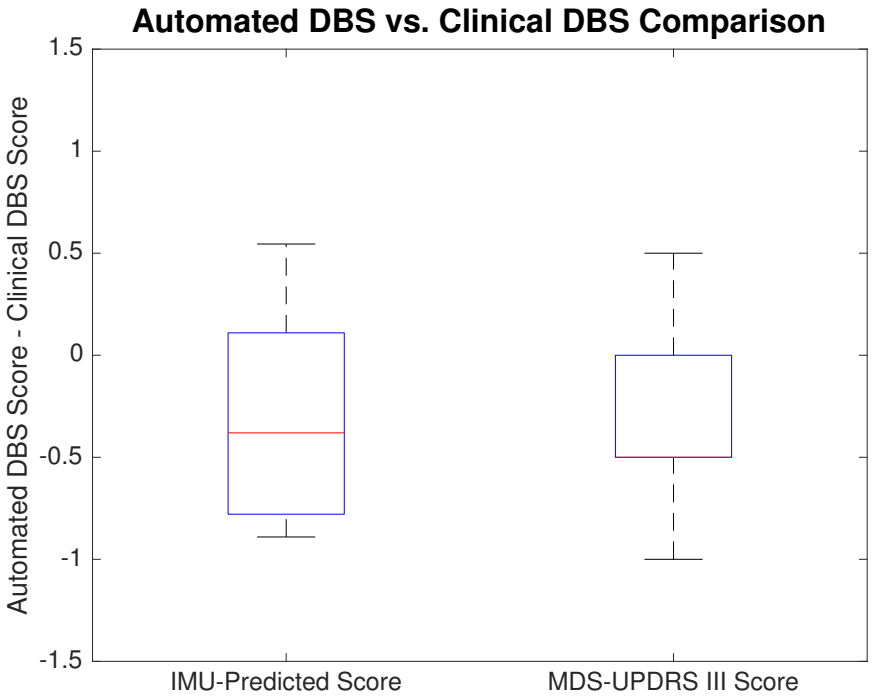

Figure 3.7: A comparison between automated DBS settings and clinical DBS settings for both IMU-predicted tremor ratings and blinded neurologist UPDRS tremor ratings. The distribution of differences between automated DBS tremor ratings and clinical DBS tremor ratings are shown, with negative values indicating that automated DBS settings had lower tremor ratings than clinical DBS settings.

DBS resulted in signficantly lower tremor scores than clinical DBS) using right and left tail Wilcoxon signed-rank tests, respectively. For the right tail test, the null hypothesis is accepted (i.e. that automated DBS scores were not significantly greater than clinical DBS scores) for both IMU-predicted ratings ($p = 0.96$) and MDS-UPDRS ratings ($p = 0.99$). For the left tail test, the null hypothesis is rejected (i.e. that clinical DBS scores were not significantly greater than automated DBS scores) for MDS-UPDRS ratings ($p < 0.05$) and accepted for IMU-predicted ratings ($p = 0.053$). These results indicate that our method for automated DBS programming for tremor performs at least as well as expert clinicians in selecting DBS parameters for tremor therapy for this group of PD and ET patients.

Finally, we plot the clinical DBS vs. automated DBS scores augmented with patient preferences in Figure 3.8. This plot illustrates how patient perceptions of level of therapy between the two modes of DBS programming delivery (automated vs. clinical) line up with sensor-based (left plot, IMU-predicted ratings) and clinician-based (right plot, MDS-UPDRS ratings) assessments of tremor severity (jitter was added to data points to help differentiate them visually). These results show that patient perceptions of therapy are not always in line with sensor- or clinic-based assessments; two patients who preferred their clinical DBS settings actually had lower automated DBS setting tremor ratings, and one patient who preferred automated DBS actually had a lower clinical DBS setting tremor rating.

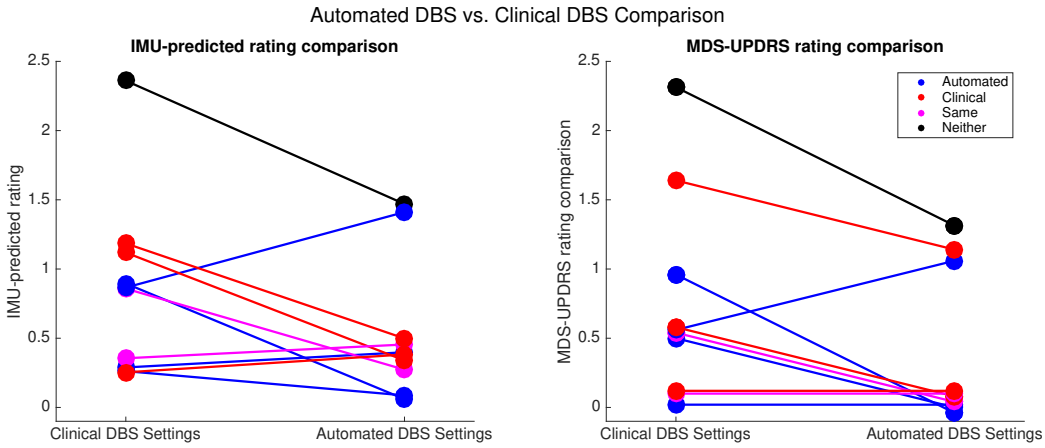

Figure 3.8: Average tremor scores for automated DBS settings and clinical DBS settings color-coded by the patient preferences for tremor therapy (blue = automated, red = clinical, magenta = same, black = neither).

3.4 Discussion

In this study we describe and validate a system for automated DBS parameter selection for tremor in PD and ET patients that performs at the level of expert human programmers. This approach relied on a commercially available smartwatch equipped with IMU, which provided sensitive motion data related to various types of tremor which were classified to

produce estimates of clinical tremor ratings based on blinded movement disorders neurologist scores. The tremor assessment was coupled with a side effect report, and this information was used to rank and select DBS parameters using a clinical programming decision algorithm and optimization procedure implemented in the same software system. The software communicated with the patient's implanted DBS systems via Medtronic's Nexus adapter to automatically change stimulation settings without human intervention. Tremor ratings in the optimized automated DBS setting were compared against each patients chronic clinical DBS settings based on their ability to suppress tremor without causing side effects.

Several limitations need to be outlined with regards to our study results. Although precision IMU data can potentially provide a finer resolution assessment of tremor severity compared with the relatively coarse, integer-based UPDRS clinical scale, this approach is not without limitations. Specifically, it is difficult to parse out all movement features in the IMU data not related to tremor, whereas trained clinicians know to ignore these aspects of movement in their evaluation of tremor. A patient may sway their arm subtly or bring it abruptly to rest against an armrest, and a neurologist will discern these features as not related to tremor; however, such movements may not be effectively filtered from the IMU data and cause an overestimate of tremor severity. For this reason, our automated programming experiments were not performed entirely without human assistance, as an accompanying researcher confirmed that each tremor test was performed without extraneous movements. In a clinical setting, tremor tests would require monitoring, or extensive instruction to patients and caregivers, so that the patient response to DBS can be accurately assessed for all tested settings. Poorly evaluated DBS settings can lead the automated method astray and can result in the selection of suboptimal DBS settings for therapy; therefore, proper tremor testing with the smartwatch is of paramount importance to the efficacy of this method.

Another limitation to this study was present in the Activa IPG system that was used for the experiments, which allowed for limited control over stimulation parameters. Only four different stimulation contact configurations can be programmed at once for the Activa IPG, while the Medtronic 3387/3389 leads enable 4 possible monopolar configurations, 12 possi-

ble bipolar configurations, and additional double monopolar, double bipolar, and interleaved settings for consideration. Therefore, the period after the monopolar screen once again required human intervention to reprogram the Activa IPG for possible advanced programming recommendations. Ideally, there would be simultaneous control over the stimulation contact configuration, amplitude, pulsewidth, and frequency, and the automated search for optimal DBS parameters could run uninterrupted.

Device power consumption can be another important factor in DBS programming decision making as high amplitude DBS settings can hasten the need for battery replacement surgery, which carries the risk of infection. However, our algorithm did not account for device power consumption in determining optimal DBS settings, and instead used only estimated tremor severity and side effects to guide programming. Current DBS systems such as Medtronic's RC series IPG can operate using rechargeable batteries, which both prolong the implanted device lifetime and potentially change the calculus on how to consider device power consumption versus the potentially greater therapeutic benefits of high amplitude DBS settings.

Decisions involving several criteria, in this case the consequences of DBS setting selection on symptoms, side effects, and device lifetime, can become difficult to reason through without careful consideration. To this end, we can combine the results of this study with power expenditure estimates from Medtronic battery manuals to obtain quantitative insight into the actual tradeoffs imposed by these criteria. Figure 3.9 shows the estimated symptoms (tremor), side effects, and DBS device lifetime of each DBS setting tested for patient 7's automated programming session. Using this plot we can introduce the notion of Pareto optimality to discuss rational decision making and how it impacts selection of DBS settings. From a clinical perspective, an optimal DBS setting is one that minimizes symptom (tremor) severity, does not induce side effects, and maximizes device battery lifetime. However, from the plot in Figure 3.9, we can see that these competing objectives are often at odds with one another: DBS settings that reduce symptoms are more likely to induce side effects and have a shorter battery lifetime, and conversely DBS settings that have the longest battery lifetimes are likely to not induce side effects and not reduce symptoms as effectively.

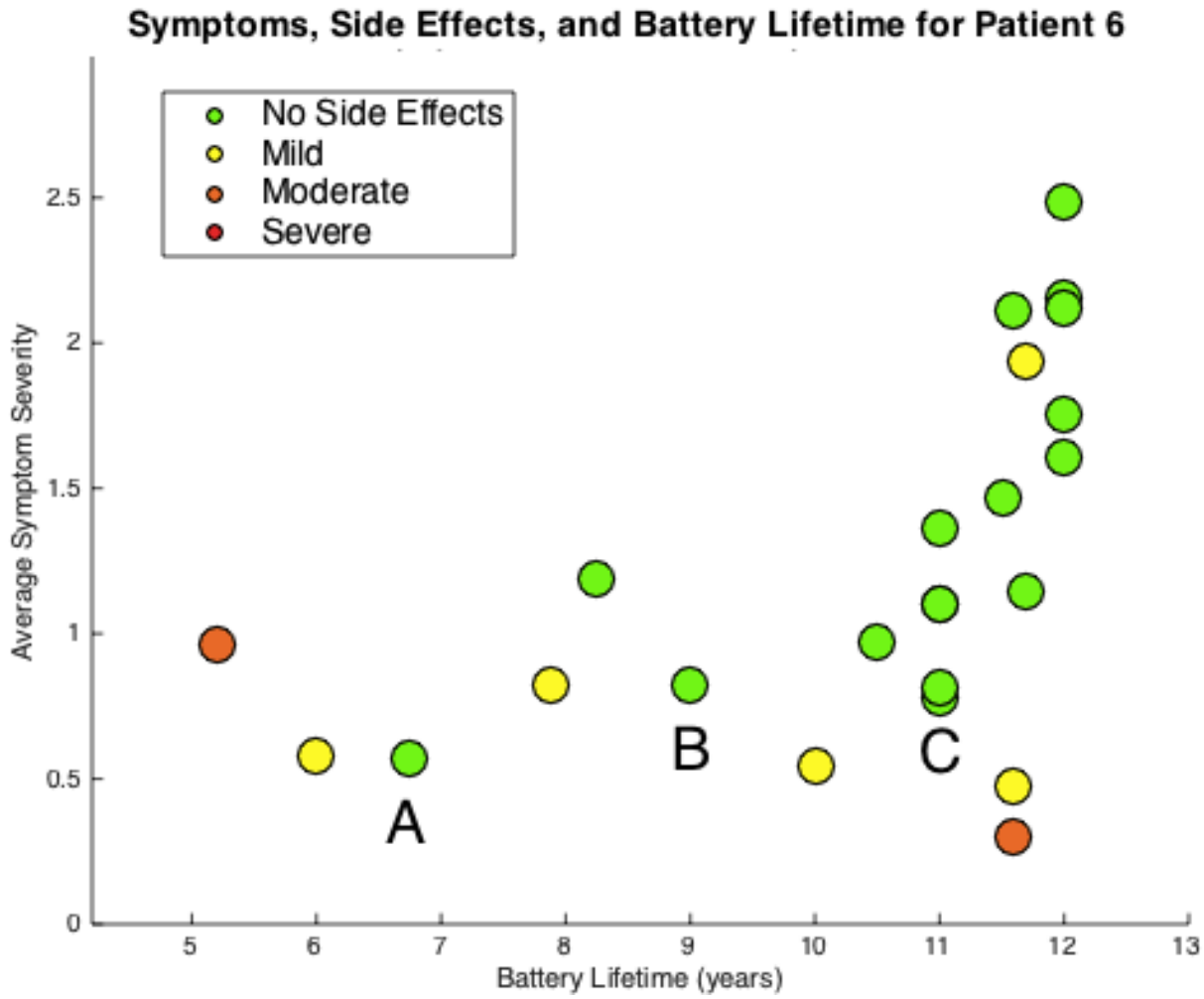

Figure 3.9: A Pareto plot showing the tradeoffs inherent to DBS programming. Each tested DBS setting during the automated DBS programming experiment for patient 6 is plotted in terms of its predicted symptom level (y-axis), estimated battery lifetime (x-axis), and side effects (color-coding).

This inherent tradeoff between DBS programming objectives requires that decision makers (clinicians and patients themselves) think carefully about how they value therapeutic, symptom-reducing benefits of DBS versus the possibilities of inducing side effects and maximizing battery lifetime. Assuming that patient 7 would not rationally choose a DBS setting that induce side effects - as no DBS settings confer such an advantage in the other two

objectives to warrant such a decision - consider the DBS settings labeled **A**, **B**, and **C** in Figure 3.9. DBS setting **A** has the lowest estimated symptom severity among the "no side effects" DBS settings, but also has the shortest estimated battery life at just under 7 years. DBS setting **B** has a slightly higher level of estimated symptom severity - about 0.25 points higher on the UPDRS scale - while also delivering 2 additional years of battery life. Further, DBS setting **C** provides about the same benefit as **B** in reducing symptoms while providing an *additional* 2 years of battery life, to an estimated lifetime of 11 years.

In order to decide between DBS settings **A**, **B**, and **C**, we can introduce the idea of dominance with respect to Pareto optimality. Dominance is perfectly illustrated by comparing DBS settings **B** and **C**. These two DBS settings are equally effective at reducing symptoms, while DBS setting **C** confers about 2 additional years of battery life. Therefore, the only rational DBS programming decision to make between **B** and **C** is to select DBS setting **C**.

It should also be noted that optimizing DBS settings for symptoms measured by the wrist-worn smartwatch might leave other aspects of PD and ET untreated. For instance, ET patients can experience head tremor and lower extremity tremors, and optimal DBS settings for hand tremor may have to be adjusted to provide coverage for all types of bodily tremor. Similarly, PD patients also commonly experience bradykinesia, rigidity, and postural instability and other gait impairments, and these symptoms may require different DBS settings than treating tremor alone. Furthermore, these symptoms respond to DBS at longer than timescales than tremor [49], which may necessitate longer-term strategies for monitoring and evaluation in order to automate DBS programming. Bradykinesia severity is typically assessed with the UPDRS using finger tapping and hand pronation/supination tests, and the quantification of these tests has been explored in prior studies using IMUs [30][31], which suggests that automated DBS programming for bradykinesia could be achieved with the system described in this Chapter. Additionally, programming could be based around hypothesized disease-state biomarkers, such as beta band synchronization in PD [50], and some candidate neural biomarkers in ET that will be explored in Chapter 4.

Other study limitations and areas for improvement can be found in the algorithms used

for automated search. The method for optimization in this study relied on formulating a patient-specific model of tremor response to DBS parameterized by the monopolar or advanced programming screen, which assessed DBS response to stimulation of varying intensity on the four possible monopolar stimulation configurations or multiple bipolar stimulation configurations. The optimization procedure predicted DBS values for untested intermediate DBS amplitude settings by interpolation of DBS values at the 1 V increments in the monopolar screen or advanced programming screen. The driving assumption behind this approach was that DBS settings with the same stimulating contact configuration and proximate stimulation amplitudes would evoke predictable and therapeutically valuable DBS responses, and the results shown in Figure 3.5 support this assumption. However, in only considering correlations between DBS settings based on stimulation amplitude, this approach neglects possible correlations between different stimulating contact configurations. For example, electric fields generated by adjacent monopolar contact configurations (e.g. C+1- and C+2-) may overlap, and thus there may be significant correlation between their respective tremor suppression and side effect inducing properties. Moreover, the electric field created by a bipolar contact configuration (e.g. 1+2-) will overlap and can be expected to share properties with these monopolar contact configurations. Therefore, a more sophisticated way to guide automated programming, advanced programming recommendations, and optimization could involve using estimates of shared volume of tissue activated (VTA) by the electric fields generated by various stimulation contacts, amplitudes, and pulsewidths in order to systematically select new DBS parameters for testing.

Future experiments for automated DBS programming will aim to expedite optimal DBS parameter selection through further algorithm innovations. Overlong automated programming sessions can be fatiguing for patients, and this may compromise the accuracy with which tremor is assessed during testing. In this study, we performed the full monopolar screen for each patient, however there are multiple ways in which the screen could be shortened based on online results of each DBS setting assessment. For one, if during the monopolar screen a DBS setting is tested that provides an adequate level of tremor therapy without inducing side

effects then the search can be focused in on that stimulation contact and amplitude through the optimization procedure, and other monopolar contacts can be effectively removed from consideration. Another possibility is that a DBS setting is found to induce side effects, which would suggest that higher amplitude settings on the same contact would also induce side effects, and so these DBS settings could also be removed from consideration. Knowledge of typical patient DBS response can be used to further optimize the search strategy for automated programming. As Figure 3.4 shows, tremor is generally more effectively treated with increasing stimulation amplitude, while stimulation-induced side effects are also more likely to be evoked. Therefore, another effective strategy for enhancing automated DBS programming may be to concentrate the search for DBS settings in this regime of moderate stimulation amplitudes where clinical benefit is expected, known as the "therapeutic window". Incorporating this logic into the automated DBS programming decision-making could significantly shorten the number of tests required for patients to achieve satisfactory levels of DBS therapy.

Chapter 4

NEURAL CORRELATES OF EFFECTIVE DEEP BRAIN STIMULATION FOR ESSENTIAL TREMOR

In this chapter we explore an extension of the automated DBS programming study of Chapter 3 to investigate possible neural biomarkers of effective DBS for essential tremor. The motivation behind this study is that tremor is an inherently random and unpredictable signal, with a number of factors influencing a patients momentary expression of tremor, including DBS setting, time since last medication dosage, stress, muscle fatigue, and many other factors. Therefore, patient tremor response to DBS during time-limited programming sessions may not reveal the true, long-term therapeutic value of any particular DBS setting. On the other hand, neural biomarkers may provide a stable signal that serves as a direct measure of DBS disruption of pathological processes in the brain related to tremor. Additionally, new investigational DBS devices, such as Medtronic's Activa PC+S, are equipped with electrocorticographic (ECoG) strips placed over motor cortex, which may be able to provide continuous insight into neural activity related to tremor and efficacy of DBS.

4.1 Background

The neurophysiological characteristics of Parkinson's disease (PD) and essential tremor (ET) pathology have been the subject of extensive study, serving both to elucidate mechanisms of disease and identify features that are causal or correlated to disease state or severity, which may be used to evaluate treatment efficacy. Although the experimental results described in this chapter concern only ET, it is instructive to also review allied studies in PD due to the noted similarities between the symptoms and neurophysiological manifestation of the

diseases, the shared platform for neuromodulation therapy, and the fact that PD has been studied in greater detail.

4.1.1 Neurophysiological mechanisms of Parkinson's disease

PD is characterized by dopaminergic cell death in the substantia nigra pars compacta (SNc), which is a small brain structure in the basal ganglia. The loss of these neurons, which provide both inhibitory and excitatory connections to the putamen, sets off a cascade of neurodynamical changes in the greater cortico-basal ganglia-thalamic loop in which the SNc is situated, a diagram of which is shown in Figure 4.1.

The SNc innervates two distinct dopaminergic pathways in the putamen: so-called "direct" and "indirect" pathways. The direct pathway is an excitatory branch from SNc to putamen that then relays an inhibitory connection from putamen to globus pallidus internus (GPi) and substantia nigra pars reticula (SNr). The indirect pathway is an inhibitory branch from SNc to putamen that then relays an inhibitory connection to the globus pallidus externus (GPe). The GPe then provides inhibitory connections to both the GPi/SNr and the subthalamic nucleus (STN), the latter of which also provides an excitatory connection to GPi/SNr. The GPi/SNr pair, in turn, sums the inhibitory connections from GPe and putamen, as well as the excitatory connections from STN, to output an inhibitory connection to the thalamus. The motor cortex receives excitatory connections from the thalamus and additionally provides excitatory connections back to thalamus and to the putamen and STN, as well as descending motor commands through the corticospinal pathways that eventually reach muscles.

The net effect of removing SNr from this vital motor pathway is exaggerated inhibition of thalamus via decreased inhibition and increased excitation of GPi/SNr. The increased inhibitory drive to thalamus weakens the excitatory connections relayed to and from motor cortex. The consequences of this reweighted neural network have been explored in numerous studies seeking biomarkers that indicate disease state and severity in PD.

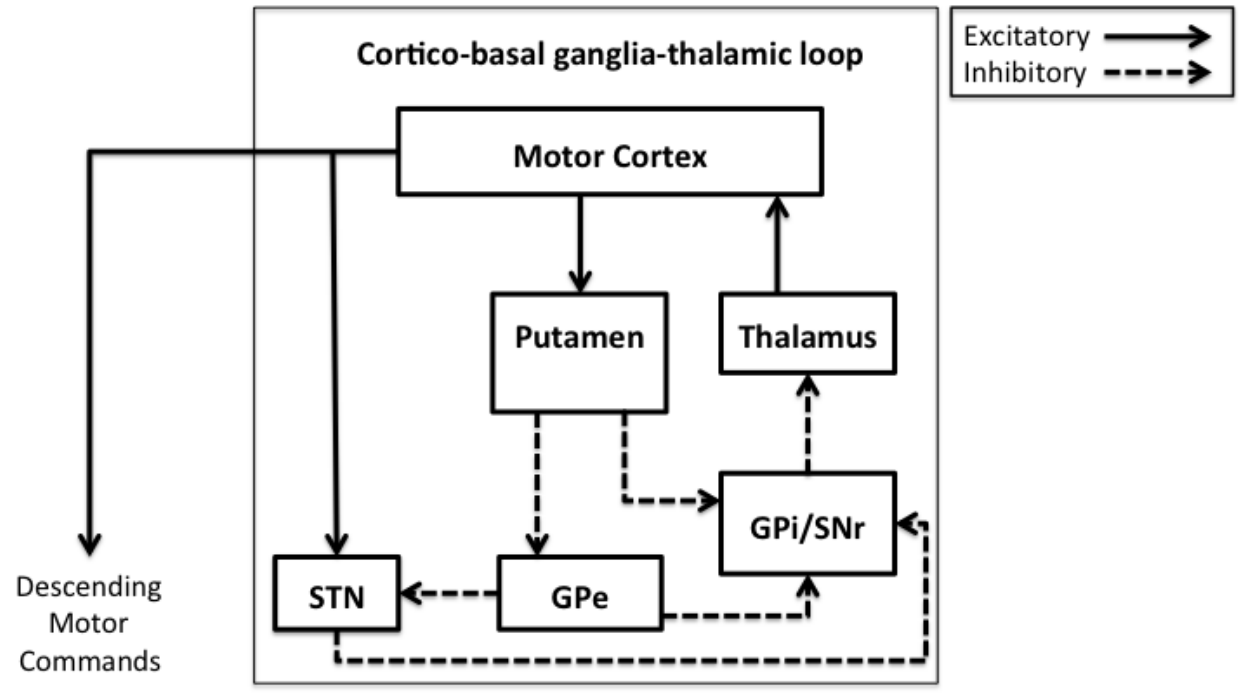

Figure 4.1: The network of brain structures implicated in the pathological cortico-basal ganglia-thalamic loop in Parkinson's disease.

4.1.2 Parkinson's disease biomarkers for DBS

The behavioral manifestations of Parkinson's disease are well known and typically obvious in patients exhibiting symptoms. Tremor, bradykinesia, rigidity, and postural instability or gait difficulties are all readily apparent and disabling motor features that afflict PD patients, however the search for neurophysiological underpinnings of such diverse and pervasive symptoms has been more difficult. Several clinical and experimental studies have outlined some of the hallmark features that arise from the degenerative cortico-basal ganglia-thalamic loop

characteristic to PD.

One of the most studied neurophysiological characteristics of PD to date has been the phenomenon of excessive beta band (13-30 Hz) synchronization, which has been observed in recordings of local field potentials (LFPs) in STN and other brain structures in the cortico-basal ganglia-thalamic loop [51]. A series of studies revealed the beta band in STN to be critical to understanding decision-making related to motor control: voluntary movements were shown to be accompanied by a reduction in beta band signal power in STN [52], and decisions to abruptly halt movement were shown to be accompanied by an increase in beta band signal power in STN [53]. Based on these studies, excessive beta band synchronization is thought to be particularly relevant to the pathogenesis of rigidity and bradykinesia in PD as it is apparently an antikinetic signal in nature. Furthermore, two of the common treatments for PD, levodopa and DBS, have been demonstrated to significantly reduce beta band signal power in STN, highlighting the potential use of this neurophysiological feature as a biomarker for treatment efficacy.

The effects of DBS are systemic and, as expected, not confined to modulating activity only within the targeted brain structures (STN, or less commonly GPi, in the case of PD). Stimulation of STN for PD in turn elicits orthodromic (i.e. downstream, postsynaptic targets) activation of GPi and antidromic (i.e. upstream, presynaptic targets) activation of motor cortex. Recent studies in animal models and human patients have demonstrated that motor cortex neurons are activated with short latency (1 ms) during therapeutically effective DBS [54][55].

In a study with human PD patients who were implanted with DBS in STN [55], clinicians tested a number of bipolar stimulation contacts, amplitudes, and frequencies while tremor was quantitatively measured and EEG activity was recorded from electrodes placed above motor cortex. Stimulation settings that were effective for eliminating tremor revealed synchronized event-related potentials (ERPs) from EEG recordings, demonstrating that cortical neurons were activated with short latency after stimulation pulses were delivered to STN. This cortical activation was determined to be the result of antidromic conduction due to the

short latency of activation, which precludes synaptic transmission through the regular downstream activation that would occur via GPi/SNr and thalamus. Furthermore, the possibility that EEG activity over motor cortex after stimulation pulses could be simply attributable to an electric artifact of stimulation was ruled out due to the EEG activity having opposite polarity of DBS and its nonlinear relationship with stimulation amplitude, unlike that of a stimulation artifact. Based on these observations, the study authors conclude that effective DBS for parkinsonian tremor synchronizes cortical activity to the stimulation frequency or one of its subharmonics, and that this effect is produced by altering the timing of cortical firing along the "hyperdirect" pathway to STN.

A comparable study in a rat model of parkinsonism expanded upon this study by using microelectrodes in cortex to examine single-unit activity in addition to LFPs in relation to the apparent desynchronization related effects of STN DBS [54]. This study recorded neural activity of Layer V neurons that project to STN, and there identified a short latency, antidromic spike associated with effective DBS as in the previously mentioned human study. Further scrutiny of antidromic activation in the Layer V neurons revealed that following the antidromic spikes, neurons underwent a biphasic shift in their firing probability that strongly suppressed activity for 1 ms and was followed by a period of increased excitability for 2 ms. Additionally, the occurrence of antidromic spiking was not uniform; therapeutically effective DBS settings for the rats (125 Hz) elicited a lower success rate (27%) yet also a higher frequency (30 Hz) for antidromic spikes, while lower, ineffective frequencies ($< 10Hz$) elicited a high success rate (80%) and lower frequency ($< 10Hz$) for antidromic spikes, and higher, ineffective frequencies (250 Hz) elicited an even lower success rate (10%) and slightly lower frequency (25 Hz) for antidromic spikes. Interestingly, the pattern of discharge for ineffective, low frequency stimulation induced antidromic spikes followed a uniform Gaussian distribution, while discharge for effective, high frequency stimulation induced antidromic spikes followed a random Poisson distribution. This latter case, in which cortical neurons randomly discharge in antidromic fashion following high frequency stimulation, suggests the possible therapeutic mechanism for DBS: pathological beta band synchronization

in the cortico-basal ganglia-thalamic loop is disrupted by replacement with more typical, randomized firing of these cortical Layer V projection neurons.

Another line of inquiry on DBS mechanisms related to pathological Parkinsonian brain states concerns the phenomenon of phase-amplitude coupling (PAC), which is believed to be a proxy measurement related to population spiking and synaptic input activity [56]. Normal motor cortical function relies on PAC between the phase of low frequency beta rhythms and amplitude of broadband activity (50-200 Hz), and movement initiation and execution is accompanied by a marked reduction in PAC. In PD patients, PAC between the phase of beta rhythms and amplitude of broadband activity is exaggerated, making movement initiation and execution difficult, and evoking the symptoms of bradykinesia and rigidity. This phenomenon is closely related to that of excessive beta band synchronization in STN mentioned previously, however it is more specific to the role of motor cortex in facilitating these rhythms, as prior studies have presented mixed results concerning whether beta band power is increased or decreased in motor cortex during clinically effective DBS. This study found unambiguously that PAC in motor cortex is markedly decreased during acute, clinically effective DBS, providing yet another possible lens through which PD therapy could be understood and quantitatively observed.

4.1.3 Neurophysiological mechanisms of Essential Tremor

Increasing evidence in animal and human studies suggest involvement of a network of distributed brain structures for the development and expression of essential tremor; these areas include the inferior olive, cerebellum, thalamus, and motor cortex [57]. The interactions of these distinct brain structures, which comprise the cerebello-thalamo-cortical loop, are outlined in detail in the following section.

The inferior olive is a structure within the medulla oblongata that is reciprocally connected with the cerebellum, receiving inhibitory inputs and sending back excitatory outputs, and its neurons contain specialized calcium channels capable of rhythmically discharging at the frequencies of peripheral action tremor [58], suggesting an involvement in essential

tremor. The inferior olive capacity for producing synchronous, tremor-frequency neuronal activity is disrupted through lesioning of the cerebellum, suggesting that cerebellar structures may be a critical mediator for expression of essential tremor [59]. Complementary to this observation are studies that show morphological changes in the cerebellum of ET patients [60], however it is not known whether these changes are the primary, or perhaps a secondary or downstream, cause or effect of neurodegeneration in ET. Oscillatory activity in cerebellum related to ET has also been observed using coherent source analysis with magnetoencephalography (MEG) and peripheral tremor sensors [61].

Evidence for thalamic involvement in ET comes from established therapies for ameliorating pathological tremor. Early approaches to ET treatment included lesions of the ventral intermediate nucleus of thalamus (VIM), which receives cerebellothalamic connections, and this was subsequently replaced by reversible, high frequency stimulation (i.e. DBS) of the same area. Studies of thalamic neurophysiological recordings have revealed tremor frequency oscillatory activity in VIM [62]. Thalamus is reciprocally connected with both the cerebellum and motor cortex, and driving oscillations coherent with peripheral muscular tremor activity have been observed in cortical EEG and MEG recordings [63], suggesting that cortex is also a mediator of pathological ET rhythms.

These findings provide a picture of ET as an intertwined network of synchronously active brain regions, and an illustrative schematic is shown in Figure 4.2. Some studies have suggested that these distributed brain regions are all simultaneously activated during pathological tremor in ET [63], while others demonstrate intermittent activity in motor cortical regions related to tremor [57]. In ET there is an apparent reciprocal coupling of activity between thalamus and motor cortex during tremor, while in healthy subjects voluntary oscillatory motion at tremor frequencies is merely accompanied by oscillatory activity transmitted from thalamus to motor cortex [64].

This discrepancy between the directionality of tremor-related thalamocortical activity in ET (bidirectional) and healthy subjects (unidirectional, from thalamus to cortex) suggests a possible mechanism of action for DBS in delivering therapy for tremor. It is possible that

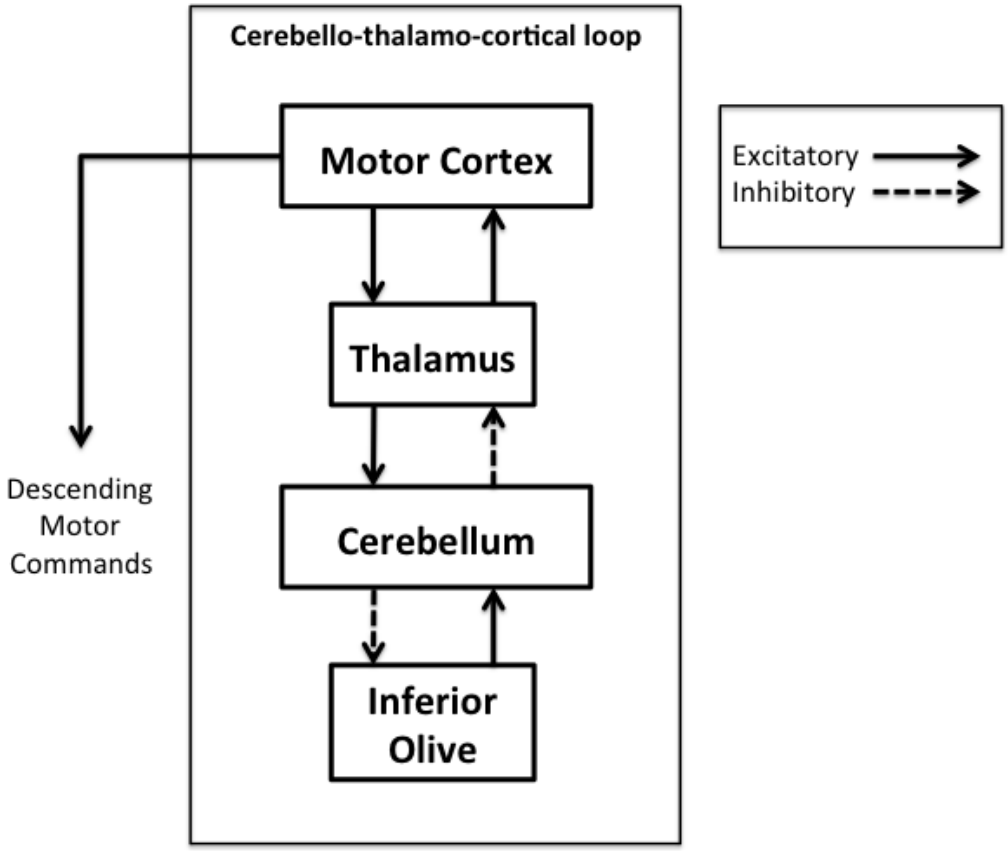

Figure 4.2: The network of brain structures implicated in the pathological cerebello-thalamo-cortical loop in essential tremor.

therapeutically effective DBS for ET acts by blocking the flow of information from motor cortex to thalamus. It is unclear, however, why stimulation must be delivered at high frequencies (typically greater than 130 Hz) to achieve this effect. The selective effectiveness of high frequency stimulation was explored in a computational study using model thalamocortical relay neurons, and it was demonstrated that stimulation frequencies above 100 Hz elicited inhibition of neuronal firing in the target nucleus while also activating downstream targets, such as motor cortex this proposed mechanism of DBS was dubbed an "informational lesion" [65]. Although high frequency thalamic stimulation is the accepted clinical

standard for both ET and PD, recent studies have demonstrated the efficacy of destructive interference stimulation, i.e. stimulation pulses delivered out of phase with and at the same frequency of centrally driven peripheral tremor [66].

4.1.4 Essential Tremor Biomarkers for DBS

In contrast to DBS for PD literature, there have been comparatively few studies examining characteristic neurophysiological activity related to DBS effectiveness for ET therapy. Notably, there have been two studies examining cortical activity in relation to DBS therapy for ET using EEG [67] and ECoG [68].

The first study, investigating recorded EEG activity over motor cortex during effective and ineffective DBS therapy for ET [67], is essentially a companion study to the biomarker EEG study previously reviewed for PD [67]. As in the PD study, clinicians tested a number of bipolar stimulation configurations, amplitudes, and frequencies for VIM DBS while tremor was quantitatively measured and EEG activity was recorded. Similar to the companion PD investigation, the study produced evidence of synchronized, short latency (1 ms) antidromic spike activity from ERPs in EEG recordings over motor cortex, and found a nonlinear relationship between stimulation amplitude and the resulting antidromic ERP amplitude and reduction in tremor. As in the PD study, the investigators conclude that effective VIM DBS for ET synchronizes cortical activity to the stimulation frequency or one of its subharmonics, and that effective DBS therefore alters the precise timing of cortical discharge to the cerebellar region of thalamus. This study suggests a possible mechanism behind the proposed "informational lesion" effect of therapeutic DBS.

Another study examining cortical activity during DBS was an intraoperative study investigating cortical LFP activity using ECoG [68]. In this study, ET patients who were undergoing neurosurgery for DBS implantation or thalamotomy had M1 and S1 ECoG activity recorded during various conditions related to movement, tremor, and therapy. This investigation focused on the effects seen in various frequency bands thought to be related to tremor and movement disorder pathology, including the theta band (4-8 Hz), alpha band

(8-13 Hz) and beta band (13-30 Hz). During high frequency DBS while the patient was at rest alpha band activity in M1 was significantly decreased and theta band activity in S1 was also significantly decreased. Compared to resting position, induction of a postural tremor pose significantly reduced theta, alpha and beta in M1. Thalamotomy, which is also effective for tremor therapy, resulted in increased theta and beta activity in M1. The study concluded that, because thalamotomy produces comparable therapeutic effects as DBS, the reduction in M1 alpha activity during high frequency DBS was probably not indicative of therapeutic efficacy. However, a very noteworthy limitation of this study was that, because it was performed intraoperatively and during the "lesion effect", which strongly suppresses tremor, seen immediately after electrode implantation, the therapeutic efficacy of DBS stimulation could not be assessed. Additionally, patients had been sedated for surgical procedures, which can cause significant changes in LFPs recorded in cortex relative to a normal waking state.

4.2 Methods

This study was conducted at the University of Washington Medical Center (UWMC), and we recruited patients who had enrolled in an ongoing study for closed-loop DBS using Medtronic's Activa PC+S through an FDA investigational device exemption (IDE). To date, 4 patients have enrolled in the study, however 2 of these patients were implanted within the last 6 months and still exhibit the lesion effect following surgery, which markedly reduces tremor and can mask the long-term therapeutic response of DBS settings. Therefore, the results presented here are only based on experiments with the first 2 patients, and subsequent patients will be tested over the next several months. All patients have essential tremor diagnoses and were implanted with unilateral DBS in VIM with the cortical ECoG strip placed over the ipsilateral arm areas of M1 and S1. Patient characteristics - including age, months since implantation, and clinical DBS settings - are shown in Table 4.2.

Table 4.1: Neural Biomarker Experiment Details

ID No.	**Age, Sex**	**Dx**	**DBS Target**	**Clinical DBS Setting**	**Experimental Settings**
P1	58, M	ET	**L** VIM	2+0-, 2.5 V, 90 μs, 140 Hz	(2+0-, 1+0-, 1+3-, 2+3-), 0 - 4 V, 90 μs, 140 Hz
P2	82, M	ET	**L** VIM	2+0-, 3.9 V, 90 μs, 140 Hz	(2+0-, 1+0-, 1+3-, 2+3-), 0 - 4 V, 90 μs, 140 Hz

4.2.1 System Description and Data Recording

The software system used in this study is identical to that described in Chapter 3, with a modification allowing for streaming and recording of neural recordings from the Activa PC+S. The Activa PC+S enables sensing and recording of neural activity from the implanted electrode (placed in VIM) and the cortical ECoG strip (placed over M1 and S1 arm areas). Nexus-D enables streaming of this data at a maximum rate of 422 Hz, which can be sampled entirely from either electrode or cortical sensors, or can be split to record and stream data from both sensors simultaneously at 211 Hz.

In this study, we recorded LFPs only from M1 (referenced against S1) at 422 Hz. Although VIM LFPs can potentially provide useful information about essential tremor and the effect of DBS, low amplitude neural activity in this region is mostly obscured by the large stimulation artifact of DBS. Cortical recordings also are affected by stimulation artifacts but to a lesser extent. From Figure 4.2 it is evident that both VIM (within thalamus) and M1 (motor cortex) are situated in the cerebello-thalamo-cortical loop, and LFPs recorded from these brain structures should provide information relevant to DBS efficacy.

4.2.2 Experiment Description

The aim of this study was to identify correlative or causative changes in recorded neural activity from motor cortex that are indicative of DBS effectiveness in ameliorating tremor

in ET patients. To accomplish this, we tested a range of DBS settings that were expected to be effective and ineffective based on each patient's clinical DBS settings, and evaluated their symptom severity in each DBS setting using the approach outlined in Chapters 2 and 3.

In this study we restrict the range of ineffective settings tested so that the frequency and pulsewidth are constant, and it is the stimulation contacts and amplitudes that are varied. It is simply not possible to test even a substantial portion of ineffective DBS settings, and, for the most part, stimulation frequency and pulsewidth are consistently set between 130-160 Hz and 60-90 μs for treatment of tremor. By instead only testing various stimulation amplitudes and contact configurations, which in turn specify the volume of neural tissue activated by DBS (along with pulsewidth), this study tests the hypothesis that effective DBS activates motor cortex via stimulation of specific downstream thalamic targets, and this line of reasoning has been employed in prior studies investigating DBS effectiveness in ET [67][68].

In addition to tremor tests (postural and kinetic tremor tests for ET patients) and side effects reports that were performed and collected for evaluation of each DBS setting, there was an additional period of "rest" lasting 10 seconds where neural activity was recorded while the patient was comfortably seated with their arms at their sides. The purpose of the rest period was to evaluate neural activity in response to a particular DBS setting in a controlled setting without the presence of potentially confounding effects of movement on cortical activity.

4.2.3 Signal Processing

All recorded neural activity was analyzed offline, and data was first filtered using a Type II Chebyshev band pass filter from 1 to 80 Hz to remove the presence of stimulation artifacts. Spectral estimates were obtained using Welch's method which was computed using 422 FFT points thereby provide 1 Hz resolution of power spectral density (PSD) estimates.

Unlike previous intraoperative studies using ECoG where neural recordings can be ref-

erenced against a truly grounded material outside the brain, the implanted Activa PC+S recordings must be referenced against another implanted electrode, which records its own electrical activity. This is one of the major challenges of recording and interpreting neural activity in a fully implanted system. In these experiments, we referenced M1 recordings against an electrode placed over S1. If we assume that M1 and S1 can be considered independent random signals, then the following relationship will hold for the PSD estimates of recordings of M1 referenced against S1:

$$PSD(M1 - S1) = PSD(M1) - PSD(S1) \tag{4.1}$$

That is, the PSD of M1 recordings referenced against S1 is equivalent to the difference between the PSD of M1 and the PSD of S1. This is an important distinction to draw when comparing results from this study against past intraoperative ECoG studies in which reference was a true ground [68]. Any change in recorded frequency band activity could be attributable to either a change in M1 or S1 or both. For example, if recorded beta band activity drops during a certain condition, it could be attributed to a drop in beta band activity in M1 relative to stationary beta band activity in S1, an *increase* in beta band activity in S1 relative to stationary beta band activity in M1, or any relative changes in which the magnitude of M1 beta band activity reduction is greater than S1 beta band activity reduction or S1 beta band activity increase is greater than M1 beta band activity increase.

It should be noted that the assumption that M1 and S1 represent independent random signals may not strictly be true, and this would result in a more complex relationship between respective PSDs of M1 and S1 as in 4.1. Particularly as the targeted M1 and S1 regions contain motor and sensory information about arm movements, there may be significant correlation between frequency bands in their respective PSDs. For example, arm movement commands are generated in M1, and proprioceptive signals related to changing arm positions will be relayed back to S1. Thus, the independence assumption between M1 and S1 would

seem not to hold during movement tasks, but may be more valid during rest when the motor execution-proprioception loop is not engaged, although there may be other sources of correlated sensorimotor activity. Therefore, we will focus our analysis on PSD estimates obtained during rest as a means to evaluate significant changes in M1 and S1 activity in various DBS settings.

4.2.4 Candidate Neural Biomarkers for ET

Based on prior studies investigating effective DBS settings for ET therapy [67][68] we focus our analysis in this chapter on a number of spectral features from recorded neural activity: subharmonic (70 Hz) power and theta (4-8 Hz), alpha (8-13 Hz) and beta (13-30 Hz) band power. Subharmonic power was implied as a biomarker by the study investigating antidromic activation of motor cortex during clinically effective DBS [Walker]. Theta and alpha band activity overlap with typical tremor frequencies expressed at the periphery by ET patients, and beta band activity is known to be related to various states of movement.

4.2.5 DBS and Tremor Conditions

Recorded neural signal power varies highly between patients due to differences in electrode placement and impedance in addition to patient specific anatomical and neurophysiological differences. Due to this, we make candidate biomarker comparisons across subjects by analyzing the difference in estimated signal power relative to a baseline measure. Specifically, we use for a baseline measurement the estimated signal power for each candidate biomarker (subharmonic, theta, alpha, and beta) while DBS is off (0 V) and the patient at rest, which is recorded 4 times throughout each experiment. We compare both effective and ineffective DBS settings for reducing tremor against this baseline measure, each of which are identified from quantified IMU-predicted tremor scores, as in Chapters 2 and 3. Effective DBS settings for tremor are those which provide at least a 90% reduction in the total tremor reduction seen across all DBS settings for each patient, and ineffective DBS settings do not satisfy this criteria and also require that stimulation is on. None of the DBS settings evaluated for these

patients induced persistent side effects, so consideration of this alongside tremor value is not necessary.

4.3 Results

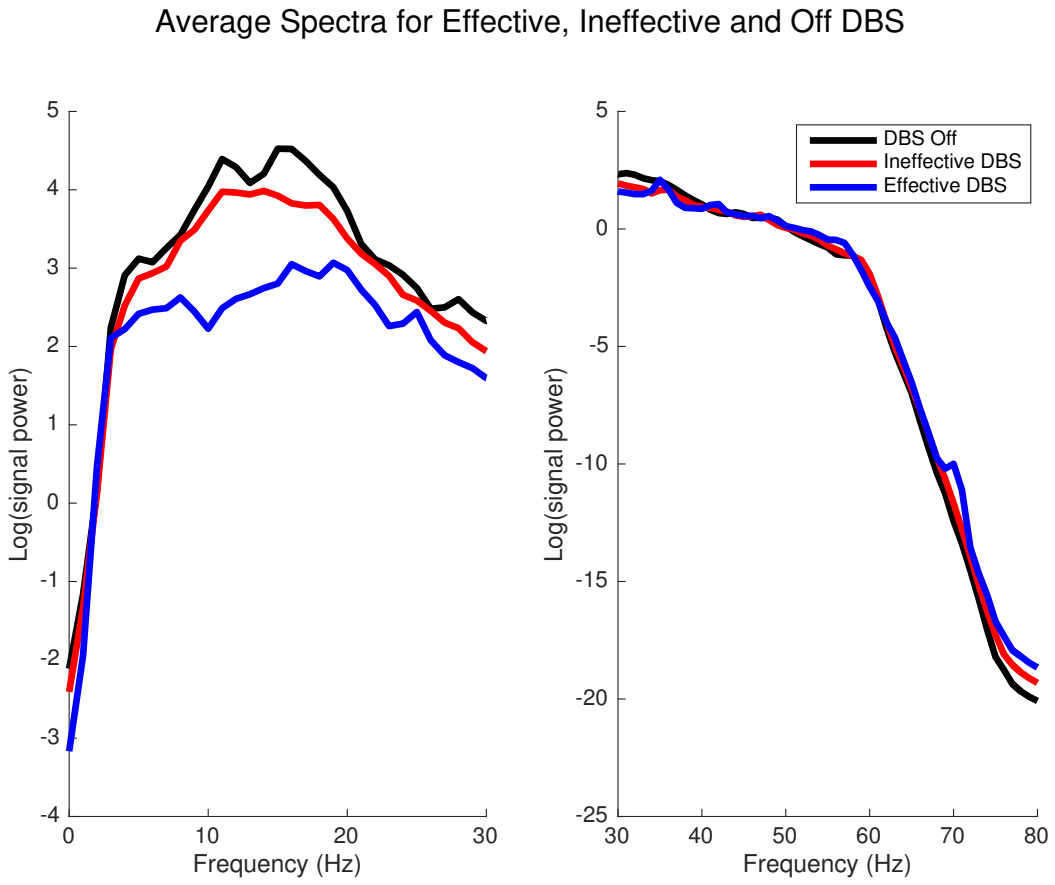

Figure 4.3: Average spectra from recorded ECoG LFPs over motor cortex for effective, ineffective, and off DBS. The plot at left shows the spectra from 1-30 Hz, and the plot at right shows the spectra from 30-80 Hz.

Based on the results of the automated programming experiment using the parameters defined in Table 4.2, there were a total of 6 *effective* DBS settings (5 for P1, 1 for P2) , 26 *ineffective* DBS settings (11 for P1, 15 for P2), and 8 "off" settings (4 for P1, 4 for P2) tested.

Figure 4.3 shows the average spectra recorded from ECoG LFPs during effective, ineffective, and off DBS conditions. From the average spectra plots, it is apparent that effective DBS generally has lower signal power in the lower frequency range comprising theta, alpha, and beta bands than ineffective DBS or off DBS. Additionally, effective DBS has higher signal power at 70 Hz than ineffective or off DBS, which is the subharmonic (f/2) associated with the stimulation frequency (140 Hz). Effective, ineffective and off DBS had indistinguishable differences in signal power level at low frequencies (¡ 5 Hz) and moderate frequencies above the beta band (30 - 65 Hz).

In order to determine whether the differences in LFP signal power were significant in the frequency bands of interest (theta, alpha, beta, and subharmonic/70Hz), we performed a grouped analysis of average signal power in the bands by the DBS condition (effective, ineffective, off). We then used a Wilcoxon rank-sum test to determine whether the average signal power in each frequency band for each of the DBS conditions belonged to the same distribution (null hypothesis) or a significantly different distribution.

The left plot of Figure 4.4 shows the average theta band (4-8 Hz) power estimated from recorded ECoG during effective, ineffective and off DBS. Wilcoxon rank-sum test results indicate that effective DBS results in significantly lower ($p < 0.01$) theta band power than both ineffective and off DBS. The right plot of Figure 4.4 shows the average alpha band (8-13 Hz) power estimated from recorded ECoG during effective, ineffective and off DBS. Wilcoxon rank-sum test results indicate that effective DBS results in significantly lower alpha band power than both ineffective ($p < 0.01$) and off DBS ($p < 0.005$).

While theta, alpha and subharmonic band activity had consistent signal power levels between the two patients tested, beta band power did not, which prevented a meaningful, direct comparison between power levels in different DBS conditions. Therefore, in order to make a meaningful comparison across subjects for beta band power between different DBS conditions we subtracted off the baseline power level recorded in off DBS (0 V). The left plot of Figure 4.5 shows the average beta band power for effective and ineffective DBS referenced against beta band power when DBS was off for each patient. Wilcoxon rank-sum tests

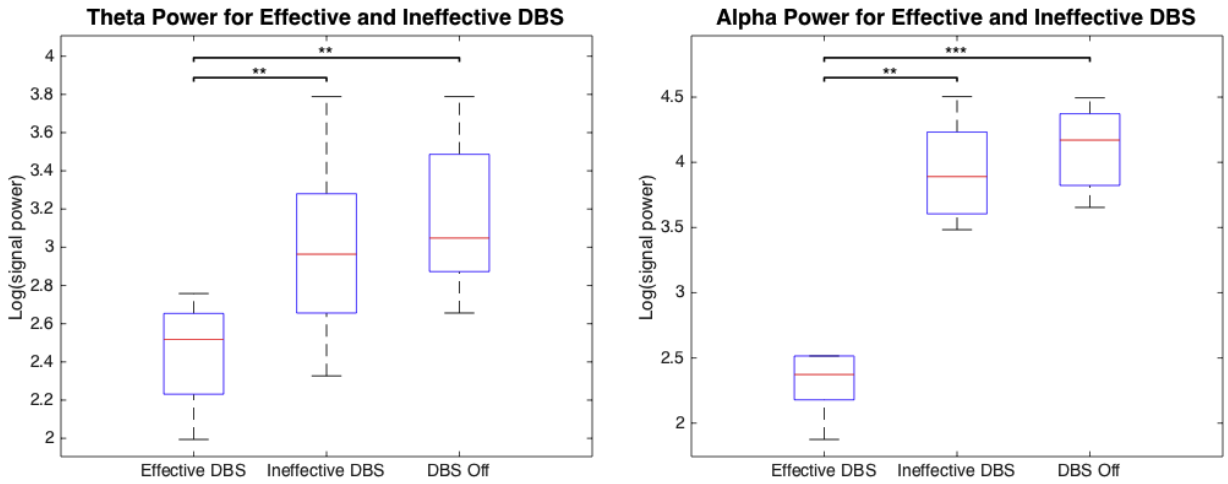

Figure 4.4: At left: average signal power in the theta band (4-8 Hz) for effective, ineffective, and off DBS conditions. Wilcoxon rank-sum tests indicate that effective DBS results in significantly lower theta band power during rest than ineffective and off DBS ($**p < 0.01$). At right: average signal power in the alpha band (8-13 Hz) for effective, ineffective, and off DBS conditions. Wilcoxon rank-sum tests indicate that effective DBS results in significantly lower alpha band power than ineffective ($p < 0.01$) and off DBS ($p < 0.005$).

indicate that beta band power is significantly lower during effective DBS than ineffective DBS ($p < 0.005$). The right plot of Figure 4.5 shows the average 70 Hz subharmonic power during effective, ineffective, and off DBS. Wilcoxon rank-sum tests indicate that the 70 Hz subharmonic power is significantly increased during effective DBS compared with ineffective DBS and off DBS ($p < 0.01$).

4.4 Data Significance

This study presented evidence of reduced theta, alpha, and beta band signal power and increased subharmonic, 70 Hz signal power from recorded ECoG LFPs from M1 referenced against S1 during effective DBS compared with ineffective and off DBS conditions during rest. These results suggest a possible mechanism for discriminating the therapeutic effect of DBS settings based on analysis of neural signals alone, circumventing the typical approach

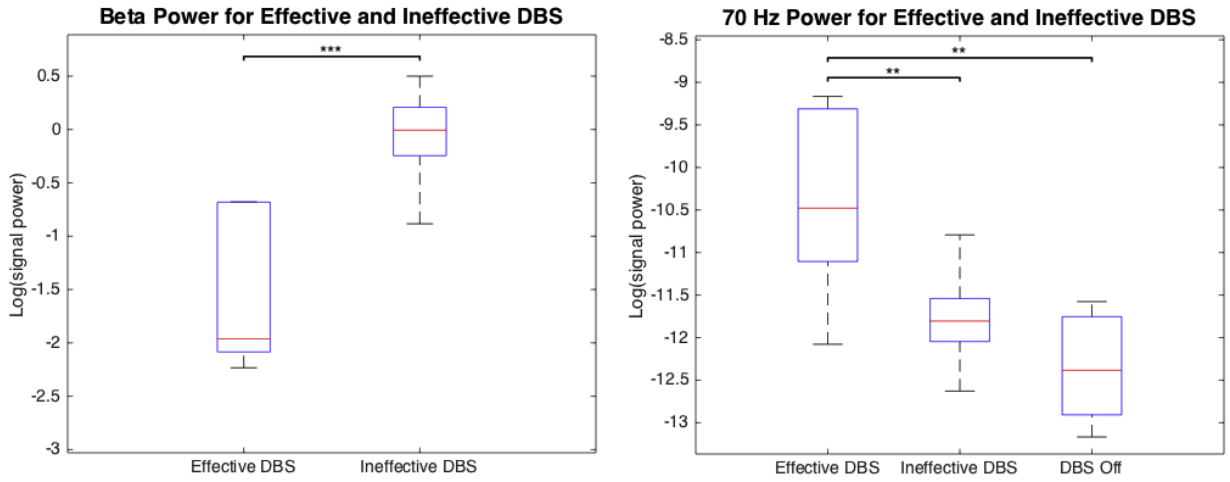

Figure 4.5: At left: average signal power in the beta band (13-30 Hz) for effective and ineffective DBS referenced against off DBS (0 V). Wilcoxon rank-sum tests indicate that effective DBS results in significantly lower beta band power during rest than ineffective DBS ($**p < 0.005$). At right: average signal power in the 70 Hz subharmonic band for effective, ineffective, and off DBS conditions. Wilcoxon rank-sum tests indicate that effective DBS results in significantly lower alpha band power than ineffective or off DBS ($p < 0.01$).

of having patients perform overt motor tasks that elicit tremor.

Theta (4-8 Hz) and alpha (8-13 Hz) bands in ECoG LFPs comprise the frequency bands overlapping with typical tremor frequencies observed in peripheral limb oscillation in essential tremor (4-12 Hz). Moreover, it has been suggested in PD that the central drive of tremor is derived from excessive synchrony at the tremor frequency (typically 4-8 Hz in PD) and *double* the tremor frequency (8-12 Hz), owing to the need to alternately activate antagonistic muscle pairs to produce the oscillations seen in tremor. Therefore, the significant reduction in theta and alpha activity seen during effective DBS compared with ineffective and off DBS could indicate a direct measure of a silencing of tremor-generating neural activity in the cerebello-thalamo-cortical loop.

It is less clear how an apparent reduction beta band power during effective DBS could be related to mechanisms of pathological tremor. Beta band desynchronization is known to be related to the initiation of movement, however the data reported here were recording during

rest. Additionally, high frequency DBS is known to cause desynchronization of beta band activity, which is indicative of the therapeutic anti-akinetic effects of DBS for bradykinesia in Parkinson's disease. It is possible that the significant reduction in beta band power observed during effective DBS compared with ineffective DBS and off DBS is actually attributable to the typically higher amplitude stimulation of effective DBS compared with ineffective DBS. Higher amplitude DBS may have more potent beta desynchronization effects than lower amplitude DBS, and thus beta band power reduction could be correlated to high stimulation amplitudes rather than therapeutic efficacy.

4.5 Future Applications

In this chapter we presented prelimiinary evidence of neural biomarkers that correlate with behavioral measures of effective DBS for reducing tremor in essential tremor patients. These neural biomarkers may provide evidence of excessively synchronized oscillatory activity in the cerebello-thalamo-cortical network, in the case of alpha and theta band activity, or they may be the result of neurophysiological effects of DBS, as in the case of reduced beta band activity and subharmonic 70Hz activity. In any case, Figures 4.4 and 4.5 provide compelling evidence that effective DBS settings for reducing pathological tremor can be identified on the basis of neural activity recorded during rest, possibly circumventing the requirement for patients to perform overt, fatiguing motor tasks to evaluate symptoms.

The ability to avoid overt tremor task performance during programming may provide several advantages in future automated DBS programming applications. For one, peripherally measured tremor can be inconsistent, and is dependent upon a number of factors, including fatigue, anxiety, and medication levels, and this may preclude optimal assessment of symptoms required to effectively select therapeutic DBS settings. By contrast, neurophysiological data may provide a direct measure of DBS-mediated disruption of tremor-related brain activity, and may therefore be a preferred surrogate measurement to tremor.

Another advantage of neural-based DBS programming is that it may provide adequate or even improved DBS programming performance while requiring significantly less time and

effort from patients. The results presented in this chapter are based on 10 seconds of recorded neural data in each DBS setting while the patients were idle at rest. By contrast, performance of each tremor test in Chapter 3 and for tremor evaluation in this study took 10 seconds, and all patients were tested on multiple tremor tests, extending testing time for each DBS setting to up to one minute plus additional for washout. When scaled by the number of DBS settings tested during programming, tremor test-based programming sessions can last up to an hour for complex cases, testing dozens of different DBS settings. The same amount of DBS settings could be tested through neural-based programming in a fraction of this time. Additionally, since neural-based programming may not require, and may actually discourage, patient movement, patients can achieve programming without expending the effort required of tremor-based testing. Patient fatigue during DBS programming sessions can, among other things, impact how effectively tremor is evaluated, thus potentially compromising the selection of DBS settings for chronic therapy. Neural-based testing can be achieved while the patient is entirely passive and may be performed while watching television to fix their attention away from incidental movement. Therefore, neural-based sensing may allow for shorter evaluation times for DBS settings, thus allowing more potential DBS settings to be tested and evaluated for selection of optimal therapy parameters.

Neural-based DBS programming could confer considerable advantages over tremor-based in terms of data collection and neuroinformatics. Due to the shorter evaluation times required, it is conceivable that neural-based DBS programming could allow considerably more DBS settings to be tested in the time of a typical DBS programming session, thereby enabling greater amounts of data concerning stimulation effectiveness to be gathered. Data-intensive discovery and research could be used to elucidate neural mechanisms of disease in PD and ET, better understand the effects of DBS on neural activity, and better understand how the tremendous variety of DBS settings are related to one another, a topic that will be explored in the next chapter.

The final advantage of neural-based testing to be addressed is that it potentially consolidates all stimulation, device control, and sensing hardware into the implanted system. The

automated DBS programming system described in Chapter 3 requires the use of external sensors and PC laptop for sensing tremor severity and making decisions and stimulation changes for the implanted system. A neural-based DBS programming session could conceivably be achieved solely by the embedded sensing and stimulation hardware. This raises the possibility that such a DBS system could periodically or continuously self-adapt to optimize patient therapy in an inscrutable manner without requiring patients to wear any additional devices or perform evaluative tests.

Chapter 5

AUTOMATED DEEP BRAIN STIMULATION PROGRAMMING GUIDED BY PATIENT-SPECIFIC ELECTRIC FIELD MODELS

In this chapter we provide additional context for automated DBS programming by realizing the physical substrate onto which DBS configurations are mapped. Every possible DBS configuration produces a volume of tissue activation (VTA) that can be accurately estimated through detailed computational modeling. The result is a sort of library of stimulation configurations that serve as the basis for an automated DBS programming "search engine". We also motivate the use of automated search algorithms and show that optimal search algorithms for DBS programming may reduce the number of tested DBS settings to achieve satisfactory therapy. This chapter does not present new experimental results, but rather reconceptualizes results from Chapter 3 to envision a more sophisticated approach to automated DBS programming that will be explored in planned future experiments.

5.1 Background

5.1.1 Volume of Tissue Activated during Deep Brain Stimulation

The most substantial efforts aimed at automated DBS programming in the literature have not actually been empirical methods like those presented in Chapters 2 and 3, but rather the use of detailed computational modeling and sophisticated medical imaging to predict the intersection of volume of tissue activated (VTA) by DBS parameters and targeted neural structures for therapy. This resource-intensive approach has been validated in some studies [45] but may also face considerable impediments to widespread clinical adoption. First, this approach relies on brain atlas data, which is based on a very limited sample of post-mortem

tissue samples, and may not be representative of full breadth of patient variability. Also, high-detailed imaging results are required, which incur a significant healthcare expense, and it may not be practical to demand such a procedure every time a patient requires re-programming. This latter point hints at perhaps the greatest detraction of the combined VTA-imaging approach to programming: a lack of flexibility in methodology that may actually *increase* the cost of programming rather than reducing it.

However, VTA-based analyses may support empirical approaches to automated DBS programming in ways that do not depend on imaging or assumptions about brain anatomy. By mapping out the shared space of VTA between different DBS settings and configurations, we can develop a model that predicts the therapeutic value of untested, possibly obscure, DBS settings based on tested DBS settings that occupy overlapping spaces. This approach may represent a scalable method for automating the entire process of DBS programming, including the algorithmic details of search.

Computational prediction of neurostimulation VTA is idealized as a coupling between finite-element modelling (FEM) of electric field data with multi-compartmental neuron models [69]. However, this approach is too computationally expensive for most applications, and would be prohibitive for the aims of this Chapter (to simulate an entire template, or library, of DBS parameters' VTAs). A simplified approach, based on determining activating functions (AFs), relies on computing the second spatial derivative of extracellular voltages emanating from the electrode [70]. In this formulation, a uniform grid of neurons are arranged in a virtual space surrounding the simulated electrode, and a neuron is included in a particular DBS configurations VTA if an action potential is elicited. More recently, this approach was extended to predict a range of stimulation configurations, including multiple cathodic (double monopolar, double bipolar) and anodic (bipolar) configurations, using artificial neural networks (ANNs) [71].

Estimating the VTA for DBS configurations is based on many parameters, some of which may be difficult to estimate. Electrode impedance data can be obtained from a module on patients' implanted IPGs, and together with nominal voltage/current, pulsewidth, and

contact configuration settings, in addition to the geometry of electrode and contact spacing, this data can be used to determine the spatial extent of electric fields generated by DBS settings. However, the physical characteristics of simulated neurons, specifically the axon diameters, cannot be easily estimated, and yet this is a major determinant of how intense an extracellular electric field is required to elicit neuronal activation. Therefore, while this approach is a sophisticated method for simulating the exact regions in neural space relative to the electrode that are activated during DBS, it is not without potential sources of error.

5.1.2 Online Search and Optimization Algorithms

In this chapter we will also explicate a strategy for performing online search and optimization of DBS settings for PD and ET therapy. There are two critical features of the DBS programming problem that will determine which methods and algorithms are appropriate for use. First, DBS programming requires that a large number of potential DBS settings be considered, and yet it is only practical to test a very limited set during actual programming sessions. Therefore, an appropriate search algorithm for DBS programming need consider many options and test them efficiently.

The second feature relevant to DBS search and optimization is that the function used to evaluate DBS settings during programming, namely the J_{DBS} equation 3.1 from Chapter 3 , is very noisy and prohibitive of accurately estimating a derivative. Specifically, patient response to DBS is highly variable, as tremor and other movement disorder features are inherently unpredictable and even side effects can be reported with some variability. This feature of DBS programming suggests that we use *derivative-free optimization* techniques in our pursuit for efficient search algorithms, as classical methods in optimization requiring gradient computations may be of little practical use.

There are many derivative-free optimization algorithms that have been developed for and applied to a variety of problem domains in the literature [72]. The most simple approach is *brute force search*, an exhaustive search technique in which all candidates are tested and evaluated. The initial monopolar screen experiment in Chapter 3 is an example of a brute

force search, and when the number of candidate DBS settings is small, this can be an effective strategy for programming. However, as many patients are likely to require more complex configurations to obtain an acceptable balance between therapeutic effects and side effects, more sophisticated methods for search will demand consideration.

The VTA method for computing the physical representation of DBS settings can provide a template or model that could be useful in directing search algorithms. For many derivative-free algorithms, search performance can be considerably enhanced through designating quantitative relationships between different candidates in consideration. A model describing DBS settings during programming may, for instance, be driven by correlations between the different DBS settings which can be estimated by their shared overlap in VTA, the logic being that DBS settings that activate similar volumes of tissue should produce similar therapy values and side effects.

Search algorithms that can capitalize on value estimates or shared correlation between candidate choices include the well-known class of *genetic algorithms* (GA) [73]. Rooted in evolutionary biology theory, GAs work by randomly seeding and testing candidates and then generating new, similar candidates in subsequent rounds of testing based on which prior candidates were the most successful or valuable, thus approximating the biological processes of mating, replication, and mutation. The downside to GAs are long convergence times that may be prohibitive for automated DBS programming applications in their current tremor-based mode of evaluation.

More recently a class of search and learning policies has emerged that works in a much more deliberate and directed manner than GAs, and these algorithms include the knowledge gradient (KG) and multi-armed bandit (MAB) [74]. These algorithms use information about each candidates estimated mean, variance, and correlation other candidates' means to drive a search policy. In brief, KG and MAB algorithms pursue testing of candidates that are either thought to be valuable or of which little is known, and in doing so form a learning policy that is considered myopically optimal. As the model fidelity is of such fundamental importance to the search process for KG or MAB algorithms, in the next section we will

outline in detail how we go about formulating and updating a VTA based model that can be used to drive automated DBS programming search.

5.2 Patient-Specific Electric Field Profiles

We use impedance data and testing results on tremor and side effects to generate VTA estimates and visualize results for the multitude of stimulation configurations that are programmable in Medtronic's Activa IPG. The figures in this section were generated by an ANN-based approach [71]. The Medtronic 3387 electrode model was used, as is present in all implanted systems of patients studied in Chapter 3, and consists of four contacts 1.5mm in width and separated by 1.5mm spacing. Although the electric fields and resulting VTAs radiate circumferentially in three dimensions from the electrode contacts, we simplify the space here to present a planar view in which only the horizontal and vertical extent of the field is of interest. This can be done without any loss of information since the electric fields are directionally uniform.

Monopolar settings on adjacent contacts (C+2- and C+3-) are plotted in Figure 5.1. Variable impedances at each electrode contact account for the different scales for the same stimulation amplitude. Black circles on the x-axis (electrode axis) denote the centers of each contact, and the space is plotted in coordinates relative to the geometric center of the four contacts. The plot shows that there is considerable VTA overlap between higher amplitude monopolar DBS settings on adjacent contacts.

Bipolar settings for one configuration (0-1+) of 12 possible are plotted in Figure 5.2. Bipolar configurations are characterized by both cathodic and anodic VTAs. Cathodic and anodic stimulation have different tissue-recruiting properties, with cathodic stimulation more effectively recruiting and activating neurons to depolarize. Additionally, bipolar electric fields are shown to be considerably smaller in extent than monopolar electric fields. For this reason, bipolar DBS settings are often recommended to narrow the electric field and limit the side effects experienced by patients (see Figure 3.3). However, it is often the case that bipolar DBS settings require high amplitude to achieve the same level of symptom control as monopolar

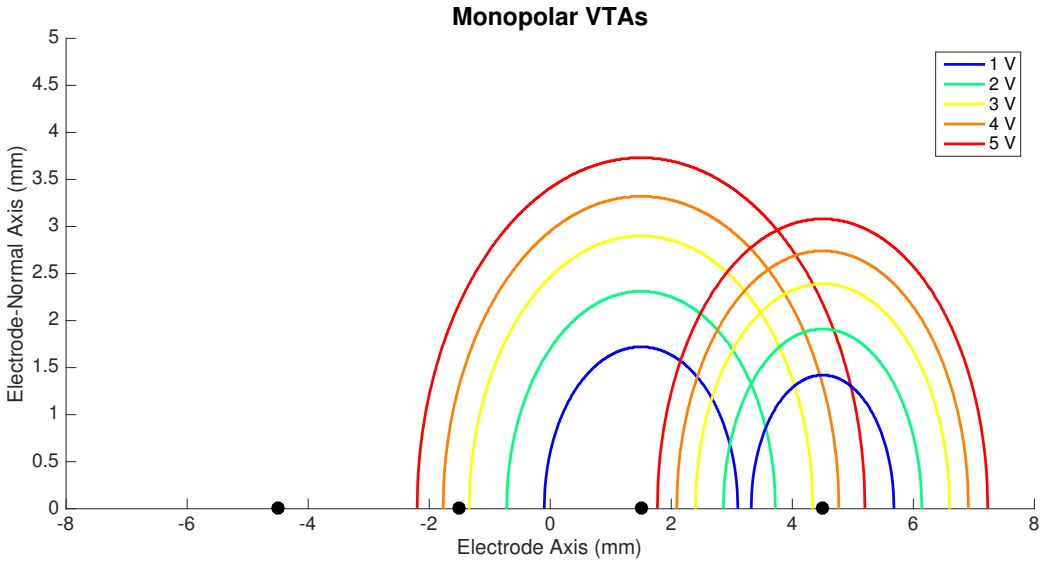

Figure 5.1: VTA ellipses for 1 - 5V on monopolar contacts C+2- and C+3-.

DBS settings, thus creating a greater burden on device power consumption. The origin of electric fields created by bipolar settings is not the same as that for monopolar settings due to interactions between the opposite polar fields. Therefore, bipolar DBS settings also allow selective stimulation for tissue volumes that cannot be isolated by monopolar DBS settings.

Double monopolar settings, in which two contacts are set as cathodes, are plotted in Figure 5.3. Double monopolar settings on adjacent contacts cause the cathodic electric field to merge into one large electric field. This makes double monopolar settings preferable in scenarios in which adequate symptom control cannot be achieved through monopolar stimulation, as the double monopolar settings cast a wider VTA.

Double bipolar settings, in which one contact is selected as anode and two contacts are selected as cathodes, are plotted in Figure 5.4. Somewhat a hybrid between bipolar and double monopolar settings, the objective of double bipolar stimulation is to stimulate as large a VTA as possible concentrated near the electrode in an attempt to affect symptoms, while limiting the extent of electric fields emanating from the electrode to limit possible side effects.

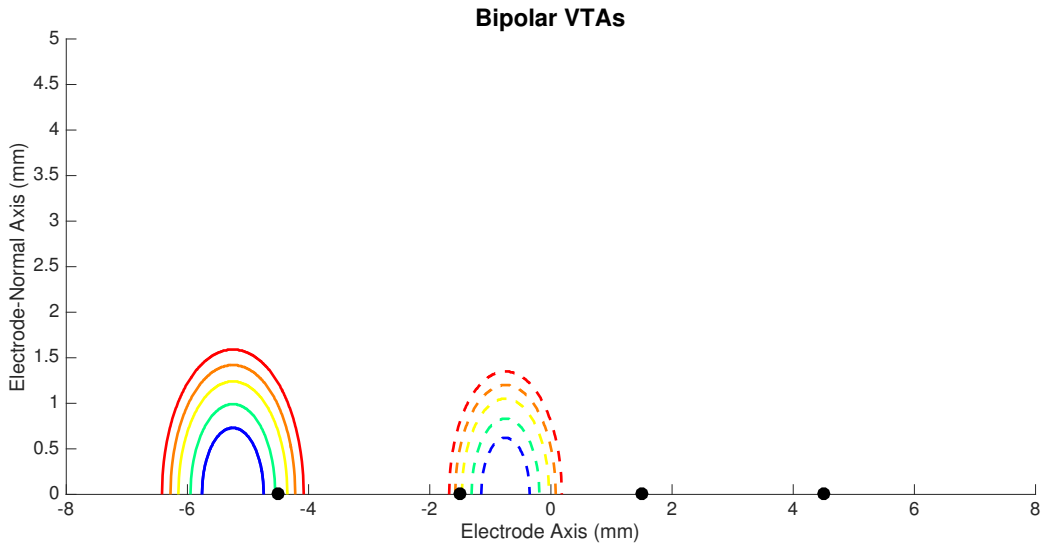

Figure 5.2: VTA ellipses for 1 - 5V on bipolar contact 0+1-. Dashed lines denote anodic VTAs, while solid lines represent cathodic VTAs.

Aside from varying stimulation amplitude and contact configuration, the other primary method for altering the VTA of DBS is through the pulsewidth. VTA scales with increasing pulsewidth, and so this provides another dimension along which DBS settings can precisely target and control the VTA.

Thus, each stimulation contact configuration possesses unique VTA properties that allow clinicians to customize therapy accordingly. The objective of the remainder of this chapter is to transform clinician intuition concerning how to use initial monopolar screening results to efficiently test more complex stimulation configurations (bipolar, double monopolar, double bipolar) to achieve optimal therapy for patients. Specifically, we aim to convert our system from Chapter 3 in which hard thresholds on symptoms and side effects are used to suggest advanced DBS contact configurations into one in which the search process is data-driven via a predictive model that captures how the many stimulation configurations are related.

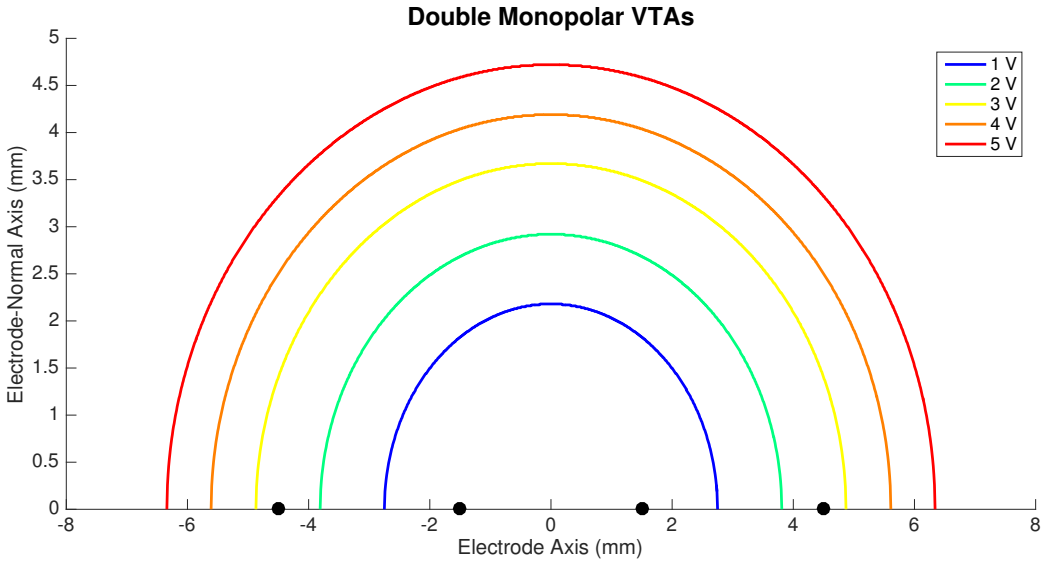

Figure 5.3: VTA ellipses for 1 - 5V on double monopolar contact C+1-2-.

5.2.1 Monopolar Screen Visualization

In this section we develop a method for assigning value to a global map of VTA based on monopolar screen results. This will inform the development of a predictive model that will allow us to select potentially therapeutically valuable DBS settings for online testing for automated search. We use the results of the monopolar screen (see Figure 3.4) to evaluate both tremor VTA model and side effect VTA model. Each unique DBS setting has a VTA analog, as shown in Figure 5.1, and many DBS settings, especially those of the same contact configuration and lesser amplitude, have overlapping VTAs. We assign value to regions of overlapping VTA of different DBS settings based on whether a tremor or side effect response was evoked. For example, if in the case of overlapping monopolar VTA as in Figure 5.1, (C+2-, 5V) had a tremor score equal to 1 and side effect score equal to 0 and (C+3-, 5V) had a tremor score equal to 2 and side effect score equal to 0.5, then their shared VTA would be assigned tremor score equal to 2 and side effect score equal to 0. Through this method we can systematically assign tremor and side effect value to VTAs associated with monopolar

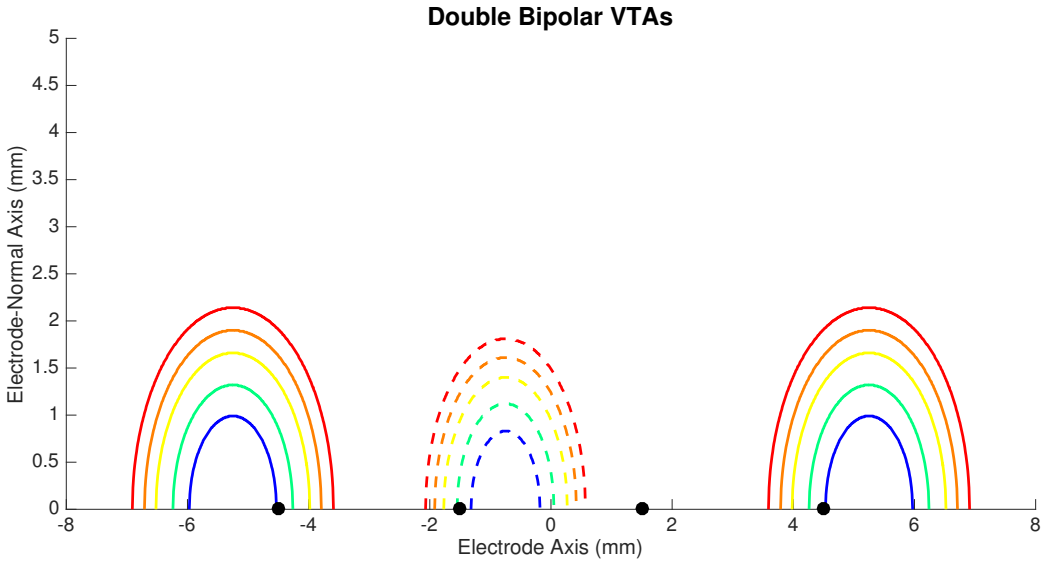

Figure 5.4: VTA ellipses for 1 - 5V on double bipolar contact 0-1+3-.

DBS settings in order to map out the most likely regions for eliciting a therapeutic, side effect-free response.

An example of this VTA-based valuation procedure is shown in Figure 5.5 for patient 4 from the Chapter 3 study (same data as in Figure 3.4). The tremor score plot shades from lighter yellow (most ineffective for treating tremor) to dark blue (most effective for treating tremor), while the side effect severity plot shades from dark blue (no side effects) to teal (mild side effects) and yellow (moderate side effects). The tremor score plot shows that the region near coordinates (-3mm, 2mm) is the most responsive in terms of reducing tremor, suggesting that the targeted region for this PD patient (STN) is located in close proximity. The side effects plot shows that mild side effect severity is reported for VTA near coordinates (0mm, 2mm), and that moderate side effects, reported for the high amplitude settings on each contact, are estimated for VTA regions at the edge of the space, suggesting that tracts to be avoided may be located in these regions.

There are some limitations to this approach of assigning value to VTA for the monopolar screen. Due to the radial VTA pattern of monopolar DBS settings, regions that are close to

the electrode-normal axis are assigned the same value as regions further from the electrode-normal axis, even though the latter is more likely to contain either the targeted brain region or tracts to be avoided. For this reason, it might be useful to augment the estimated values with a measure of uncertainty to reflect that the VTA and its associated values are spatially inexact.

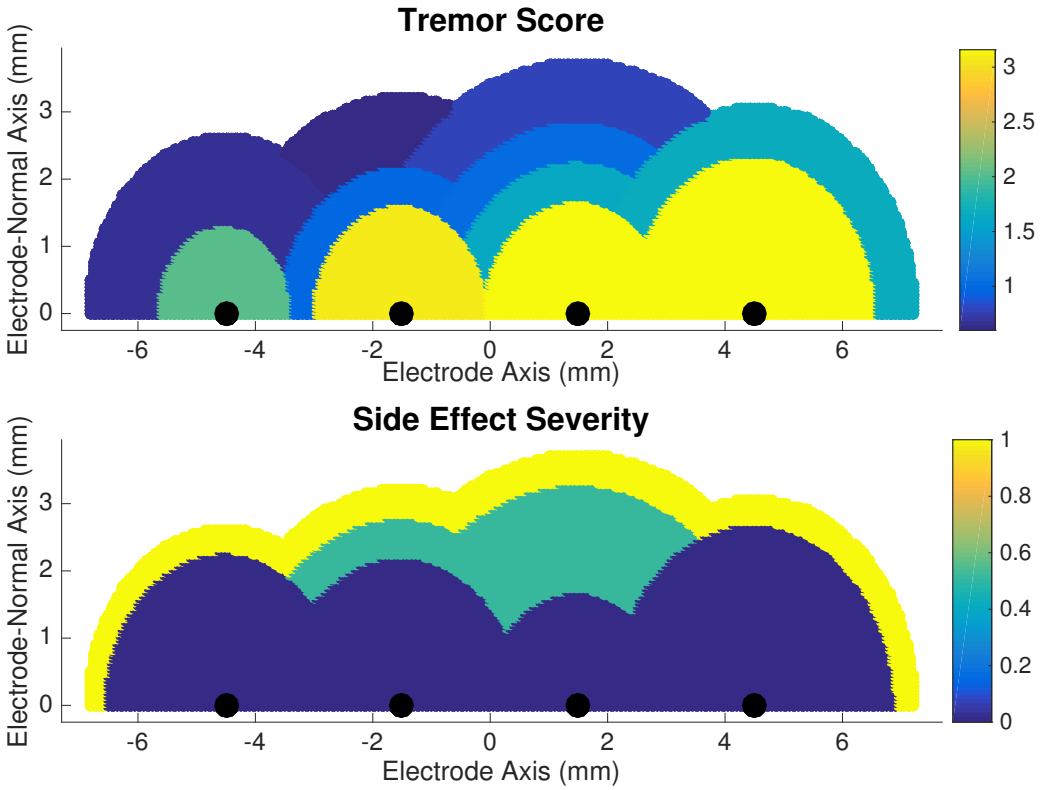

Figure 5.5: A synthesized value-based VTA map for a monopolar screen.

5.2.2 Predicting Valuable DBS Settings

Next, we combine the results of the previous two sections to obtain a model that predicts the value of untested DBS settings, particularly the advanced DBS settings such as bipolar, double monopolar, and double bipolar outlined in Figure 3.3, based on tested monopolar

DBS settings as in Figure 5.5. Each candidate DBS setting is assessed based on its VTA and the known properties of response from other previously tested settings.

The monopolar screen results in Figure 5.5 provide a physical substrate upon which other unknown DBS settings can be tested. Since the VTAs for monopolar DBS settings are spatially inexact, as mentioned in the previous section, a thresholding function is used to determine the tremor and side effect value for VTAs carved out by candidate DBS settings. Estimate DBS value is then computed in the same manner as introduced in Chapter 3.

A candidate bipolar DBS setting predicted to have high value according to this method is shown in Figure 5.6. This particular bipolar setting is 4.5V on contact 0-1+ with 90μs pulsewidth, and its VTA boundaries clearly carve out area associated with low tremor score and avoid areas associated with side effects.

This method can be extended to systematically select new DBS parameters for testing, similar to what was done with the optimization procedure in Chapter 3. Through iterative testing of many candidate DBS settings, the underlying brain region targeted by stimulation can become illuminated through VTA-based modeling. In the next section we will motivate search algorithms that can efficiently and optimally navigate the VTA-stimulation parameter space.

5.3 Search Algorithms for Automated DBS Programming

In this section we outline the details of the knowledge gradient algorithm and test and illustrate its application in automatically guiding the monopolar screen from data recorded from Chapter 3 experiments.

We consider a set of DBS setting candidates $\mathcal{X} = \{DBS_1, ..., DBS_M\}$, where M is the total number of candidates. In an automated programming application, we assume we have a measurement budget of N measurements, which amounts to testing N DBS settings and obtaining a measure J_{DBS} (Eq 3.1) for each. Each measurement i of candidate DBS_j yields a value $J^i_{DBS_j}$ which we use to update vectors of sample means and variances, $\mu^i_{DBS_j}$ and $\sigma^i_{DBS_j}$, respectively. After N measurements, we select the DBS setting that satisfies the

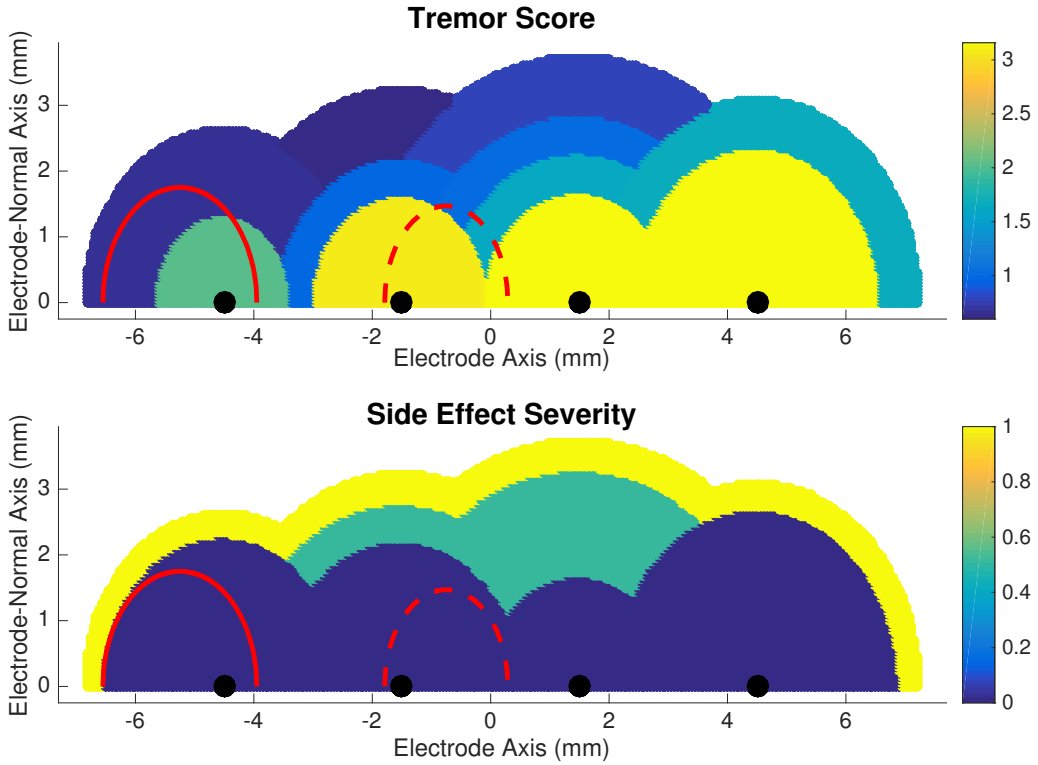

Figure 5.6: A bipolar DBS setting (4.5V, 0-1+, 90μs) with high predicted value.

optimization criterion:

$$DBS^n = \max_{DBS \in \mathcal{X}} \mu^n_{DBS} \tag{5.1}$$

The knowledge gradient (KG) policy is an offline policy, meaning that the search is considered separately from the systems operation; we tolerate testing suboptimal candidates in an offline policy so that we can more effectively explore the space and select the apparent optimal candidate at the end of testing. As such, the objective function for the knowledge gradient policy can be stated as

$$\max_{\pi \in \Pi} \mathbb{E}^{\pi} \mu_{x^N} \tag{5.2}$$

The full derivation of the KG algorithm is detailed and is beyond the scope of this chapter, but it is worth outlining some key computations to illustrate its operation. The KG policy operates, at each instance of candidate selection for measurement, by choosing the candidate that has the highest probability of exceeding the currently estimated optimum, given estimates of each candidate's mean θ_x^n and variance σ_x^n, assuming Gaussian distributions. This is done by first computing the normalized influence of decision x, which is the number of standard deviations from the current optimum for each candidate:

$$\zeta_{DBS}^n = -\left| \frac{\mu_{DBS}^n - \max_{DBS' \neq DBS} \mu_{DBS'}^n}{\sigma_{DBS}^n} \right| \tag{5.3}$$

ζ is then used to compute the tail probability of observing, for each candidate, a value greater than the current maximum, using properties of the normal cumulative distribution function

$$f(\zeta) = \zeta \Phi(\zeta) + \phi(\zeta) \tag{5.4}$$

where Φ is the cumulative distribution function and ϕ is the probability density function. Finally, the knowledge gradient is given by

$$\nu_{DBS}^{KG,n} = \sigma_{DBS}^n f(\zeta_{DBS}^n) \tag{5.5}$$

and the KG policy can be formulated as

$$DBS^{KG,n} = \arg\max_{DBS \in \mathcal{X}} \nu_{DBS}^{KG,n} \tag{5.6}$$

Thus, the KG policy computes and selects for testing the candidate DBS setting with optimal knowledge gradient. Implementing this algorithm in practice may be quite challenging, as *a priori* specification of means, variances, and correlations may significantly bias the search. Because of this, deployment of KG policies in an actual automated DBS programming application necessitates a heuristic approach, and we will make use of past patient

programming data from Chapter 3 to demonstrate an effective search strategy.

5.3.1 Learning a Model for DBS Programming

In this final section of the Chapter we simulate the KG search policy and illustrate its potential for applications in automated DBS programming. As our data collection in Chapter 3 was primarily limited to monopolar settings, we will focus on replicating this process as an initial test for automated DBS programming. However, the intention is that this method can scale to incorporate additional stimulation configurations (bipolar, double monopolar, double bipolar, etc.) following the example shown in Figure 5.6.

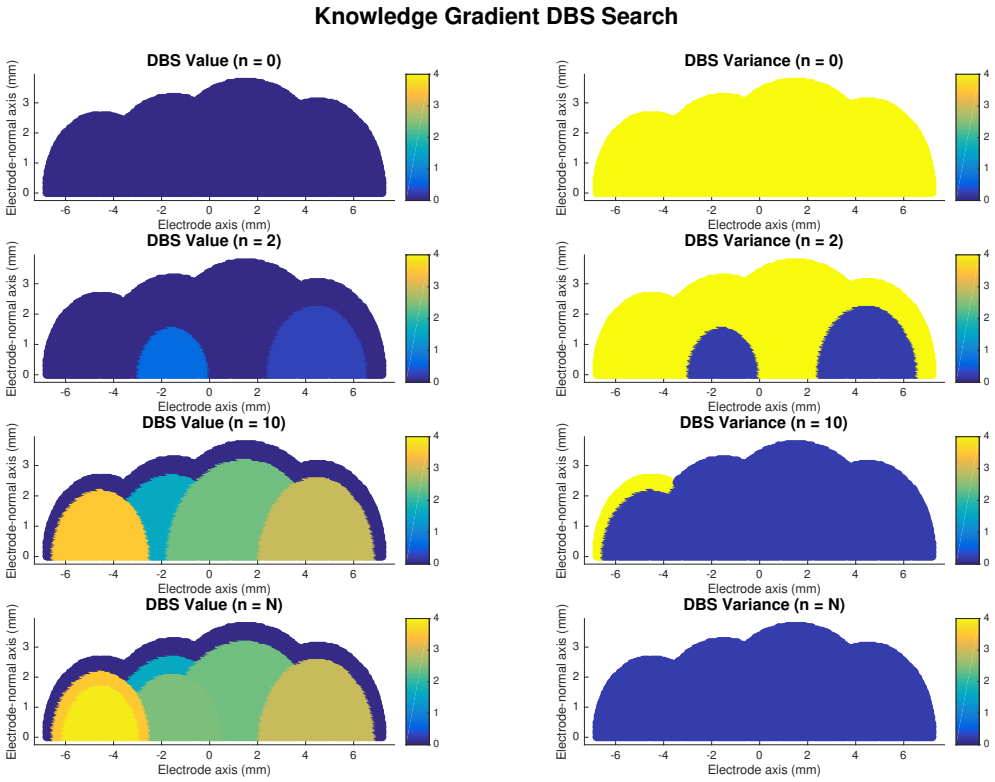

Figure 5.7: Knowledge gradient search applied to automated DBS programming (monopolar screen).

An example of the KG algorithm applied to the monopolar screen is shown in Figure 5.7. The left column shows DBS value J_{DBS}, which represents the mean value assigned to each candidate DBS setting DBS_j, and the right column shows the variance of candidate settings, σ_{DBS_j}, which can be interpreted as brain regions whose response to DBS is unknown.

The entire space mapped by the monopolar settings, which is limited to DBS settings that induce moderate side effects, is seeded with $DBS_j = 0$ and $\sigma_{DBS_j} = 4$ to reflect uniform uncertainty concerning where the optimal DBS setting will be located in VTA space at the beginning of search ($n = 0$). At $n = 2$, the plot shows that two low amplitude DBS settings have been tested on non-overlapping monopolar contacts (C+1- and C+3-), and the J_DBS plot is updated to display their values while the variance plot shows these regions as having much lower variance compared with the rest of the untested space. At $n = 10$ much of the space has been mapped out, and there is a region of high J_{DBS} emerging at the left of the VTA space on contact C+0-. Note that the periphery of the space has low value, which can either reflect untested space (for C+0- on the variance plot), or VTA regions that induced side effects which penalize J_{DBS}. Finally at $n = N$, or at the end of our "measurement budget" for the monopolar screen, the space is completely mapped out, which is indicated by the entire region having low variance, and 2V on C+0- has emerged as the most valuable DBS candidate.

5.4 Future Directions

Future planned experiments will extend the results of Chapter 3 with the methodology presented in this chapter. These experiments will seek to accomplish several benchmark goals related to the fitness of VTA models in automated DBS programming applications.

First, experiments applying the VTA method of stimulation parameter quantification will allow careful scrutiny of both the accuracy and usefulness of the VTA line of research at scale. There have been past studies that investigate the combined use of imaging and VTA data to predict DBS settings for patient therapy [71], however there have not been studies investigating VTA data related to therapeutic efficacy of several DBS settings nor

have there been studies that examine the interrelatedness of VTA data related to many DBS settings in a patient-specific application. Therefore, experiments applying the VTA method of stimulation quantification to automated DBS programming will allow an unprecented examination of the value of such heavily researched models.

Automated DBS programming experiments involving VTA predictions will also attempt to optimize the search procedure by reducing the number of parameters needed for testing and providing greater levels of therapy. The knowledge gradient search policy could be tuned to discard many DBS settings deemed unlikely to be effective, and thus reduce the number of DBS settings tested. By evading exhaustive search, as was done in Chapter 3, the knowledge gradient algorithm could achieve acceptable performance with significantly fewer tests and shorter programming times overall. Additionally, the VTA data could allow knowledge gradient policies to test more obscure DBS settings earlier in the search, which may provide patients with therapy levels not experienced.

Chapter 6

MODEL-BASED CLOSED-LOOP CONTROL OF DEEP BRAIN STIMULATION

In this chapter we move beyond the problem of programming DBS for therapy and turn to the development of closed-loop control strategies for optimizing DBS therapy and performance continuously. Closed-loop DBS is borne out of multiple observations of typical patient therapy: 1) some patients cannot achieve adequate symptom relief without some disabling side effects, so a strategy for effectively trading off between these two modes of therapy (symptom-free and side effect-free) is necessitated; and 2) many symptoms of Parkinson's disease and essential tremor are dynamic or context-dependent, suggesting that stimulation is not always needed. In this chapter we motivate the use of system identification experiments complemented with hybrid systems modeling to put forth a robust methodology for performing optimal, closed-loop DBS control.

6.1 Background

Closed-loop deep brain stimulation (CLDBS) is an emerging framework for optimizing treatment strategies for patients with Parkinson's disease (PD), essential tremor (ET), and dystonia [75]. Current DBS clinical practices use persistent, open-loop stimulation strategies, which may be inefficient due to the dynamic nature of symptoms for diseases treated by DBS. By delivering stimulation only when symptoms are expected, CLDBS promises to reduce device power consumption and side effects induced by DBS, thus extending device lifetime and improving patient quality of life.

Several clinical and simulation-based studies have been performed in pursuit of practical CLDBS methods. These studies aim to modulate DBS on the basis of biomarker data

from neural or external sensor recordings. Most simulation studies make use of the Rubin and Terman biophysical model of DBS in PD [76] and develop control policies based on, for example, time-varying estimates of synaptic conductances in pathological deep brain structures [77]. This approach is complicated by the prohibitive computational expense in simulating hundreds of neurons governed by Hodgkin-Huxley dynamics in order to make predictions in real-time, and it does not account for the variability in implanted DBS locations and other inter-patient differences that may compromise model performance.

Clinical studies to date have typically taken a more measured approach in using biomarker thresholds to trigger CLDBS. A prominent intraoperative study recorded local field potentials (LFPs) from subthalamic nucleus (STN) in PD patients and used beta band power estimates (13-30Hz) to trigger stimulation, demonstrating that both patient motor scores and stimulation time were significantly reduced using CLDBS compared to standard open-loop DBS [78]. However, this study benefited from using high-fidelity LFP recording and processing equipment that far exceeds the technical capabilities of current implanted DBS systems. Another study aimed to use tremor band power (4-8Hz) estimates from inertial measurement unit (IMU) data from a smartwatch to trigger CLDBS [79]. While this method of CLDBS proved capable of both reducing tremor band power compared to baseline (DBS off) and reducing mean stimulation amplitude compared to conventional open-loop DBS, triggering DBS on a threshold also proved prone to instability due to the time-delayed effect of DBS on observable changes in tremor.

A more promising approach involves identifying patient-specific models of the interaction between DBS and biomarkers to develop CLDBS strategies, and this approach will be explored in detailed in this chapter. The use of empirical models sidesteps the issues with the more rigid biophysical modeling approaches while also allowing the flexibility inherent to threshold-based approaches.

6.2 System Identification for DBS

6.2.1 DBS Mechanisms

Past studies investigating DBS mechanisms can provide useful aids for designing system identification experiments. The dynamics of tremor in PD at STN DBS onset and offset has been studied extensively, with multiple studies noting rapid reduction in tremor amplitude at DBS onset and a gradual return of maximal tremor amplitude after DBS offset following prolonged stimulation [80][81]. Another study investigated the dynamics of beta-band desynchronization due to STN DBS in PD patients and found that the beta-band profile was attenuated during DBS and remained desynchronized after DBS offset for a period dependent on the length of stimulation time [9]. These studies are suggestive of a potential charging/discharging mechanism inherent to STN DBS in PD, a phenomenon that could be exploited for both system identification and development of CLDBS strategies.

6.2.2 System Identification Experiment

This study was approved by the Stanford University Institutional Review Board for human subjects testing. In the system identification experiments, patients were seated comfortably in a chair with the affected arm supported against gravity on an armrest for testing of PD rest tremor. We designed a pseudo-random binary sequence (PRBS) as an input signal suitable for linear system identification [82], and we chose a switching time of 30 seconds as past studies of tremor dynamics indicated this may be an appropriate period over which we could observe a significant change in tremor severity. The PRBS alternately tested the clinical stimulation amplitude in the ON state and no stimulation in the OFF state. The PRBS input signal was applied using the Medtronic Nexus-D platform to communicate with the Activa PC+S implanted on the side contralateral to the patient's affected arm. Each system identification session lasted 30 minutes and inertial measurement unit (IMU) data was streamed over Bluetooth from an LG Smartwatch fitted securely to the patient's wrist. The purpose of the system identification experiment is to investigate the dynamical change

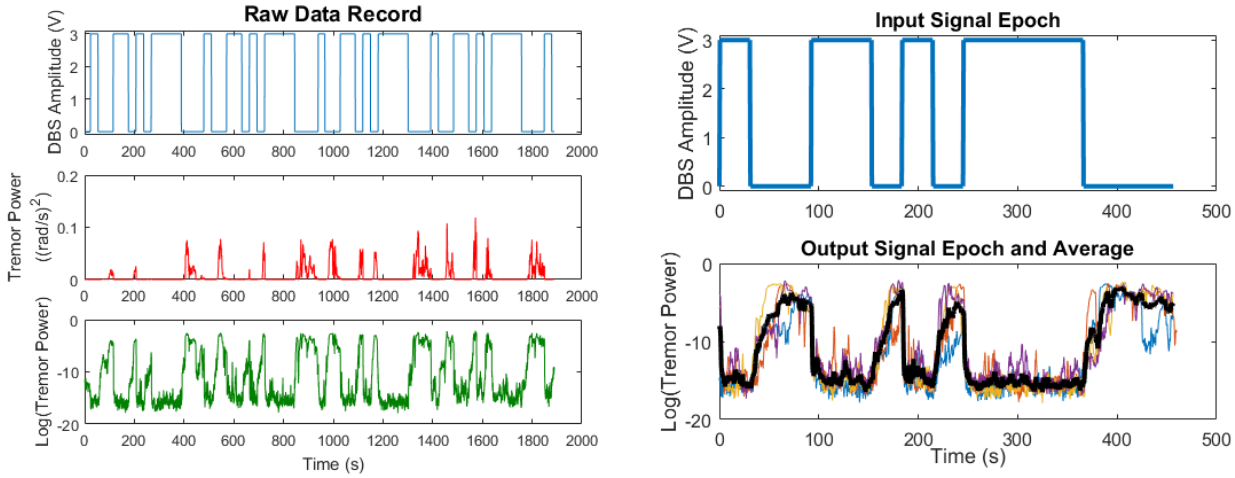

Figure 6.1: The results of a system identification experiment investigating the dynamics of Parkinsonian rest tremor due to switching DBS on and off. Left: the full 30-minute experimental record, with DBS amplitude at top, an estimate of tremor band power (4-8Hz) in middle, and the logarithm of tremor band power at bottom. Right: the same data compressed into a single epoch for the periodic PRBS used as input signal. The input signal was applied four times over the course of an experiment, and the output response is averaged over each period to produce an estimate with less noise. The averaged log(tremor power) data is used as output for identification of model parameters. The plots demonstrate the rapid reduction of tremor band power when DBS is switched on, and the more gradual return of tremor band power when DBS is switched off.

in biomarker activity as a result of switching DBS on and off.

Figure 6.1 shows for one system identification experiment the DBS amplitude input signal, an estimate of tremor band power (4-8Hz) from gyroscopic data, and the logarithm of tremor band power, the last of which has been shown to correlate highly to clinical ratings of tremor severity [28]. Tremor band power was estimated using a short-time Fourier transform with Hanning window of 1 second and was calculated every 0.2 seconds. From these plots we note the effect of DBS on PD rest tremor: when DBS is turned on there is a rapid decrease in tremor band power, and when DBS is turned off tremor band power gradually returns to its steady state value. This observation is in agreement with past studies investigating DBS mechanisms.

For this experiment we used a periodic PRBS, which was repeated four times over the course of the 30-minute experimental session. The purpose of using a periodic PRBS is twofold: first, we obtain an average output signal that is superior for producing model parameter estimates with less variability; second, it allows for output signal noise estimates, which can be useful for assessing modeling and control application performance through simulation studies, as will be demonstrated later in this paper. The input signal epoch and average output signal are shown in right plots of Figure 6.1, and it is from these data we estimate model parameters.

6.2.3 Hybrid Systems Modeling for DBS

In order to develop a model for tremor response to switching DBS on and off, we make use of a general input-output model, the autoregressive model with external inputs (ARX), which has the following form for linear, discrete-time, single-input single-output systems:

$$A(q^{-1})y(t) = B(q^{-1})u(t) + \epsilon(t) \tag{6.1a}$$

where $\epsilon(t) \in \mathcal{N}(0, \sigma^2)$ and A and B are polynomials of order n in the backward shift operator q^{-1}:

$$A(q^{-1}) = 1 + a_1 q^{-1} + a_2 q^{-2} + \ldots + a_n q^{-n} \tag{6.1b}$$

$$B(q^{-1}) = b_1 q^{-1} + b_2 q^{-2} + \ldots + b_n q^{-n} \tag{6.1c}$$

To fit an ARX model to data collected in the system identification experiments, we consider $y(t)$ as the logarithm of estimated tremor band power and $u(t)$ as the DBS stimulation amplitude. The model parameters for the ARX model can be found efficiently using linear least squares regression.

Hybrid models are typically used in systems that feature a switch mechanism or some other change in context that necessitates the use of separate models to describe system behavior. In DBS applications, the incorporation of a switching term is natural - we expect

patient tremor to behave in a wholly different manner depending on whether DBS is on or off, and this is evident from Figure 6.1. Thus, we identify a model for each condition and obtain the coefficients (A_{on}, B_{on}) and (A_{off}, B_{off}). This modeling framework has greater potential use in DBS applications, however, as many symptoms in PD and ET are context-dependent, e.g. intention or kinetic tremors while a patient is moving their arm, or freezing of gait while a patient is walking in particular environments. In these applications, we may have several models to describe the different activity states and DBS states that are needed for effective therapy.

Typically in hybrid systems applications the transitions between different models are determined by the lapse of certain time periods (time events) or system states crossing specified thresholds (state events). For the present DBS application we are considering when and how to switch between $DBS\ ON$ and $DBS\ OFF$ states in order to optimize therapy. Following the prior DBS studies suggesting a charge/discharge mechanism involved in the DBS effect on PD rest tremor, we propose that the transition from $DBS\ ON$ to $DBS\ OFF$ models be governed by a time event requiring a hold time to achieve the tremor attenuation effect, and that the transition from the $DBS\ OFF$ to $DBS\ ON$ model be governed by a state event when tremor is detected to exceed some threshold. Figure 6.2 shows this process in a conceptual model, which represents the high-level control policy for this hybrid system. We now outline the MPC algorithm that enables optimized switching between our hybrid models for CLDBS.

6.3 Model Predictive Control for DBS

6.3.1 MPC Formulation

MPC is an advanced process control algorithm that has gained popularity in recent years as computing power has increased, and is even being used in some medical devices such as closed-loop insulin pumps [83]. MPC involves prediction of system evolution over some finite time horizon N over which the optimal set of inputs is computed according to optimization

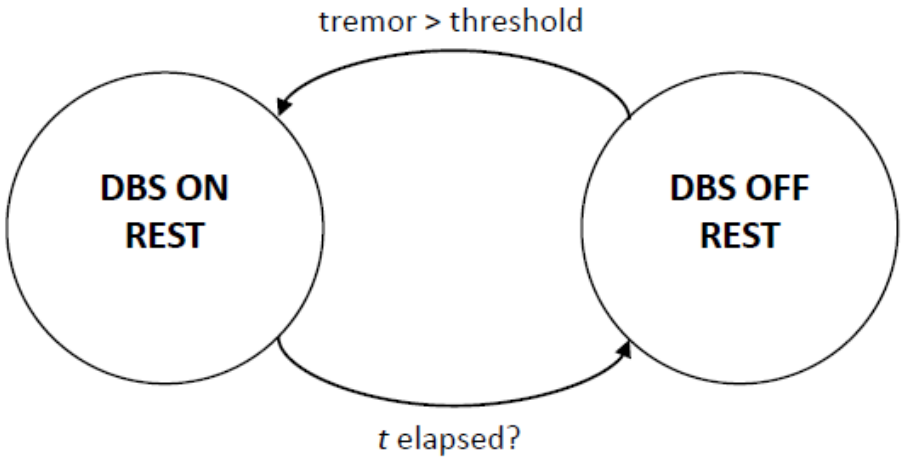

Figure 6.2: A hybrid model conception for CLDBS control of PD rest tremor. The transition from the $DBS\ ON$ to $DBS\ OFF$ models occurs after DBS is on for a certain time period, and the transition from the $DBS\ OFF$ to $DBS\ ON$ models occurs when tremor has returned above a threshold.

criteria with constraints. In practice, constraints may be required on the input signal for safe operation, and this is especially true in DBS applications as too high stimulation amplitudes and rates of change may induce side effects in the patient. By encapsulating a model of symptom response to DBS, an explicit optimization problem, and input constraints for patient safety and minimization of side effects, the MPC formulation offers an all-in-one solution for CLDBS. Thus, we consider the following MPC problem formulation for a constrained, finite-horizon linear quadratic regulator:

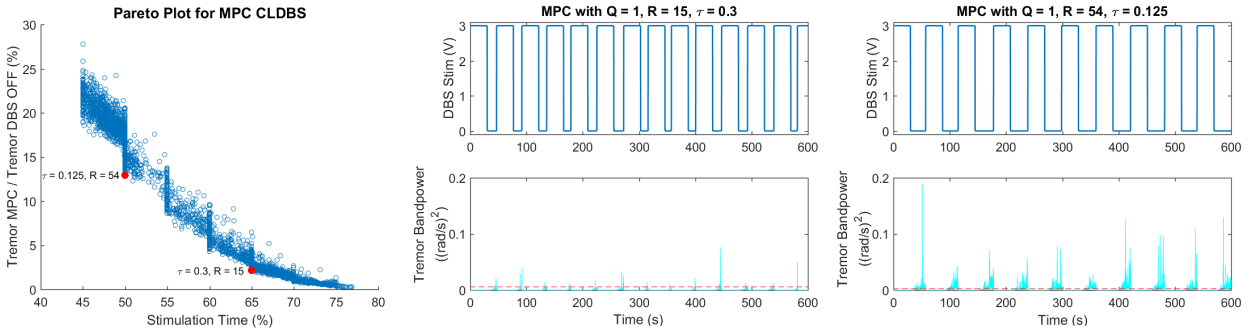

Figure 6.3: Results from the MPC simulation study. Left: a Pareto plot showing the tradeoffs in performance for various values for R and τ for the multiobjective CLDBS problem. The Pareto front is the set of points on the lower left edge of the collection of points on the plot that are closest to the origin, and we highlight two of these points. Middle: a simulation of MPC for PD rest tremor with $R = 15$, which more aggressively treats tremor at the expense of more stimulation. Right: a simulation of MPC for PD rest tremor with $R = 54$, showing that more tremor is allowed but stimulation time is considerably less. The dashed line in the MPC simulation plots indicates the tremor threshold used to trigger the optimal MPC switching sequence.

$$\begin{aligned} \min_{u} \quad & \sum_{n=1}^{N-1} x_n^T Q x_n + \sum_{n=0}^{N-1} u_n^T R u_n \\ \text{subject to} \quad & x_{n+1} = A x_n + B u_n \\ & u_{min} \leq u_n \leq u_{max} \\ & \Delta u_{min} \leq u_n - u_{n-1} \leq \Delta u_{max} \\ & n = 0, 1, \ldots, N-1 \end{aligned} \tag{6.2}$$

In order to solve (6.2) it is useful to first convert our ARX model (6.1) to a state-space controllable canonical realization:

$$A = \begin{bmatrix} 0 & 1 & 0 & \dots & 0 \\ 0 & 0 & 1 & \dots & 0 \\ \vdots & \vdots & \vdots & \ddots & \vdots \\ 0 & 0 & 0 & \dots & 1 \\ -a_n & -a_{n-1} & -a_{n-2} & \dots & -a_1 \end{bmatrix} \quad B = \begin{bmatrix} b_n \\ b_{n-1} \\ \vdots \\ b_1 \end{bmatrix}$$

$$\mathrm{C} = \begin{bmatrix} 0 & \dots & 0 & 1 \end{bmatrix}$$

where $C \in \mathbb{R}^{1\times n}$ for the single-input single-output system. Then (6.2) can be solved by conversion to the following convex quadratic program:

$$\begin{aligned} \min_{u} \quad & \frac{1}{2}u^T H u + f^T u \\ \text{subject to} \quad & A_c u \leq b_c \end{aligned} \tag{6.4}$$

where $H \in \mathbb{R}^{N\times N}$ is the Hessian matrix and is defined by $H = V^T Q V + R$ and $f^T = V^T Q v x_k$. V and v are state prediction matrices satisfying the equation $x = vx_0 + Vu$ and have the following forms:

$$V = \begin{bmatrix} CB & 0 & 0 & \dots & 0 \\ CAB & CB & 0 & \dots & 0 \\ CA^2B & CAB & CB & \dots & \vdots \\ \vdots & \vdots & \vdots & \ddots & 0 \\ CA^{N-1}B & CA^{N-2}B & CA^{N-3}B & \dots & CB \end{bmatrix} \quad v = \begin{bmatrix} CA \\ CA^2 \\ \vdots \\ CA^N \end{bmatrix}$$

Finally, the constraint matrices A_c and b_c collate the input and input rate-of-change con-

straints in the following manner:

$$A_c = \begin{bmatrix} I^{N\times N} \\ -I^{N\times N} \\ \Phi^{N\times N} \\ -\Phi^{N\times N} \end{bmatrix} \quad b_c = \begin{bmatrix} U_{max} \\ -U_{min} \\ \Delta U_{max} \\ -\Delta U_{min} \end{bmatrix} + \begin{bmatrix} \emptyset \\ \emptyset \\ I_0 \\ I_0 \end{bmatrix} u_{k-1}$$

where I is the identity matrix; U_{max}, U_{min}, ΔU_{max}, and ΔU_{min} are column vectors of length N containing the appropriate constraints; $\emptyset$ is a column vector of length N consisting of all zero entries; and $\Phi \in \mathbb{R}^{N\times N}$ and $I_0 \in \mathbb{R}^{N\times 1}$ are defined to satisfy the constraints in the following way:

$$\Phi = \begin{bmatrix} 1 & 0 & 0 & \dots & 0 \\ -1 & 1 & 0 & \dots & 0 \\ 0 & -1 & 1 & \dots & 0 \\ \vdots & \vdots & \ddots & \ddots & \vdots \\ 0 & 0 & \dots & -1 & 1 \end{bmatrix} \quad I_0 = \begin{bmatrix} 1 \\ 0 \\ \vdots \\ 0 \end{bmatrix}$$

Additional considerations are required for solving the MPC problem for hybrid systems. As the system evolution depends on the model used for prediction ($DBS\ ON$ and $DBS\ OFF$), we must enumerate all possible switching instances in order to obtain the correct solution, as outlined in [84]. The MPC problem (6.4) is then solved for each switching sequence, and the switching sequence with minimum cost according to (6.2) is selected at each time step.

6.3.2 MPC Simulation Study

We now perform a simulation study to investigate the performance of the MPC approach to CLDBS for PD rest tremor using the patient-specific models obtained from system identification experiments. The MPC formulation (6.2) contains penalty weighing terms Q and R that determine the tradeoff between minimizing tremor and stimulation time. As R increases the priority is increasingly shifted towards conserving power at the expense of allowing additional tremor. Using the hybrid state transition model shown in Figure 6.2, we also have a threshold term that determines when MPC is used to determine the optimal switching sequence. Thus, our simulation study aims to clarify how these various controller parameters influence CLDBS outcome measures, which include the percentage of tremor during MPC compared to tremor when DBS is off and the percentage of time stimulation is on.

We hold $Q = 1$, as only the relative penalty weights are essential in optimization problems, and we perform a parameter sweep across R and the tremor threshold, τ, to assess the performance of MPC in terms of amount of tremor and stimulation time for different sets of parameters. For each parameter set, we simulate the hybrid ARX model (6.1) for 10 minutes with a 30-second hold-time for the $DBS\ ON$ model. Once DBS is switched off, tremor gradually returns according to the $DBS\ OFF$ model as observed experimentally, and when tremor reaches the threshold τ, the MPC problem is solved to determine the optimal switching sequence. We use a horizon of $N = 100$ timesteps (or 20 seconds) for the MPC for illustrative purposes, although in practice it may not be computationally feasible to use a horizon of this length.

The result of this parameter sweep is shown at left in Figure 6.3, which displays a Pareto plot with the performance of each parameter set plotted as a point. Pareto plots are useful tools for investigating achievable performance in multi-objective optimization problems, where each axis represents the performance on a single objective [14]. The Pareto front is the collection of points on a Pareto plot that are non-dominated, meaning that their performance in one of the objectives cannot be improved unless at the expense of weakening

performance in another objective. Thus, the Pareto front is a set of optimal solutions for this multi-objective optimization problem, and it is sensible to choose any of the parameters from this set according to one's preferences for optimizing therapy. On the Pareto plot we highlight two points that are non-dominated on the Pareto front, and we plot their simulated MPC operation for CLDBS. The middle plot shows a simulation with $R = 15$ and $\tau = 0.3$ that demonstrates modest power savings but does not allow much tremor; by contrast, the right plot shows a simulation with $R = 54$ and $\tau = 0.125$ that demonstrates greater power savings at the expense of allowing more tremor.

6.4 Discussion

In this chapter we have demonstrated a method for identifying patient-specific hybrid models through the use of system identification experiments, and we leveraged these empirical models to propose a model predictive control approach to CLDBS that allows for customizable and optimized therapy. Prior studies investigating the mechanisms of DBS on PD symptoms suggest that both hybrid modeling practices and the use of model predictive control can be applied for CLDBS control for many symptoms. In PD patients, the symptoms of tremor, bradykinesia, rigidity, and freezing of gait have all been reported to exhibit the type of charge/discharge mechanism due to switching DBS on and off outlined earlier in this chapter [49]. Although it is unclear how these PD symptoms and their associated dynamics may change after prolonged CLDBS operation, the use of linear models permits adaptation of model parameters through simple recursive algorithms which can be computed during online operation [82].

Our approach may have other operational advantages for DBS systems not afforded by the clinical approaches suggested in the literature [78][79]. These studies have used CLDBS algorithms that require continuous sensing capabilities, which is inefficient for device power resources, and also may change stimulation levels frequently, possibly inducing additional patient side effects. Instead, our hybrid MPC approach to CLDBS minimizes both the sensing resources needed and the stimulation changes by capitalizing on the charge/discharge

mechanism in PD. The issues of sensing resources and stimulation changes are downstream considerations in most CLDBS studies to date, yet they are important areas to assess the feasibility of CLDBS systems in clinical applications.

We have also presented a novel method for tuning CLDBS controllers to achieve optimized performance. In CLDBS applications there is an implicit goal of optimizing the effect of DBS on patient symptoms, side effects, and device power consumption. In this chapter we showed that, in simulation of a model derived from patient response to DBS, we could achieve a modest power savings (75% stimulation time) without sacrificing much added tremor compared to continuous, open-loop stimulation (see Figure 6.3). Additional power savings could be achieved at the expense of allowing greater tremor, and this is a preference that some patients or clinicians may have in order to prolong the DBS device lifetime and delay the need for battery replacement surgery, which carries the risk of infection. Indeed, CLDBS may reduce costs associated with DBS healthcare and its use may allow DBS to be an economically-viable option for more patients. Pareto plots and multiobjective optimization analysis could be used to facilitate equitable treatment protocols between patients and healthcare payers, who may have to contend with limited budgets in funding therapy [85].

Future work in this domain will apply the MPC method to CLDBS in clinical studies for PD patients with rest tremor. We will also apply the hybrid modeling methodology to other DBS applications, for instance in ET patients with implanted neural sensing to classify neural signals during certain states of movement that connote different types of tremor. We then plan to use a similar approach to develop MPC controllers for kinetic/intention tremors in ET patients using a hybrid model describing the state of movement.

6.4.1 Hybrid Models for DBS Applications

In this chapter we presented a hybrid model approach to describe the dynamics of PD rest tremor in response to switching DBS on and off. Hybrid models may have much greater applicability in the domain of CLDBS, and may be used to describe many scenarios in which context-dependent changes drive changes in signal dynamics, interpretability, and the ability

to effectively modulate therapy for patients.

In PD patients, several particular movement disorder features may be effectively addressed with hybrid modeling. While DBS is used to treat the symptoms of tremor, bradykinesia, rigidity and freezing of gait, it is also possible that excessive stimulation will induce dyskinesia, a hyperkinetic motor state characterized by involuntary movements. A recent study showed that dyskinesia induced by DBS in PD patients is characterized by a spectral peak appearing at half the stimulation frequency in LFPs recorded from motor cortex [86], thus being amenable to quantification unlike most side effects caused by DBS. Dyskinesia is a serious adverse side effect of DBS that requires modulation of stimulation input in order to resolve, and this feature suggests that it is an ideal candidate for CLDBS. A cascaded hybrid system model in which symptoms (e.g. tremor) and side effects (e.g. dyskinesia) are characterized by their response to DBS being switched on and off may be used together with an MPC algorithm that continuously weighs the importance of addressing symptoms vs. side effects to achieve the desired CLDBS therapy. This illustrates the potential complexity of competing motor states encountered by PD patients in their every day lives, and hybrid modeling may be a powerful tool to describe the myriad scenarios that need be accounted for and addressed by CLDBS strategies.

Moving from the isolated, controlled environment of clinical studies for CLDBS to real-world, unstructured settings may also necessitate the use of hybrid models. In present CLDBS studies, patients are typically asked to perform discrete sets of movements while sitting, and corresponding changes in neural activity in various cortical and subcortical regions are used to trigger stimulation changes. However, it is unlikely these neural signals are stationary, especially in subcortical regions, during vastly different states of behavior that are exhibited during activities of daily living - sitting, standing, walking, talking, and more could all be associated with, possibly subtly, different features of neural activity. Thus, a responsive CLDBS system will need to account for these different activity states and accompanying markers of pathological activity in order to deploy successfully in practical situations. Hybrid systems modeling offers one approach to solving this problem.

Another application for system identification, hybrid systems modeling, and model predictive control for CLDBS concerns strategies for using multiple input DBS setting that can be switched between during online therapy. The work in Chapter 3, and specifically in Figure 3.4 informs this idea, as clearly different DBS settings (contact, amplitude, etc.) have variable effects on patient symptoms and side effects. Therefore, a potential strategy for CLDBS management is to switch between different modes of operation using a model of expected symptom and side effect outcomes for each.

Chapter 7

CONCLUSIONS

In this dissertation we introduced, developed, and validated approaches to data-driven optimization of deep brain stimulation for the movement disorders of Parkinson's disease and essential tremor. Specifically, we trained data from a smartwatch platform to accurately predict movement disorder neurologist ratings (Chapter 2), and we embedded this feature into a platform for DBS device control that allowed automated programming of DBS parameters for patient therapy (Chapter 3), which was shown to be at least as effective as expert clinicians at identifying DBS settings for therapy. We extended these methods to investigate neural biomarkers for effective DBS in essential tremor patients and found that several spectral features from motor cortical data were significantly altered during effective DBS (Chapter 4), raising the possiblity of neural-based DBS programming. We integrated computational models of volume of tissue activated (VTA) by DBS settings to produce a scalable method to predict valuable DBS settings and guide automatic search routines for future automated programming applications. Finally, we addressed closed-loop DBS and formulated a model-based approach that combined system identification experiments, hybrid systems modeling, and model predictive control.

We conclude the dissertation with a discussion that looks towards future applications and the challenges and opportunities for implementing many of the ideas and methods put forth here in widespread DBS clinical practice. We focus on two primary issues that will determine the lasting importance of this dissertation: telemedicine and the future of healthcare delivery, and advances in DBS technology.

7.1 Telemedicine and the Future of Healthcare Delivery

Although this dissertation has addressed the questions of whether remote monitoring of PD and ET symptoms and automated DBS programming are possible in conception, whether and how they are possible in clinical practice are separate questions entirely. Healthcare systems have been notoriously slow to adopt new practices and approaches to treatment, and stringent healthcare insurer policies create an inertia that is difficult to overcome.

As discussed in Chapter 1, remote delivery of DBS programming updates can potentially lead to huge savings in healthcare costs and patient time and personal costs. Recent review articles have critically examined telemedicine and its viability as an approach for delivering healthcare in PD patients [87][88]. There are several factors in the long-term treatment of movement disorders that support the use of telemedicine: unequal access to neurologists especially in rural areas, treatment regimens that can require frequent updating (DBS programming), and the fact that patients with movement disorders by definition may have difficulty traveling long distances for regular appointments. Telemedicine for PD patient care can include remote monitoring of patient symptoms and reports from live video assessments or wearable sensors, and may eventually encompass systems in which DBS systems are updated through neurologist-directed adjustments or even automatically by software algorithms as has been presented in this dissertation.

Generally, PD patients have responded favorably to telemedicine as it significantly reduces the time and cost of visits [89]. However the most frequently cited reasons for dissatisfaction have been that sessions were plagued by technical difficulties and patient desire for in-person care [90]. Elderly patients may in particular have difficulty using smartphone and smartwatch technology required for telemedicine care, and implementation of automated remote DBS re-programming may require the assistance of a skilled, or capable, caregiver. Additionally, patients' lifetime histories of interacting with physicians may impede the adoption of automated technologies that would make therapy decisions without obvious input from humans. These factors represent a serious barrier to telemedicine and will take careful con-

sideration and strategizing to overcome. However, the effort should be seen as worthwhile as the cost savings and enhancements in patient quality of life could be considerable.

Telemedicine implementation also requires access to high-quality internet connection which, even in 2017, is not entirely uniform across the U.S. and especially in other countries. In the U.S., 73% of all adults have access to broadband, while fewer (63%) rural residents do, even fewer elderly adults (51%), and less still those without a high school degree (34%) [91]. With DBS implantations already having a noted significant demographic disparity, with DBS typically being provided to wealthier rather than poorer patients, telemedicine as a mode of care delivery could exacerbate this disparity even more.

Another notable barrier to telemedicine adoption in DBS care is the strict implementation and provision of healthcare services by insurance providers. Medicare provides reimbursement coverage for telemedicine healthcare if the provider and receiving patient meets a battery of requirements [92]: care must be delivered to a "qualified originating site", which can include a physician's office, rural health clinic, hospital, or skilled nursing facility; the "qualified originating site" must be located outside a major metropolitan area or in a rural hospital shortage area; providers must be credentialed and a license to practice medicine in the patient's state. Notably, telemedicine healthcare cannot currently be delivered to a patient's home in the U.S.

Thus, the current state of affairs in American and worldwide healthcare does not permit the use of at-home automated DBS programming. However, automated DBS programming as described in this dissertation could be provided outside specialty clinics and at rural health centers, and this is a possibility in the current Medicare environment and represents a significant step forward in increasing access to this advanced healthcare resource. Increased acceptance of neuromodulation and other neurotechnologies for medical applications will likely go hand-in-hand with changing approaches to how telemedicine is viewed and accepted. The timescale of therapy adjustments in neurotechnologies simply outpaces the rate at which the current healthcare system is able to attend to patients, and it needs to adapt in order to best deliver DBS healthcare for future patients.

7.2 Advances in DBS Technology

There are several areas in which DBS technology is expected to advance as usage increases and demands are raised for optimized patient therapy. The most notable is the concept of directional current steering that is to be enabled by segmented electrode leads [11]. The Medtronic leads used in experiments described in this dissertation produce electic fields that radiate circumferentially from the impanted electrode, whereas segmented leads would allow electric fields to be concentrated in specific directions around the electrode. While segmented leads would thus greatly expand the number of possible DBS settings for therapy, the potential for creating patient-tailored stimulation patterns that precisely stimulate targeted brain structures while being more capable of avoiding side effect inducing tracts is greatly desired. Clinicians may be unable to efficiently program such current steering-enabled systems, and this may be one area of DBS therapy in which automated programming methods are especially needed. Particularly, the results of Chapter 3 and 5, in which symptom assessment and device control are embedded in an automated system, and the volume of tissue activated (VTA) is used to guide selection of new DBS settings for testing, may be of particular utility in future DBS systems with segmented leads.

Another aspect of DBS technology that is likely to improve is the fidelity of implanted neural activity recording and processing systems. Neural activity recorded at higher sampling rates will lend greater insight into dynamics of neural activity both in response to DBS and as part of the underlying pathological brain network. Through these advances, system identification experiments as in Chapter 6 could be designed to probe changes in neural activity in response to changes in DBS at shorter timescales, which would allow moment-by-moment control over DBS settings and patient symptoms, rather than the somewhat crude on/off strategies supported by current research.

BIBLIOGRAPHY

[1] R. Bartholow. Experimental investigations into the functions of the human brain. *American Journal of the Medical Sciences*, 134:305–313, 1874.

[2] L. B. Kalinowsky. History of convulsive therapy. *Annals of the New York Academy of Sciences*, 462:1–4, 1986.

[3] J. B. Reswick C. N. Shealy, J. T. Mortimer. Electrical inhibition of pain by stimulation of the dorsal columns: preliminary clinical report. *Anasthesia and Analgesia*, 46(4):489–491, 1967.

[4] P. D. Wall R. Melzack. Pain mechanisms: a new theory. *Science*, 150(3699):971–979, 1965.

[5] K. J. Tracy. The inflammatory reflex. *Nature*, 420(6917):853–859, 2002.

[6] L. V. Borovikova et al. Vagus nerve stimulation attenuates the systemic inflammatory response to endotoxin. *Nature*, 405(6785):458–462, 2000.

[7] P. Larson K. Sillay and P. Starr. Deep brain stimulator hardware-related infections. *Neurosurgery*, 62(2):360–367, 2008.

[8] R. Mehanna and E. Lai. Deep brain stimulation in parkinson's disease. *Translational Neurodegeneration*, 2(1):22, 2013.

[9] H. Yu and J. Neimat. The treatment of movement disorders by deep brain stimulation. *Neurotherapeutics*, 5(1):26–36, 2008.

[10] T. D. Halbig et al. Subthalamic deep brain stimulation and impulse control in parkinson's disease. *European Journal of Neurology*, 16(4):493–497, 2009.

[11] C. Butson and C. McIntyre. Current steering to control the volume of tissue activated during deep brain stimulation. *Brain Stimulation*, 1(1):7–15, 2008.

[12] K. Wirdefeldt, H. Adami, P. Cole, D. Trichopoulos, and J. Mandel. Epidemiology and etiology of parkinson's disease: a review of the evidence. *European Journal of Epidemiology*, 26(1):1–58, 2011.

[13] Y. Agid. Parkinson's disease: pathophysiology. *The Lancet*, 337(8753):1321–1324, 1991.

[14] P. LeWitt. Levadopa for the treatment of parkinson's disease. *New England Journal of Medicine*, 359(23):2468–2476, 2008.

[15] C. Goetz et al. Movement disorder society-sponsored revision of the unified parkinson's disease rating scale (mds-updrs): Scale presentation and clinimetric testing results. *Movement Disorders*, 23(15):2129–2170, 2008.

[16] S. Miocinovic, S. Somayajula, S. Chitnis, and J. Vitek. History, applications, and mechanisms of deep brain stimulation. *JAMA Neurology*, 70(2):163, 2013.

[17] JP Hubble, KL Busenbark, R Pahwa, K Lyons, and WC Koller. Clinical expression of essential tremor: effects of gender and age. *Movement Disorders*, 12(6):969–972, 1997.

[18] E. D. Louis, R. Ottman, and W. A. Hauser. How common is the most common adult movement disorder? estimates of the prevalence of essential tremor throughout the world. *Movement Disorders*, 13(1):5–10, 1998.

[19] J. Benito-León and E. Louis. Essential tremor: emerging views of a common disorder. *Nature Clinical Practice Neurology*, 2(12):666–678, 2006.

[20] A. Gironell and J. Kulisevsky. Review: Diagnosis and management of essential tremor and dystonic tremor. *Therapeutic Advances in Neurological Disorders*, 2(4):215–222, 2009.

[21] J. Volkmann, E. Moro, and R. Pahwa. Basic algorithms for the programming of deep brain stimulation in parkinson's disease. *Movement Disorders*, 21(14):S284–S289, 2006.

[22] K. Stroupe, F. Weaver, L. Cao, D. Ippolito, B. Barton, I. Burnett-Zeigler, R. Holloway, B. Vickrey, T. Simuni, and K. Follett. Cost of deep brain stimulation for the treatment of parkinson's disease by surgical stimulation sites. *Movement Disorders*, 29(13):1666–1674, 2014.

[23] V. A. Jourdain and G. Schechtmann. Health economics and surgical treatment for parkinson's disease in a world perspective: results from an international survey. *Stereotactic and Functional Neurosurgery*, 92:71–79, 2014.

[24] Erwin B. Montgomery Jr. *Deep brain stimulation programming: mechanisms, principles and practice*. Oxford University Press, 2nd edition, 2016.

[25] R. Elble et al. Reliability of a new scale for essential tremor. *Movement Disorders*, 27(12):1567–1569, 2012.

[26] A. Beuter, A. de Geoffroy, and P. Cordo. The measurement of tremor using simple laser systems. *Journal of Neuroscience Methods*, 53(1):47–54, 1994.

[27] A. Salarian et al. Quantification of tremor and bradykinesia in parkinson's disease using a novel ambulatory monitoring system. *IEEE Transactions on Biomedical Engineering*, 54(2):313–322, 2007.

[28] J. Giuffrida, D. Riley, B. Maddux, and D. Heldman. Clinically deployable kinesia™ technology for automated tremor assessment. *Movement Disorders*, 24(5):723–730, 2009.

[29] M. M. Koop et al. Improvement in a quantitative measure of bradykinesia after microelectrode recording in patients with parkinson's during deep brain stimulation surgery. *Movement Disorders*, 21(5):673–678, 2006.

[30] J-W. Kim et al. Quantification of bradykinesia during clinical finger taps using a gyrosensor in patients with parkinson's disease. *Med Biol Eng Comput*, 49:365–371, 2011.

[31] J. Stamatakis et al. Finger tapping clinimetric score prediction in parkinson's disease using low-cost accelerometers. *Computational Intelligence and Neuroscience*, 10:717–730, 2013.

[32] N. E. Piro et al. Analysis and visualization of 3d motion data for updrs rating of patients with parkinson's disease. *Sensors*, 16:930–945, 2016.

[33] O. Martinez-Manzanera et al. A method for automatic and objective scoring of bradykinesia using orientation sensors and classification algorithms. *IEEE Transactions on Biomedical Engineering*, 63(5):1016–1024, 2016.

[34] V. Sharma et al. Spark: Personalized parkinson's disease interventions through synergy between a smartphone and a smartwatch. *DUXU 2014, Part III, LNCS 8519*, pages 103–114, 2014.

[35] H. Dubey et al. Echowear: Smartwatch technology for voice and speech treatments of patients with parkinson's disease. *ACM Wireless Health 2015*.

[36] R. LeMoyne et al. Implementation of an iphone for characterizing parkinson's disease tremor through a wireless accelerometer application. *32nd Annual International Conference of the IEEE EMBS*, pages 4954–4958, 2010.

[37] D. A. Salazar et al. Comparison between svm and logistic regression: which one is better to discriminate? *Revista Colombiana de Estadistica*, 35(2):223–237, 2012.

[38] G. E. Hinton A. Krizhevsky, I. Sutskever. Imagenet classification with deep convolutional neural networks. *Communications of the ACM Magazine*, 60(6):84–90, 2017.

[39] M. Zeng et al. Convolutional neural networks for human activity recognition using mobile sensors. *2014 6th International Conference on Mobile Computing, Applications and Services (MobiCASE)*, pages 197–205, 2014.

[40] E. Moro et al. Subthalamic nucleus stimulation: improvements in outcome with reprogramming. *Archives of Neurology*, 63(9):1266–1272, 2006.

[41] S. Farris et al. Retrospective review of factors leading to dissatisfaction with subthalamic nucleus deep brain stimulation during long-term management. *Surgical Neurology International*, 4(1):69, 2013.

[42] A. Castrioto et al. Postoperative management of deep brain stimulation in parkinson's disease. *Handbook of Clinical Neurology*, 116:129–146, 2013.

[43] X. Feng et al. Optimal deep brain stimulation of the subthalamic nucleus - a computational study. *Journal of Computational Neuroscience*, 23(3):265–282, 2007.

[44] D. Brocker et al. Optimized temporal pattern of brain stimulation designed by computational evolution. *Science Translational Medicine*, 9(371):eaah3532, 2017.

[45] A. Frankemolle et al. Reversing cognitive-motor impairments in parkinson's disease patients using a computational modeling approach to deep brain stimulation programming. *Brain*, 133(3):746–761, 2010.

[46] A. Connolly et al. Guiding deep brain stimulation contact selection using local field potentials sensed by a chronically implanted device in parkinson's disease patients. *2015 7th International IEEE/EMBS Conference on Neural Engineering (NER)*, pages 840–843, 2015.

[47] C. Pulliam et al. Motion sensor strategies for automated optimization of deep brain stimulation in parkinson's disease. *Parkinsonism and Related Disorders*, 21(4):378–382, 2015.

[48] T. Mera et al. Kinematic optimization of deep brain stimulation across multiple motor symptoms in parkinson's disease. *Journal of Neuroscience Methods*, 2(280-286):2011, 198.

[49] P. Temperli et al. How do parkinsonian signs return after discontinuation of subthalamic dbs? *Neurology*, 60(1):78–81, 2003.

[50] A. Kuhn et al. High-frequency stimulation of the subthalamic nucleus suppresses oscillatory activity in patients wiht parkinson's disease in parallel with improvement in motor performance. *Journal of Neuroscience*, 28(24):6165–6173, 2008.

[51] P. Brown. Bad oscillations in parkinson's disease. *J Neural Transm*, 70:27–30, 2006.

[52] M. Cassidy et al. Movement-related changes in synchronization in the human basal ganglia. *Brain*, 125(6):1235–1246, 2002.

[53] A. A. Kuhn et al. Event-related beta desynchronization in the human subthalamic nucleus correlates with motor performance. *Brain*, 127(4):735–746, 2004.

[54] Q. Li et al. Therapeutic deep brain stimulation in parkinsonian rats directly influences motor cortex. *Neuron*, 76(5):1030–1041, 2012.

[55] H. C. Walker et al. Short latency activation of cortex during clinically effective subthalamic deep brain stimulation for parkinson's disease. *Movement Disorders*, 27(7):864–873, 2012.

[56] C. de Hemptinne et al. Therapeutic deep brain stimulation reduces cortical phase-amplitude coupling in parkinson's disease. *Nature Neuroscience*, 18(5):779–786, 2015.

[57] J. Raethjen. The oscillating central network of essential tremor. *Clinical Neurophysiology*, 123:61–64, 2012.

[58] Y. G. Park. Ca(v)3.1 is a tremor rhythm pacemaker in the inferior olive. *Proceedings of the National Academy of Sciences*, 107:10731–10736, 2010.

[59] T. E. Milner et al. Emg analysis of harmaline-induced tremor in normal and three strains of mutant mice with purkinje cell degeneration and the role of the inferior olive. *Journal of Neurophysiology*, 73:2568–2577, 1995.

[60] G. Nicoletti et al. Diffusion tensor mri changes in cerebellar structures of patients with familial essential tremor. *Neurology*, 74(988-994), 2011.

[61] A. Schnitzler et al. Synchronized brain network associated with essential tremor as revealed by magnetoencephalography. *Movement Disorders*, 24:1629–1635, 2009.

[62] S. E. Hua and F. A. Lenz. Posture-related oscillations in human cerebellar thalamus in essential tremor are enabled by voluntary motor circuits. *Journal of Neurophysiology*, 93:117–127, 2005.

[63] B. Schelter et al. Assessing the strength of directed influences among neural signals using renormalized partial directed coherence. *Journal of Neuroscience Methods*, 179:121–130, 2009.

[64] B. Pollok et al. The cerebral oscillatory network of voluntary tremor. *Journal of Neurophysiology*, 554:871–878, 2004.

[65] W. M. Grill and S. Miocinovic. Deep brain stimulation creates an informational lesion of the stimulated nucleus. *Neuroreport*, 15(7):1137–1140, 2004.

[66] H. Cagnan et al. Stimulating at the right time: phase-specific deep brain stimulation. *Brain*, 140:132–145, 2017.

[67] H. C. Walker et al. Short latency activation of cortex by clinically effective thalamic brain stimulation for tremor. *Movement Disorders*, 27(11):1404–1412, 2012.

[68] E. L. Air et al. Acute effects of thalamic deep brain stimulation and thalamotomy on sensorimotor cortex local field potentials in essential tremor. *Clinical Neurophysiology*, 123(11):2232–2238, 2012.

[69] D. R. McNeal. Analysis of a model for excitation of myelinated nerve. *IEEE Transactions on Biomedical Engineering*, 23(4):329–337, 1976.

[70] C. R. Butson et al. Patient-specific analysis of the volume of tissue activated during deep brain stimulation. *Neuroimage*, 34(2):661–670, 2007.

[71] A. Chaturvedi. Artificial neural network based characterization of the volume of tissue activated during deep brain stimulation. *Journal of Neural Engineering*, 10(5):056023, 2013.

[72] L. M. Rios et al. Derivative-free optimization: a review of algorithms and comparison of software implementations. *Journal of Global Optimization*, 56(3):1247–1293, 2013.

[73] M. Mitchell. *An Introduction to Genetic Algorithms*. MIT Press, 1998.

[74] W. Powell and I. Ryzhov. *Optimal Learning*. Wiley, 2012.

[75] P. Afshar et al. A translational platform for prototyping closed-loop neuromodulation systems. *Frontiers in Neural Circuits*, 6, 2013.

[76] J. Rubin and D. Terman. High frequency stimulation of the subthalamic nucleus eliminates pathological thalamic rhythmicity in a computational model. *Journal of Computational Neuroscience*, 16(3):211–235, 2004.

[77] S. Schiff. Towards model-based control of parkinson's disease. *Philosophical Transactions of the Royal Society A: Mathematical, Physical and Engineering Sciences*, 368(1918):2269–2308, 2010.

[78] S. Little et al. Adaptive deep brain stimulation in advanced parkinson disease. *Annals of Neurology*, 74(3):449–457, 2013.

[79] M. Malekmohammadi et al. Kinematic adaptive deep brain stimulation for resting tremor in parkinson's disease. *Movement Disorders*, 31(3):426–428, 2016.

[80] C. Blahak et al. Rapid response of parkinsonian tremor to stn-dbs changes: direct modulation of oscillatory basal ganglia activity? *Movement Disorders*, 24(8):1221–1225, 2009.

[81] M. Titcombe et al. Dynamics of parkinsonian tremor during deep brain stimulation. *Chaos*, 11(4):766–773, 2001.

[82] L. Ljung. *System Identification*. Prentice Hall, 1st edition, 1997.

[83] Y. Wang et al. Closed-loop control of artificial pancreatic beta-cell in type 1 diabetes mellitus using model predictive iterative learning control. *IEEE Transactions on Biomedical Engineering*, 57(2):211–219, 2010.

[84] F. Borelli et al. Dynamic programming for constrained optimal control of discrete-time linear hybrid systems. *Automatica*, 41(10):1709–1721, 2005.

[85] J. Branke. *Multiobjective Optimization*. Springer-Verlag, 1st edition, 2008.

[86] N. C. Swann et al. Gamma oscillations in the hyperkinetic state detected with chronic human brain recordings in parkinson's disease. *Journal of Neuroscience*, 36(24):6445–6458, 2016.

[87] M. Achey et al. The past, present, and future of telemedicine for parkinson's disease. *Movement Disorders*, 29(7):871–883, 2014.

[88] R. B. Schneider and K. M. Biglan. The promise of telemedicine for chronic neurological disorders: the example of parkinson's disease. *The Lancet*.

[89] J. R. Wilkinson et al. High patient satisfaction with telehealth in parkinson's disease: a randomized controlled study. *Neurol Clin Pract*, 6:241–251, 2016.

[90] R. Schneider et al. Innovative approaches in caring for people with parkinson's disease: filling the gaps. *Neurol Clin Pract*, 6:203–205, 2016.

[91] Pew research center. internet/broadband fact sheet, November 2017.

[92] Legal information institute, November 2017.

VITA

Andrew Haddock grew up near St. Louis, MO and received the B.S. in Electrical Engineering from the University of Missouri, Columbia in May 2012. He began graduate school at the University of Washington in Fall 2012, and received the M.S. in Electrical Engineering in March 2015, followed by the Ph.D. in Electrical Engineering in December 2017, with concentrations in Systems, Robotics, and Controls. His research interests are in neural engineering, deep brain stimulation, neuromodulation, motor disorders, motor control, digital/mobile health delivery, and personalized medicine, and his technical expertise is mostly in control systems and theory, signal processing, machine learning, and artificial intelligence.